Quantification of hepatic vascular regeneration after 70% partial hepatectomy in mice: Tools and application

in partial fulfillment of the requirements for the degree of doctor of medicine (Dr. med.)

submitted to the Faculty Council of the School of Medicine

at Friedrich Schiller University Jena

by Chichi Xie

Born on 25.08.1987 in Hangzhou, Zhejiang, China

Gutachter:

1. Prof. Dr. med. Uta Dahmen

Experimentelle Transplantationschirurgie,

Klinik für Allgemein-, Viszeral- und Gefäßchirurgie, Universitätsklinikum Jena

2. Prof. Dr. rer. nat. med. habil. Jürgen R. Reichenbach

AG Medizinische Physik, Institut für Diagnostische und Interventionelle Radiologie,

Universitätsklinikum Jena

3. Prof. Dr. med. Fabian Kiessling

Institute for Experimental Molecular Imaging, RWTH Aachen University

Datum der Verteidigung: 06.12.2016

Contents

1 Zusammenfassung

Einleitung: Leberregeneration erfordert die Regeneration des Parenchyms und des Gefäßbaumes. Bisher stand die Regeneration des Leberparenchyms im Fokus des wissenschaftlichen Interesses, nicht zuletzt aufgrund der technischen Limitationen die Regeneration des Gefäßbaumes quantitativ zu beschreiben. Daher zielt diese Untersuchung darauf ab, die Techniken zur Quantifizierung der vaskulären Leberregeneration am Mausmodell zu verbessern.

Ziele: Wir definierten vier Teilziele: Etablieren einer intraoperative Monitoringtechnik zur Erfassung der Hämodynamik der Leber in der Maus, Etablieren eines Arbeitsablaufes zur Kontrastierung einer Mausleber, Bildgebung mittels µCT und 3D-Rekonstruktion des Gefäßbaumes, Entwicklung eines Verfahrens zur computerunterstützten Quantifizierung des regenerierenden Gefäßbaumes und die Untersuchung der parenchymalen und vaskulären Leberregeneration nach Modulation der CXCR4-CXCR7-SDF-1 Achse mit Hilfe der neu entwickelten Verfahren.

Methoden und Ergebnisse: Im ersten Schritt wurde die technisch schwierige MonitoringTechnik am Mausmodell etabliert um hämodynamische Parameter der Leber wie den portalen und leberarteriellen Blutfluß und den portalen Druck zu messen. Diese Parameter wurden sowohl in Normaltieren, während einer selektiven partiellen Ischämie und vor, während und im Verlauf nach einer 70%igen partiellen Hepatektomie gemessen. Die Ergebnisse lassen erkennen, dass die angewandte Monitoringtechnik hinreichend empfindlich ist, um kleine Veränderungen im portalen Druck und der portalen Flussrate festzustellen.

Im zweiten Schritt wurde ein Verfahren zur Visualisierung und Quantifizierung des Gefäßbaumes entwickelt. Der Gefäßbaum wurde durch die Injektion eines Silikonpolymers kontrastiert. Anhand der hämodynamischen Parameter aus den MonitoringExperimenten wurde die optimale Flussrate zur Injektion des Polymers festgelegt (0.2ml/min). Die kontrastierten Lebern wurden explantiert und im µCT gescannt. Mit Hilfe eines schwellenwertbasierten Algorithmus (Imalytics Preclinical Software) wurden die Gefäßbäume 3D rekonstruiert und ausgewählte Parameter wie z.B. die maximale Gefäßlänge und der Radius der rechten unteren Portalvene, interaktiv vermessen.

Im dritten Schritt wurde das Wachstumsmuster der Leber im Rahmen der Regeneration betrachtet. Dazu wurde eine Serie von portalvenös und lebervenös

kontrastierten Präparaten zu verschiedenen Zeitpunkten nach 70%PH (unmittelbar, 2, 3 und 7 Tage, n=3/Gruppe) per µCT untersucht. Mit Hilfe des Schwellenwertverfahrens wurden die Gefäßbäume 3D-rekonstruiert und selektiv vermessen. Zusätzlich erfolgte die Segmentierung und 3D-Rekonstruktion von Leberterritorien und Gefäßbäumen mit Hilfe des Programms HepaVision um das Lebervolumen und kumulative Gefäßparameter (z.B. Gesamtlänge der Gefäße) berechnen zu können. Wie zu erwarten korrelierten Lebervolumen und Lebergewicht, sodass im Weiteren das Lebervolumen als Maß der parenchymatösen Regeneration verwendet wurde. Basierend auf der Gefäßgeometrie wurde eine Reihe von kumulativen Gefäßparametern zur Quantifizierung des Gefäßbaumes berechnet: Gesamtlänge und Gesamtgefäßvolumen. Gefäßdichte, (Gesamtlänge/ Lebervolumen und vaskulärer Volumenanteil) wurden erhoben. Mit Hilfe des HepaVision-Programms wurde ein virtuelles Resektionsmodell entwickelt, um den Effekt der resektionsbedingten portalen Hypertension auf die Gefäßparameter zu eliminieren. Die quantitativen Gefäßparameter nach virtueller Resektion wurden mit denen am siebten Tag nach chirurgischer Resektion verglichen. Obwohl bei qualitativer Betrachtung eine scheinbar homogene 3D-Größenzunahme zu beobachten war, konnten die quantitativen Gefäßparameter die Hypothese des isotropen Wachstums des Leberparenchyms und der Gefäßstrukturen nicht bestätigen.

Viertens wurden die Techniken der Silikoninjektion und µCT-Bildgebung angewendet um die parenchymatöse und vaskuläre Regeneration nach Modulation des CXCR4-Signalwegs zu quantifizieren. Die Leberregeneration konnte durch die Gabe von AMD3100, einem CXCR4-Antagonisten, nicht beeinflusst werden. Jedoch wurden die parenchymale Leberregeneration und das Gefäßwachstum durch die Gabe von TC14012, das sowohl als CXCR4-Antagonist als auch als CXCR7-Agonist agiert, beeinträchtigt.

Zusammenfassung: Im Rahmen dieser Arbeit zwei technisch schwierige chirurgische Methoden etabliert: zum einen die Monitoringtechnik zur Beurteilung hämodynamischer Auswirkungen der partiellen Hepatektomie und zum anderen der Arbeitsablauf zur Visualisierung und Quantifizierung der Gefäßbäume mittels µCT. Es wurden quantitative Parameter zur Beschreibung des Gefäßwachstums identifiziert und mit deren Hilfe der Zusammenhang zwischen parenchymatöser und vaskulärer Regeneration untersucht. Zum Schluss wurden die beschriebenen Gefäßparameter genutzt, um das verzögerte und geminderte Gefäßwachstum nach

Modulation der CXCR4-CXCR7-SDF-1-Achse im Mausmodell nach 70%iger partieller Hepatektomie zu quantifizieren.
Schlußfolgerung Insgesamt stellt diese Untersuchung eine Verbesserung der technischen Möglichkeiten zur Untersuchung der vaskulären Leberregeneration nach Leberresektion dar.

1 Summary

Liver regeneration consists of parenchymal regeneration and also vascular growth. Due to technical limitation in quantifying vascular regeneration, more efforts were spent on studying parenchymal liver regeneration rather than vascular regeneration. However, vascular liver regeneration is as important as parenchymal liver regeneration. Thus, this study aims for improving techniques for quantifying hepatic vascular regeneration in mice. We defined four goals: to adapt an intraoperative monitoring procedure for determining hepatic hemodynamics to be used for mice, to develop a workflow consisting of injecting a contrasting compound, micro-CT imaging of the explanted liver visualization of the vascular tree, to establish a computational technique for assessing vascular regeneration based on vascular geometry, and to investigate the effect of modulating the CXCR4-CXCR7-SDF-1 axis on hepatic vascular and parenchymal regeneration.

First, we established a delicate monitoring procedure suitable for mice in order to measure hepatic hemodynamic parameters. Blood flow of portal vein and hepatic artery and portal venous pressure (PVP) were measured in normal mice as well as during the procedure of 70% PH and in liver lobe clamping experiments. The results indicated that this monitoring procedure was sensitive and suitable for detecting small changes in portal pressure and portal flow rate.

Second, we wanted to assess hepatic vascular growth during regeneration after 70%PH. Contrasting silicone compound injection prior to micro-CT scanning was used for visualization of hepatic vasculature. We adapted the silicone injection method for visualizing both hepatic vascular systems in mice. The biggest challenge for modifying this procedure was the determination of the adequate perfusion rate for the silicone compound. Based on the hepatic hemodynamic parameters acquired by the monitoring technique, we defined the perfusion rate for the silicone compound, 0.2 ml/min. Maximal vessel length and radius of right inferior portal vein and hepatic vein were measured after digitalizing and visualizing the hepatic vascular trees based on µCT data in Imalytics Preclinical software.

Third, based on this imaging workflow we developed a method to quantify hepatic parenchymal regeneration and vascular growth after 70%PH to investigate the underlying growth pattern. µCT data were converted into 3D vascular and territory reconstructions using HepaVision software. Total hepatic volume indicative of parenchymal regeneration was determined. Total hepatic volume and liver weight

were highly correlated, indicating that the increase of hepatic volume could be utilized as basis for the subsequent quantitative analysis of hepatic parenchymal regeneration. Then, cumulative vascular regenerative parameters, total edge length and total vascular volume, were computed based on vascular geometry. At last, parameters describing the vascular density, total edge length/ hepatic volume and the vascular volume fraction, were determined. We created a virtual resection model in HepaVision in order to eliminate the effect of portal hypertension induced by the extended hepatectomy. We compared parameters obtained after virtual resection and on POD 7 for exploring the growth pattern of liver regeneration after 70%PH. Despite the seemingly homogeneous 3D-growth, the observed vascular parameters were not compatible with the hypothesis of isotropic expansion of liver parenchyma and vascular structures.

Forth, we applied the newly established work flow consisting of contrasting the specimen, image acquisition and data analysis to quantify the vascular regeneration after modulating the CXCR4 signaling pathway. Liver regeneration was not affected by administrating AMD3100, a CXCR4 antagonist. However, liver parenchymal regeneration (recovery of liver body weight ratio) and vascular growth (circumscribed vascular parameters) was impaired by applying TC14012, acting as both CXCR4 antagonist and CXCR7 agonist, pointing to the relevance of this pathway for liver regeneration.

In conclusion, we explored vascular liver regeneration in a meso- and macroscopic scale. We started by adapting two delicate surgical tools, hepatic hemodynamic monitoring technique and intravascular silicone injection technique, for accessing the immediate effects of partial hepatectomy and for studying the vascular growth during the first week post-PH. Next, we reported hepatic hemodynamic parameters and vascular regenerative parameters which can be utilized as the basis for exploring vascular growth in normal and partially hepatectomized mice. Furthermore, we investigated the growth pattern of hepatic vascular trees for better understanding the relationship between parenchymal liver regeneration and vascular liver regeneration. Last but not least, using the circumscribed vascular parameters we quantified the delayed and reduced vascular growth after modulating the CXCR4-CXCR7-SDF-1 axis in 70%PH mouse model.

Altogether, this study provides technical tools to further and deeper explore and understand hepatic vascular regeneration after liver resection.

2 Introduction

2.1 Hepatic vascular regeneration

The liver has the remarkable capacity to fully regenerate after major loss of parenchyma. Liver regeneration requires reconstitution of liver parenchyma and vascular structures. Once liver injury or loss of hepatic tissue occurs, not only hepatocytes but also non-parenchymal cells, i.e LSECs, biliary epithelial cells as well as stellate cells, are involved in programmed liver regeneration (DeLeve 2013). Replication of hepatic parenchymal and non-parenchymal cells leads to the increase of liver mass and growth of blood vessels.

Vascular liver regeneration mainly includes the proliferation of LSECs and the liberation of angiogenic factors (growth factors, cytokines and chemokines). About 2 decades ago, Jacquelyn Maher first hypothesized that LSECs contribute to liver regeneration (Schwier et al. 2013). Now, evidence is accumulating that angiogenesis, the formation of new microvasculature from preexisting blood vessels, is essential for liver regeneration to proceed to completion. Although LSECs are known to contribute to the angiogenesis that accompanies parenchymal regeneration, emerging data now suggest a more complex and multifaceted role for LSECs in liver regeneration through their effects on other hepatic cells (Ding et al. 2014, Ding et al. 2010).

Therefore, studying regeneration of hepatic vasculature can facilitate the understanding of the pivotal role of vascular growth in liver regeneration. Assessing vascular parameters quantitatively can contribute to elucidate the underlying mechanism of vascular growth and serve as a basis to develop novel therapeutic strategies.

Due to the lack of adequate methods, nowadays, most studies are mainly focused on parenchymal liver regeneration rather than vascular liver regeneration. However, hepatic vascular growth and remodeling seems to be crucial in the progression of hepatic regeneration. Thus, it is urgently needed to establish methods for visualizing and quantifying vascular growth.

2.2 Hepatic hemodynamic parameters

The hemodynamic consequence of partial hepatectomy is the trigger for the activity of hepatocytes and LSECs, and further directs liver regeneration in an explosive rate. The relationship of altered hepatic hemodynamics and the regulation of hepatocyte proliferation after liver resection have been studied extensively. A dramatic hemodynamic stimulus occurs at the time of surgical removal of liver lobes. Despite

the fact that LSECs enter into DNA synthesis between 72 and 96 h after PH, the increase in the fenestration diameter and porosity indicative of the changes in the sinusoidal structure are observed within 5 min after the operation (Kandilis et al. 2010). The changes in portal blood flow serve as the initial trigger for the activation of a complex cascade of events leading to cellular proliferation.

The technical procedure of measuring hepatic hemodynamic parameters for rats was reported before by our group (Huang et al. 2010). However, due to the small size, adaptation of this procedure to the mouse represented a technical challenge. Technical details of the challenging intraoperative monitoring procedure suitable for the mouse were rarely described. Thus, it was urgently needed to establish and disseminate a method for acquiring the hepatic hemodynamic parameters, including portal blood flow and portal vein pressure. So, as a first step, we aimed at establishing a delicate procedure for monitoring the changes of hepatic hemodynamics in normal mice and in mice subjected to 70%PH.

2.3 Visualization of vascular regeneration

In parallel to the development of imaging techniques, several approaches for visualizing vascular growth on the lobule or organ scale in different organ vascular systems became available (Upputuri et al. 2015). The two main methods for contrasting the vascular tree prior to ex-vivo imaging are the vascular corrosion casting and silicone contrast compound injection technique. Both techniques allow subsequent μCT scanning to visualize hepatic vasculature and principally also the quantification of vascular and parenchymal parameters with the help of computational techniques. However, visualization of hepatic vasculature based on corrosion cast needs the digestion of liver parenchyma. In contrast, silicone injected specimen enables the subsequent histological work up including serial sectioning and histological analysis. Injection of the contrast compound allows imaging of the whole organ, the prerequisite for visualization and 3D reconstruction of hepatic parenchyma as well as vasculature. In contrast, corrosion casting only allows visualization of the injected vascular trees.

Silicone contrast compound injection together with micro-CT (μCT) imaging technique can serve to characterize and describe the changes of vascular parameters under different circumstances associated with vascular regeneration. Silicone compound can be used to fill and opacify microvessels as well as large vessels prior to explanting the organ for ex-vivo imaging. Following injection, microfil

compound has to cure to form a three-dimensional cast of the vasculature. The 3D vascular trees can be visualized and subsequent vascular regenerative parameters can be quantified. This technique has been successfully used for assessing the vasculature in multiple organs(Ghanavati et al. 2014, Ehling et al. 2014b, Jing et al. 2012) and in tumors (Downey et al. 2012, Ehling et al. 2014a).

Typically, silicone compound is perfused systematically via the left ventricle instead of direct injection into the vascular system of interest. However, given the fact that the hepatic vascular system consists of two vascular trees, it is difficult to ensure equal homogenous perfusion of both trees after systemic perfusion with a highly viscous solution. Thus, we wanted to modify the silicone injection procedure making it suitable for visualizing portal vein and hepatic vein separately.

2.4 Quantification of vascular regeneration

Micro-CT data acquired from contrasted specimen can facilitate not only visualizing but also quantifying the vascular growth. Quantifying vascular growth requires quantifying changes in parameters appropriate for describing the geometry of vascular systems. Such parameters include vessel diameter/ thickness (Ehling et al. 2014b, Ehling et al. 2014a), vessel length (Mittal et al. 2005, Wan et al. 2002), vessel volume (Langheinrich und Ritman 2006, Downey et al. 2012), vessel density (Bolland et al. 2008, Gayetskyy et al. 2014), branching angles (Parker et al. 1997), vessel number (Ghanavati et al. 2014, Downey et al. 2012), and vessel cross-section area (Huang et al. 1996). Parameters can be determined for individual vessel segments or as cumulative quantities. However, there is no widely accepted standard yet to describe vascular geometries. Thus, we wanted to quantify hepatic vascular regenerative parameters during the liver regeneration process. We also wanted to study the relationship between parenchymal regeneration and vascular regeneration by quantifying vascular density. Doing so, we wanted to explore the underlying growth pattern by comparing the observed to the expected growth pattern with isotropic expansion.

2.5 The role of CXCR4-CXCR7-SDF-1α pathway in liver regeneration

Once established, we wanted to demonstrate the added value of assessing hepatic vascular growth in a pilot study exploring the role of CXCR4-CXCR7-SDF-1α pathway.

Stromal-derived factor-1 alpha (SDF-1α, also known as CXCL12) binds to G-protein-coupled CXCR4 and CXCR7. This chemokine plays an important and unique role in vasculogenesis and angiogenesis (Liekens et al. 2010) as well as in the regulation of stem/progenitor cell trafficking (Rosenkilde et al. 2004).

Within the liver, SDF-1α/CXCL12 is mainly produced by cholangiocytes and hepatic progenitor cells (Tsuchiya et al. 2012), biliary epithelial cells, hepatic stellate cells and LSECs (Hu et al. 2014). CXCL12 is upregulated in response to injury to initiate regeneration by switching on its receptors CXCR4 and CXCR7. It was reported that the expression levels of CXCR4 and CXCL12 increased after liver injury (Wilson et al. 2015, Jiang et al. 2012). Thus, we hypothesized that CXCR4- SDF-1α pathway is involved in liver regeneration. We wanted to explore the role of this axis in liver regeneration especially for hepatic vascular regeneration in the mouse 70%PH-model. As a first step in this pilot experiment, we selected CXCR4 antagonist, AMD3100, which can block CXCR4 and subsequently interfere with cell proliferation as indicated in Figure 1 from (Faber et al. 2007) below. We hypothesized that, liver regeneration will be impaired by administration of AMD3100.

Figure 1 in (Faber et al. 2007)

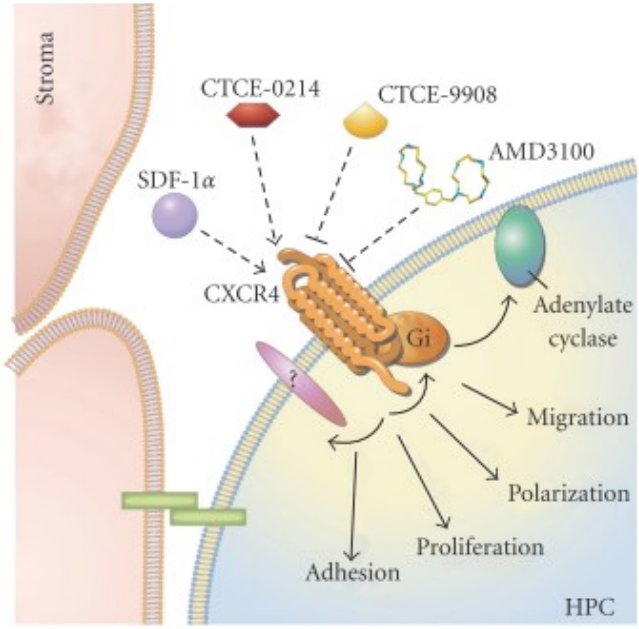

FIGURE 1: SDF-1α/CXCR4 axis and interaction with small molecules. The chemokine stromal cell-derived factor-1 alpha (SDF-1α or CXCL12) is secreted by stromal cells with various effects on hematopoietic progenitor cells (HPCs). It binds to the CXCR4 receptor and this interaction can be influenced by the peptide agonist CTCE-0214 as well as by the peptide antagonists CTCE-9908 or the nonpeptide antagonist AMD3100.

Figure 1 in (Duda et al. 2011)

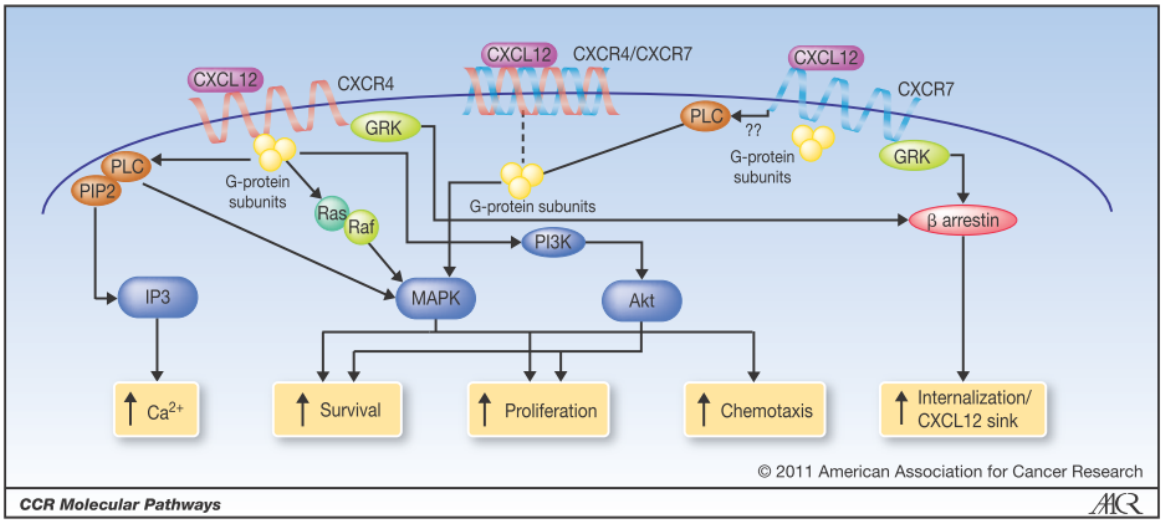

Figure 1. CXCL12 pathway. CXCL12 binds to CXCR4 and CXCR7, which are GPCRs that can form homodimers or heterodimers. In the latter case, CXCR7 changes the conformation of the CXCR4/G-protein complexes and abrogates signaling. Activation of CXCR4 by CXCL12 leads to G-protein–coupled signaling through PI3K/Akt, IP3, and MAPK pathways, which promote cell survival, proliferation, and chemotaxis. In addition, the β-arrestin pathway can be activated through GRK to internalize CXCR4. When CXCR7 binds CXCL12, the classical GPCR mobilization of Ca^{2+} does not occur, and activation of the β-arrestin pathway may lead to scavenging of CXCL12. In certain cancer cells (e.g., gliomas), CXCR7 can also signal through PLC/MAPK to increase cell survival.

However, as indicated in the Figure 1 from Duda (Duda et al. 2011), SDF-1α has interactions not only with CXCR4 but also with CXCR7. Thus, next, we selected the CXCR4 antagonist and CXCR7 agonist, TC14012, for blockade of CXCR4 and activation of CXCR7. In this way, TC14012 may activate the β-arrestin pathway via activation of GRK, leading to internalization of CXCR4 and scavenging of CXCL12. Inhibiting the role of CXCL12 might impair tissue regeneration after injury. Thus, we hypothesized that liver regeneration will be impaired by giving TC14012.

The results obtained from this pilot experiment can serve as the basis for a thorough investigation of this pathway in the future.

2.6 Experimental design and aims

2.6.1 Establish a method to determine hepatic hemodynamics in mice

A reliable technique to monitor hepatic hemodynamics in mice is needed. Establishment of the monitoring procedure was achieved in three steps (see Table 1) using normal mice (step 1) and mice subjected to selective clamping (Step 2) and to liver resection (Step 3).

Table 1. Group distribution for monitoring hepatic hemodynamics in mice

	Objective of each step in monitoring study	**Animal numbers**
Step 1	Establish monitoring procedure and acquire normal values of hepatic parameters	N=10
Step 2	Measure hepatic hemodynamic parameters in clamping/ declamping liver lobe experiment for detecting small changes using monitoring technique	N=5
Step 3	Measure hepatic hemodynamic parameters before and immediately after 70%PH	N=25

2.6.2 Establish a method to visualize vascular regeneration

Vascular liver regeneration is as important as parenchymal liver regeneration. However, the kinetics of vascular growth during the process of liver regeneration is not well described yet.

Thus, the goal of this step was to observe the time course of hepatic vascular regeneration in 70%PH mouse model (Table 2). In order to achieve this goal, a method suitable for visualizing hepatic vasculature is needed. Contrasting the vascular trees using silicone injection was chosen for this purpose. This technique also has the potential benefit resulting from a detailed analysis of the specimen using µCT and the subsequent detailed histological workup of the same specimen using serial sections for analyzing vascular liver regeneration. This silicone injection technique was demonstrated in detail in Manuscript II.

Table 2. Group distribution for visualizing hepatic vascular regeneration in mice

Group	**Animal numbers**		**Success rate**
	Unsuccessful cases	**successful cases**	
Portal venous system	N=10	N=12	55%
Hepatic venous system	N=3	N=24	89%

2.6.3 Establish a method to quantify vascular regeneration

After achieving the visualization of vascular growth, we further wanted to study hepatic vascular regeneration in a qualitative and quantitative way. Traditionally, quantification of liver regeneration usually includes determination of cell proliferation rates and liver weight recovery, but not the assessment of vascular growth.

This study aimed at (1) quantitatively describing parenchymal and vascular regeneration, and (2) determining their relationship. Both together are needed to (3) characterize the underlying growth pattern. The changes of these regenerative parameters (as listed in the Table 3) after 7 days' regeneration were described and elucidated in Manuscript III.

Table 3. Parameters computed to describe hepatic regeneration and vascular growth

Parameters	Unit	Explanation	Software
Total hepatic volume	ml	Volume of total liver or RIL	HepaVision
In/Outflow vascular radius	mm	Radius of entry point to RIL	Imalytics
Maximal vessel length	mm	Intravascular distance from root to most distant tip	Imalytics
Total edge length	mm	Sum of lengths of all edges in vascular tree	ATA
Total vascular volume	ml	Sum of volumes of all edges in vascular tree	ATA
Total edge length/ hepatic volume	mm/ml	Vascular length per liver volume	(derived parameter)
Vascular volume fraction	ml/ml	Vascular volume per liver volume	(derived parameter)

(ATA is the automatic tree analysis using the tools from (Schwen und Preusser 2012).

2.6.4 Explore the role of CXCR4-CXCR7-SDF-1α pathway in liver regeneration

In this first preliminary experiment we wanted to assess the value of quantifying hepatic vascular growth. We aimed at interfering with liver regeneration especially with hepatic vascular regeneration after 70%PH in mice by modulating CXCR4-CXCR7-SDF-1 pathway using AMD3100 and TC14012, CXCR4 antagonist and CXCR4 antagonist+CXCR7 agonist respectively (Table 4).

We determined body weight recovery and liver enzymes as indicator for the overall surgical stress and damage to the liver, liver weight recovery and total BrdU proliferation index to assess parenchymal regeneration and the selective parameter maximal vessel length and inflow vascular radius of right inferior portal vein to quantify vascular growth.

Table 4. Interfering with liver regeneration by modulating CXCR4-CXCR7-SDF-1 axis

Post-operative day(POD) / Group	**Naïve**	**Sham op**	**AMD3100 exp.**		**TC14012 exp.**	
			70%PH +PBS	**70%PH +AMD3100**	**70%PH**	**70%PH+ TC14012**
0	N=6					
POD2		N=6	N=6	N=6	N=6	N=4
POD3		N=6	N=6	N=6	N=6	N=4
POD7		N=6	N=6	N=6	N=6	N=4

Table 5. Silicone injection after modulating CXCR4-CXCR7-SDF-1 axis by TC14012 in 70%PH mouse model

Post-operative day (POD)	**70%PH**	**70%PH+TC14012**
POD 2	N=3	N=3
POD 7	N=3	N=3

3 MANUSCRIPT

3.1 Manuscript I

Monitoring of Systemic and Hepatic Hemodynamic Parameters in mice

Chichi Xie, Weiwei Wei, Tao Zhang, Olaf Dirsch, Uta Dahmen

J. Vis. Exp. e51955, doi:10.3791/51955 (2014).

The video component of this article can be found at
http://www.jove.com/video/51955/

Authorship

First author

Authors' contributions

Chichi Xie: Established microsurgicall procedure, cutting and editing the film, analyzing the results and writing of the manuscript.
Weiwei Wei: Assisting in microsurgical procedure development
Tao Zhang: Involved in establishing the microsurgical procedure
Olaf Dirsch: Guidance and supervision of the project
Uta Dahmen: Supervising the project

Summary

In this study, we demonstrated a real-time monitoring procedure, for acquiring systemic and hepatic hemodynamic parameters suitable for mice. This monitoring procedure is useful in experimental research in mice that require obtaining systemic and hepatic hemodynamic parameters related with vascular liver regeneration. We applied this procedure to monitor the changes of hepatic hemodynamic parameters, including portal blood flow and portal venous pressure, before and immediately after 70% partial hepatectomy and during clamping and declamping experiment in mice. In conclusion, this monitoring procedure is sensitive to detect small changes of vascular perfusion.

jove Journal of Visualized Experiments www.jove.com

Video Article

Monitoring of Systemic and Hepatic Hemodynamic Parameters in Mice

Chichi Xie[1,3], Weiwei Wei[1], Tao Zhang[1], Olaf Dirsch[2], Uta Dahmen[1]

[1]Department of General, Visceral and Vascular Surgery, Jena University Hospital

[2]Institute of Pathology, Jena University Hospital

[3]Reproductive Medicine Center, The First Affiliated Hospital of Wenzhou Medical University

Correspondence to: Uta Dahmen at uta.dahmen@med.uni-jena.de

URL: http://www.jove.com/video/51955
DOI: doi:10.3791/51955

Keywords: mice, hemodynamics, hepatic perfusion, CAP, CVP, surgery, intraoperative monitoring, portal vein pressure, blood flow

Date Published: 5/27/2014

Citation: Xie, C., Wei, W., Zhang, T., Dirsch, O., Dahmen, U. Monitoring of Systemic and Hepatic Hemodynamic Parameters in Mice. *J. Vis. Exp.* (), e51955, doi:10.3791/51955 (2014).

Abstract

The use of mouse models in experimental research is of enormous importance for the study of hepatic physiology and pathophysiological disturbances. However, due to the small size of the mouse, technical details of the intraoperative monitoring procedure suitable for the mouse were rarely described. Previously we have reported a monitoring procedure to obtain hemodynamic parameters for rats. Now, we adapted the procedure to acquire systemic and hepatic hemodynamic parameters in mice, a species ten-fold smaller than rats. This film demonstrates the instrumentation of the animals as well as the data acquisition process needed to assess systemic and hepatic hemodynamics in mice. Vital parameters, including body temperature, respiratory rate and heart rate were recorded throughout the whole procedure. Systemic hemodynamic parameters consist of carotid artery pressure (CAP) and central venous pressure (CVP). Hepatic perfusion parameters include portal vein pressure (PVP), portal flow rate as well as the flow rate of the common hepatic artery (table 1). Instrumentation and data acquisition to record the normal values was completed within 1.5 h. Systemic and hepatic hemodynamic parameters remained within normal ranges during this procedure.

This procedure is challenging but feasible. We have already applied this procedure to assess hepatic hemodynamics in normal mice as well as during 70% partial hepatectomy and in liver lobe clamping experiments. Mean PVP after resection (n= 20), was 11.41±2.94 cmH_2O which was significantly higher ($P<0.05$) than before resection (6.87±2.39 cmH_2O). The results of liver lobe clamping experiment indicated that this monitoring procedure is sensitive and suitable for detecting small changes in portal pressure and portal flow rate. In conclusion, this procedure is reliable in the hands of an experienced micro-surgeon but should be limited to experiments where mice are absolutely needed.

Video Link

The video component of this article can be found at http://www.jove.com/video/51955/

Introduction

The overall goal of this video was to demonstrate a real-time monitoring procedure for acquiring systemic and hepatic hemodynamic parameters. The rationale for developing this procedure is its great value for experimental interventions in mice that require obtaining systemic and hepatic hemodynamic parameters. The procedure can be applied to naïve animals and during or after a given hepato-biliary experimental surgical intervention, such as partial hepatectomy, portal vein ligation and liver transplantation.

Acquisition of hepatic hemodynamic data in rodents requires the proposed invasive procedure. Hepatic perfusion cannot be obtained non-invasively. However, there are alternatives for the acquisition of the systemic blood pressure. Monitoring techniques such as the tail cuff technique[8] have been utilized for acquiring the blood pressure in both rats and mice. The tail cuff technique can be applied in conscious animals. When measuring the blood pressure, the animal needs to be placed and fixed in a specific uncomfortable position. In the manual of the tail-cuff device, the manufacturer states that mice may become nervous and stressed which may diminish the circulation in the tail. Under that circumstance, the peripheral blood pressure acquired in the tail may be much lower than the central blood pressure.

The full monitoring procedure was performed with an integrated multiple-channel monitor using a series of sensors for data acquisition. The blood pressure was obtained by inserting a catheter into the respective vessel after careful microsurgical dissection and exposure under the microscope. The flow rate was measured by placing a transonic flow probe around each vessel.

We already reported a similar intraoperative monitoring procedure for rats resulting in a comprehensive series of physiological hemodynamic data comparable to single data reported from other groups[7]. Therefore we considered this procedure to represent a good basis for adapting it to the mouse, a species 10-fold smaller than the rat. The key difference to the rat procedure is the use of Millar catheters for acquiring blood pressure data instead of a fluid-based catheter system. Flow data were also acquired with transonic flow probes, just much smaller ones than for the corresponding rat vessels.

Due to the small size of the animal, instrumentation of mice is technically challenging, but feasible. Once instrumentation is completed, data acquisition and primary life data analysis is simple, since a predefined setting file can be used. The setting file has to be defined once at the beginning of a series of experiments and can be stored and used for all subsequent experiments.

Up to now we applied this procedure to assess hepatic hemodynamic effects in acute experiments. We measured CAP and PVP before and immediately after 70% partial hepatectomy (PH) and in clamping/de-clamping experiments. We clamped the hepato-duodenal ligament of the right lobe representing 20% of the liver mass followed by brief (5min) clamping of the median and left lateral lobe representing totally 90% of the liver mass. De-clamping started with releasing the clamp from the right lobe followed by freeing the median and left lateral lobe. Maximal clamping time was below 10min.

Protocol

Housing and all procedures carried out were in accordance with German Animal Welfare Legislation.

1. Sensors calibration. (Follow manufactures instructions for sensors calibration).

1.1) Millar catheter calibration. Pre-soak the tip of the catheter in sterile water or saline for 30 minutes prior to balance (zeroing) and calibration.

1. Connect the millar sensor to the millar1 channel of bridge amplifier and insert the millar sensor tip into water column.
2. Set the water column value to 0 cmH_2O. In data analysis software window, choose bridge amplify and zero it. The baseline value 0 cmH_2O can be set.
3. Set the water column value to 20 cmH_2O. Run data analysis software window progress, and stop. Choose "units" in the window of bridge amplify, set the baseline of 0 and 20 cmH_2O accordingly. Adjust the "unit" to cmH_2O.
4. Calibrate the millar2 for measuring CAP in the same way (set two base line 90 and 110 cmH_2O).

1.2) Blood flow probe calibration

1. Put the probe into deionised water. Connect the probe with transonic flow probe system.
2. In data analysis software window, choose Input amplify to zero the flow probe. Adjust the units.
3. Press the button to "test channel" to collect the signal: if the signal has 3-4 bars, it means the signal is good. In case a good signal is acquired, the procedure can be continued.
4. Press the button to "zero channel" and scale channel to see whether the value has been calibrated or not.
5. Press the button to "measure channel" for later measuring.

2. Prepare the mouse for the surgical procedure

1. Place the mouse in an induction chamber and anesthetize the mouse with 2% isoflurane and 0.3ml/min oxygen. The operation can be performed if the toe-pinch withdrawal reflex of the mouse is absent.
2. Shave the fur of surgical regions, which include the left neck and abdomen.
3. Place the mouse on the operation table and fix it using tapes. Use vet ointment on eyes to prevent dryness during the operation period.
4. Place a gauze cushion under the neck for optimal exposure of the operation field of neck.
5. Disinfect the operation field and place sterilized gauzes to cover the mouse only leaving the surgical field open.

3. Vital parameters measurement

1. Insert the ECG needles subcutaneously into the paws of mouse.
2. Place the respiratory sensor under the back of the mouse.
3. Place the temperature probe into the rectum of the mouse.
4. Record temperature, ECG and respiratory rate of the mouse in data analysis software.

4. Neck operation for systemic cardiovascular monitoring

4.1) Vessel dissection

1. Identify the middle line of the neck, middle point of clavicle, the angle of mandible.
2. Make a 2cm longitudinal incision from the angle of mandible to the middle point of clavicle which is 0.5cm to the left side of the middle line.
3. Dissect the submandibular gland, turn it over and cover it with saline soaked gauze.
4. Identify the jugular vein, dissect it and place three 6-0 silk sutures under the vein for later ligation and fixation.
5. Identify the sternocleidomastoid muscle, separate it from the superior belly of omohyoid and posterior belly of digastric muscle, and pull it with a retractor for easy exposure of the carotid artery.
6. Dissect the carotid artery and place three 6-0 silk sutures under the artery for later ligation and fixation.

4.2) Carotid artery blood flow measurement

1. Place the transonic probe around the carotid artery, keep it stable, and optimize the contact using ultrasound gel or saline.
2. Record blood flow velocity of the carotid artery as indicated on the small screen of the transonic device using data analysis software

3. Remove the probe after completing the measurement

4.3) Carotid artery pressure measurement (CAP)

1. Ligate the distal end of the carotid artery and clamp its proximal end.
2. Place 2 fixing sutures around the carotid artery. Use 10-0 prolene for the stay suture.
3. Make a small incision on the anterior wall of the vessel.
4. Insert the millar catheter and fix it with pre-placed sutures.
5. Record the CAP in data analysis software.

4.4) Jugular vein blood flow measurement

1. Lift the jugular vein and place the transonic flow probe to measure the flow rate.
2. Record the flow rate in data analysis software.

4.5) Central venous pressure measurement (CVP)

1. Clamp the proximal end of the jugular vein and ligate the distal end.
2. Cut a small incision using microscissors on the anterior wall of the vessel.
3. Insert the fluid-filled catheter and fix it with the pre-placed suture lines.
4. Record the CVP in data analysis software.

5. Abdominal operation for acquisition of hepatic hemodynamics

5.1) Vessel identification

1. Make a transverse incision on the abdomen.
2. Eventerate the intestines to the left side and cover with wet gauze.
3. Identify the inferior vena cava, the portal vein, the common hepatic artery and the proper hepatic artery.
4. Drop some warm saline in the abdomen and on the surface of the intestines every five minutes during the whole monitoring procedure.

5.2) Measurement of portal blood flow

1. Dissect the portal vein.
2. Place 6-0 silk under the portal vein to facilitate lifting of the vessel when placing the flow probe.
3. Place the transonic flow probe around the portal vein and measure its blood flow rate.
4. Record the blood flow rate of the portal vein.

5.3) Measurement of Common hepatic artery flow

1. Dissect the common hepatic artery cautiously.
2. Place one 6-0 silk suture around the vessel to facilitate lifting of the vessel.
3. Place the flow probe around the artery.
4. Measure its blood flow and acquire the data.

5.4) Measurement of portal vein pressure (PVP)

1. Choose one branch of the mesenteric vein with few side branches, which drains straight into the portal vein.
2. Ligate the distal end of the selected mesenteric vein. Make sure that ligation is close to the intestinal tube. Ligate its small branches
3. Place 2 fixing sutures using 6-0 prolene around the vein. The key point of this procedure is to avoid touching the mesenteric artery when ligating the vein.
4. Clamp the proximal end of the portal vein.
5. Place 2 stay sutures using 10-0 prolene. Some bleeding will occur since the stay suture should penetrate the vascular wall of the fine mesenteric vein.
6. Make a small incision on the vein using a microscissor obliquely at a 45 degrees angle.
7. Insert the Millar catheter through the mesenteric vein into the portal vein and fix it
8. Record the portal vein pressure. At the end of the procedure, sacrifice the mice by exsanguination under anesthesia.

Representative Results

Vital parameters of the mice such as respiratory rate and heart rate are obviously much higher than in rat. Mean systemic blood pressure and jugular vein pressure are similar to rat values and even similar to the human data.

Hepatic hemodynamic data are obviously different. We obtained normal values from 8 mice. Portal blood flow in normal mice ranged between 1.6 to 2.3ml/min. Flow in the common hepatic artery ranged from 0.10 to 0.35 ml/min. Portal vein pressure in normal animals was in the wide range from 4.4 to 11.2 cmH_2O with a mean value of 8.09 ± 2.47 cmH_2O (Table 1). This wide range may lead to small but not significant differences when comparing the mean value of small groups of normal animals.

Since we observed considerable inter-individual differences especially in the portal pressure, we tested whether small intra-individual differences could be detected with this technique. We evaluated this procedure in two different experimental settings: partial hepatectomy and liver lobe clamping/de-clamping. Portal pressure before and immediately after 70% partial hepatectomy (n=20) in the same animal (Figure1) increased

by 2-fold from 6.87±2.39 and 11.41±2.94cmH_2O (P =<0.001). These results were in a similar range as observed in other species [5,12] and also in humans [7].

Normal portal vein pressure and portal pressure before resection were acquired from two different groups (one from normal monitoring parameters group, the other from 70%PH group). Due to the wide range of portal pressure in normal mice (4 to 11 cmH_2O), the mean values of small groups of animals may be slightly different, as observed in our experiment (8.09 ± 2.47 cmH_2O versus 6.87±2.39 cm H_2O). However, when analyzing the data, we found that there was no statistically significant difference between these two groups (P = 0.237).

The clamping/de-clamping experiment was designed to demonstrate that the procedure is sensitive enough to pick up even smaller changes in the portal pressure. Clamping of the right lobe representing 20% of the liver mass resulted in an increase of about 17%. Further clamping of the median and left lateral lobe caused an increase of at least 2-3 folds compared to the starting portal pressure. Portal pressure returned gradually to the starting pressure, when releasing the clamp from the right lobe resulting in clamping of 70% of the liver. The pressure returned to the starting level when removing the clamp from the left portal vein supplying the median and left lateral lobe (Figure2 and Table2). The MAP of the sham operation group remained stable within 1h after opening the abdomen. The MAP of mice in the control group, obtained at the comparable time point as in the clamping experiment, had no significant difference compared with the MAP of the experimental group. The results of both experiments revealed that even small intra-individual changes of less than 20% could be detected with this procedure.

Typical complications like severe bleeding and congestion may occur during the procedure. Since severe blood loss would cause significant decrease of MAP as well as PVP, the results of mice with this complication should be eliminated. To avoid venous congestion and thrombosis when performing liver lobe clamping experiment, we suggest injecting a small dose heparin (500U/kg) intra-operatively before clamping. Common hepatic artery can undergo a transient vessel spasm upon handling such as lifting the vessel and placing the probe. This might cause a transient brief ischemia of the liver. In general, the spasm may resolve spontaneously within minutes. A short vascular spasm in the CHA is not posing a serious problem to the life of the animal, but might interfere with experimental results, when focusing on hepatic ischemia reperfusion injury.

In conclusion, this procedure is challenging but feasible. It requires some training even for experienced micro-surgeons. Due to the high inter-individual variability comparison of pressure data obtained in different animals before and after an intervention may not lead to conclusive results. Therefore we recommend this procedure to study short term regulation of hepatic hemodynamics in acute experiments by acquiring the data before and after the intervention within the same animal.

Parameters		Own data obtained	Parameters reported
Vital parameters	Heart rate (n=8)	418±55 BPM	389(353-566) BPM [1]
	respiratory rate (n=2)	162±11 BPM	254 ± 28 BPM [2]
	Temperature (n=8)	33.56±0.54°C	36.1–36.6°C [11]
Systemic blood pressure (CAP) (n=8)		130.54 ± 20.47cmH_2O (=96.02 ± 15.06 mmHg)	94 ± 15 mmHg [9]
Central venous pressure (CVP) (n=2)		8.90 ± 3.25 cmH_2O	5.9 ± 2.0 cmH_2O [11]
Hepatic hemodynamics	Portal vein flow (n=6)	2.03 ± 0.24 ml/min	3.0 (2.5-3.1) ml/min [1]
			3.3 ml/min [1]
	Common hepatic artery flow (n=6)	0.20 ± 0.09 ml/min	Not found
	PVP (n=8)	8.09 ± 2.47 cmH_2O (=5.95 ± 1.82mmHg)	5.3±1.4 cm saline [3]
			8.7 ± 2.1 mmHg [4]
			4mmHg [6]

Table 1. Normal systemic and hepatic hemodynamic parameters of mice acquired using this monitoring procedure. CAP: carotid artery pressure; MAP: mean arterial pressure; CVP: central venous pressure; PVP: portal vein pressure.

jove Journal of Visualized Experiments www.jove.com

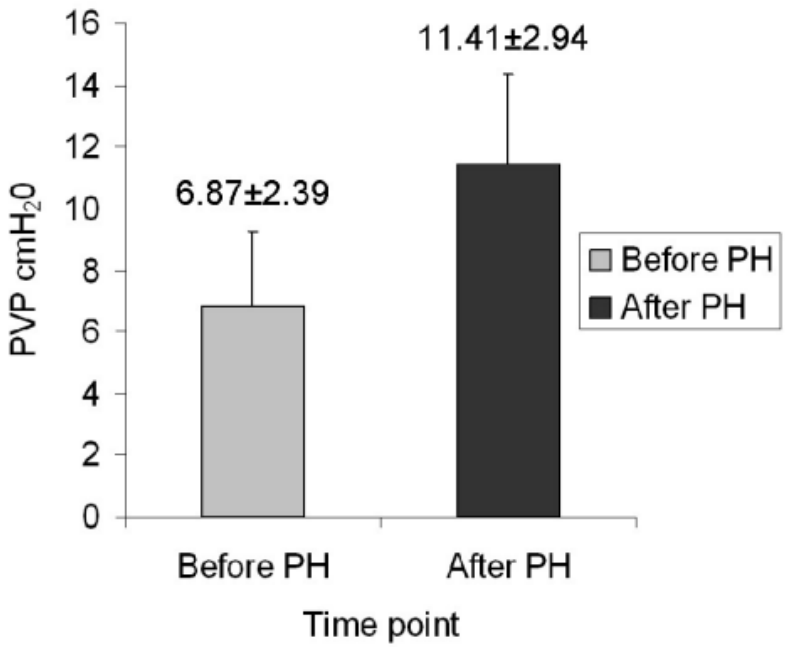

Figure 1. PVP before and after 70%PH. Portal vein pressure before and after 70%partial hepatectomy (n=20) were 6.87±2.39 and 11.41±2.94cmH_2O. Please click here to view a larger version of this figure.

Parameters (cmH2O)	After laparotomy	After clamping 20% of liver (RL)	After clamping 90% of liver (RL+ML+LLL)	After clamping 70% of liver (ML+LLL)	At the end (release all clamps)
PVP - Clamping exp group (n=10)	9.59±4.00	10.45±3.89	25.78±8.99	16.91±9.86	11.14±4.48
Mean CAP - Clamping exp group (n=10)	121.50±18.67	95.89±32.76	74.41±35.35	93.88±42.96	89.44±44.20
Mean CAP - Sham group (n=3)	123.33±12.42	121.0±5.57	124.00±8.66	127.33±7.23	123.00±8.89

Table 2. Hemodynamic response after clamping and declamping of different liver lobes (n=10). RL: right lobe, ML: median lobe (including right median lobe and left median lobe), LLL: left lateral lobe.

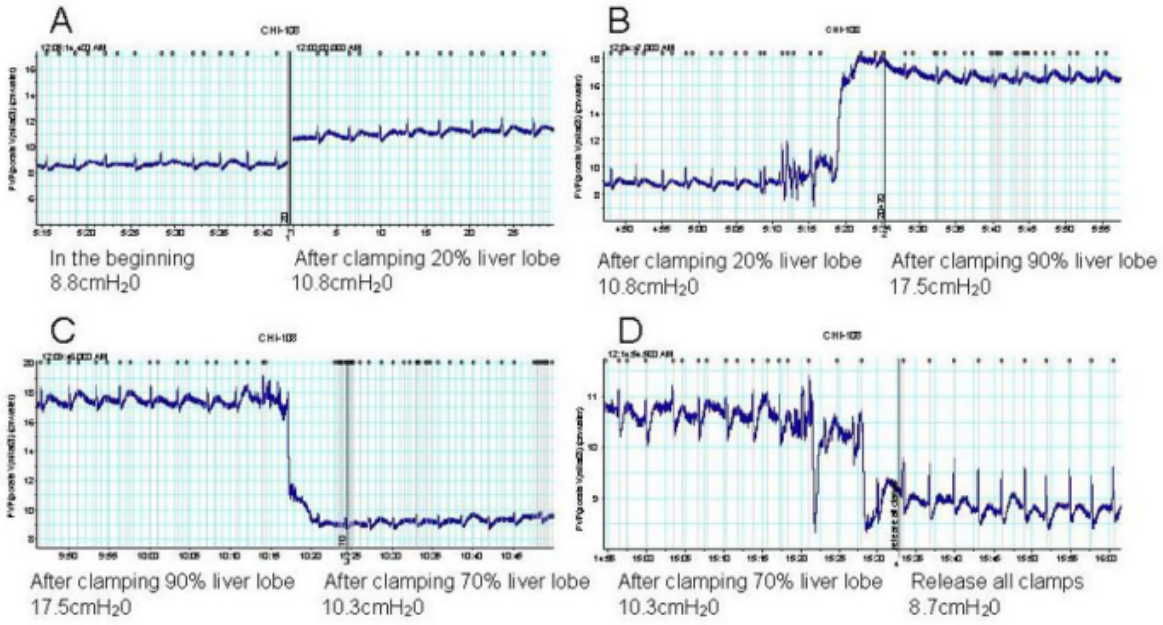

Figure 2. Hemodynamic response after clamping and declamping of different liver lobes (animal ID: CHI-108). A. PVP right after inserting the millar catheter was 8.8cmH_2O. PVP after clamping 20% liver lobe was 10.8cmH_2O. B.PVP rose to 17.5cmH_2O after clamping 90% liver lobe. C. PVP decreased to 10.3cmH_2O when releasing the clamp of the right lobe. D.PVP went back to 8.7cmH_2O as in the beginning after releasing all the clamps. Please click here to view a larger version of this figure.

Discussion

Monitoring of hepatic hemodynamics is an important research tool in hepatology and hepatobiliary surgery. Acquisition of hepatic hemodynamic data helps to characterize the effect of hepatobiliary procedures on the circulatory system. Acquisition of hepatic hemodynamic data is also needed to study the effect of drugs affecting portal pressure and portal flow, e.g. as needed in studies evaluating vasoactive drugs.

Despite the small size, the vital parameters, systemic and hepatic hemodynamics can be monitored in mice. The critical steps within the protocol were as follows: First, it is important to place the animal on a warming pad during the whole procedure to avoid hypothermia which may lead to circulatory dysfunction. Second, it is crucial to be very cautious when dissecting the vessels of a mouse, since the vessel wall of mouse is very fragile and thin. It seems best to fix the vessel wall by grabbing some fat tissue on the surface instead of grabbing the vessel wall itself. Third, it is vital to avoid accidental ligation of mesenteric artery for not impairing the arterial supply when placing the fixing sutures around the mesenteric vein.

However, the invasive mentoring echnique has some limitations. The **first** one is its invasiveness by itself. This monitoring technique is an invasive method, which requires a surgical intervention. Therefore the monitoring procedure itself may cause side effects for the animals. Hence, we only used this procedure to acquire hemodynamic parameters in normal animals and in acute experiments, but not in survival experiments. In a next step, we want to evaluate this technique in survival experiments. The **second** limitation of this procedure is that it requires substantial microsurgical experience. Hemodynamic monitoring in mice should only be performed by specifically trained microsurgeons. The most difficult part of this monitoring procedure is the insertion of the Millar catheter in the small mesenteric vein, since this vein is extremely fragile. In our hands, about 10 training operations were needed for an experienced microsurgeon prior to technically mastering this procedure. Experience was defined of having successfully performed more than 50 vascular anastomosis (carotid artery, jugular vein) in rats or mice. The **third** limitation is that the portal pressure obtained with this method may be below the physiological range for a normal animal. Mesenteric vein ligation and catheter insertion may reduce the total volume of blood draining into the portal vein by an estimated 10%. However, this physiological range cannot be acquired using the currently available devices. Similarly, the effect of anesthesia itself on PVP cannot be excluded[13]. However, since all animals are subjected to the same intervention, the potential error would be a systematic error. Therefore, data interpretation should be done with caution focusing on relative changes within an animal and not necessarily on absolute differences between animals.

However, there are little alternatives to the invasive hemodynamic monitoring in rodents. Non-invasive monitoring is limited to the acquisition of the systemic blood pressure. Portal pressure or portal flow cannot be determined non-invasively in mice. Telemetric monitoring is also limited to the acquisition of the systemic blood pressure. No reports were found regarding the telemetric acquisition of other hemodynamic parameters.

This full intraoperative monitoring procedure is needed to understand hepatic physiological processes such as regulation of liver perfusion, liver regeneration and hepatobiliary surgery comprehensively. The ability to monitor and collect data of laboratory animals intraoperatively in real-time thus represents a significant advance in the study of liver disease and portal hypertension.

Disclosures

The authors declare that they have no competing financial interests.

Acknowledgements

This research was supported by the German Federal Ministry for Education and Research (BMBF) funded "Virtual Liver Network". I'd like to thank Frank Schubert and Rene Gumpert from the media center of Jena University Hospital for their help in producing the video and creating the animation and Isabel Jank for recording the audio.

References

1. Albuszies, G. *et al.* Effect of increased cardiac output on hepatic and intestinal microcirculatory blood flow, oxygenation, and metabolism in hyperdynamic murine septic shock. *Crit Care Med.* **33** (10), 2332-2338, doi: 10.1097/01.CCM.0000182817.20977.E9, (2005).
2. Bernhard, W. *et al.* Phosphatidylcholine molecular species in lung surfactant: composition in relation to respiratory rate and lung development. *Am.J.Respir.Cell Mol.Biol.* **25** (6), 725-731, doi: 10.1165/ajrcmb.25.6.4616, (2001).
3. Cheever, A.W., & Warren, K.S. Portal vein ligation in mice: portal hypertension, collateral circulation, and blood flow. *J.Appl.Physiol.* **18** 405-407, (1963).
4. Costa, G., Aguiar, B.G., Coelho, P.M., & Cunha-Melo, J.R. On the increase of portal pressure during the acute and chronic phases of murine schistosomiasis mansoni and its reversibility after treatment with oxamniquine. *Acta Trop.* **89** (1), 13-16, doi:10.1016/S0001-706X(03)00202-X, (2003).
5. Cui, S., Shibamoto, T., Zhang, W., Takano, H., & Kurata, Y. Venous resistance increases during rat anaphylactic shock. *Shock.* **29** (6), 733-739, doi:10.1097/shk.0b013e31815c42f1, (2008).
6. Geerts, A.M. *et al.* Comparison of three research models of portal hypertension in mice: macroscopic, histological and portal pressure evaluation. *Int.J.Exp.Pathol.* **89** (4), 251-263, doi: 10.1111/j.1365-2613.2008.00597.x, (2008).
7. Huang, H., Deng, M., Jin, H., Dirsch, O., & Dahmen, U. Intraoperative vital and haemodynamic monitoring using an integrated multiple-channel monitor in rats. *Lab Anim.* **44** (3), 254-263, doi: 10.1258/la.2009.009055, (2010).
8. Krege, J.H., Hodgin, J.B., Hagaman, J.R., & Smithies, O. A noninvasive computerized tail-cuff system for measuring blood pressure in mice. *Hypertension.* **25** (5), 1111-5, doi: 10.1161/01.HYP.25.5.1111, (1995).
9. Kuga, N. *et al.* Rapid and local autoregulation of cerebrovascular blood flow: a deep-brain imaging study in the mouse. *J. Physiol.* **587** (Pt 4), 745-752, doi: 10.1113/jphysiol.2008.163253, (2009).
10. Muraki, T., & Kato, R. Strain difference in the effects of morphine on the rectal temperature and respiratory rate in male mice. *Psychopharmacology (Berl).* **89** (1), 60-64, (1986).
11. Nielsen, J.M. *et al.* Left ventricular volume measurement in mice by conductance catheter: evaluation and optimization of calibration. *Am.J.Physiol Heart Circ.Physiol.* **293** (1), H534-H540, doi: 10.1152/ajpheart.01268.2006, (2007).
12. Sakamoto, M. *et al.* Improvement of portal hypertension and hepatic blood flow in cirrhotic rats by oestrogen. *Eur.J.Clin.Invest.* **35** (3), 220-225, doi: 10.1111/j.1365-2362.2005.01476.x, (2005).
13. Reverter, E. et al. Impact of deep sedation on the accuracy of hepatic and portal venous pressure measurements in patients with cirrhosis. *Liver Int.* **34** (1), 16-25, doi: 10.1111/liv.12229, (2014).

3.2 Manuscript II

Visualization of vascular and parenchymal regeneration after 70% partial hepatectomy in normal mice

Chichi Xie, Weiwei Wei, Andrea Schenk, Lars Ole Schwen, Sara Zafarnia, Michael Schwier, Felix Gremse, Isabel Jank, Olaf Dirsch, Uta Dahmen

The Journal of Visualized Experiments - ***Accepted***

J. Vis. Exp. e53935, doi:10.3791/53935 (2016)

Authorship

First author

Authors' contributions

Chichi Xie: established microsurgical procedure, cutting and editing the film, analyzing the results and writing of the manuscript.
Weiwei Wei: assisting in microsurgical procedure development, revising manuscript
Andrea Schenk: providing 3D vascular and territories reconstructions and manuscript revising
Lars Ole Schwen: computing vessel parameters and manuscript revising
Sara Zafarnia: micro-CT scanning of microfil samples
Michael Schwier: providing 3D vascular reconstructions based on serial sections
Felix Gremse: providing Imalytics Preclinical software and manuscript revising
Isabel Jank: audio recording and manuscript revising
Olaf Dirsch: Guided and supervised the project
Uta Dahmen: Supervising the project and manuscript revising

Summary

In this study, we established and demonstrated the delicate silicone injection technique required to achieve optimal contrasting both vascular systems (portal vein and hepatic vein) and showed the potential benefit resulting from a detailed analysis of the resulting specimen using µCT and histological serial sections for subsequent analysing vascular liver regeneration. The vascular growth at each postoperative day was visualized and vascular regenerative parameters, such as maximal vessel length and radius, were obtained enabling for further analysis. In conclusion, this technique has the potential to be extensively applied to studies concerning vascular anatomy and growth in various animal and disease models.

Visualization of vascular and parenchymal regeneration after 70% partial hepatectomy in normal mice

***Chichi Xie*[1]**, *Weiwei Wei*[1], *Andrea Schenk*[2], *Lars Ole Schwen*[2], *Sara Zafarnia*[3], *Michael Schwier*[2], *Felix Gremse*[3], *Isabel Jank*[1], *Olaf Dirsch*[4], *Uta Dahmen*[1]

1 Department of General, Visceral and Vascular Surgery, Jena University Hospital Jena, Germany
2 Fraunhofer Institute for Medical Image Computing MEVIS, Bremen, Germany
3 Experimental Molecular Imaging, RWTH Aachen University, Aachen, Germany
4 Klinikum Chemnitz gGmbH, Institute of Pathology, Chemnitz, Germany

Corresponding author:
Prof. Dr. med. Uta Dahmen
1 Department of General, Visceral and Vascular Surgery
Jena University Hospital
Jena, Germany
Uta.Dahmen@med.uni-jena.de
telephone: +49 3641 9325351

Address:
Exp.Transplantationschirurgie,
Drackendorfer Str. 1,
07747, Jena, Germany

KEY WORDS:
mice; portal vein; hepatic vein; µCT; 3D vascular reconstruction; vascular liver regeneration; parenchymal liver regeneration; partial hepatectomy

SHORT ABSTRACT:

Tools used for visualizing vascular regeneration require methods for contrasting the vascular trees. This film demonstrated a delicate injection technique used to achieve optimal contrasting of the vascular trees and illustrate the potential benefits resulting from a detailed analysis of the resulting specimen using µCT and histological serial sections.

LONG ABSTRACT:

A modified silicone injection procedure was used for visualization of the hepatic vascular tree. This procedure consisted of *in-vivo* injection of the silicone compound, via a 26G catheter, into the portal or hepatic vein. After silicone injection, organs were explanted and prepared for *ex-vivo* micro-CT (µCT) scanning. The silicone injection procedure is technically challenging. Achieving a successful outcome requires extensive microsurgical experience from the surgeon. One of the challenges of this procedure involves determining the adequate perfusion rate for the silicone compound. The perfusion rate for the silicone compound needs to be defined based on the hemodynamic of the vascular system of interest. Inappropriate perfusion rate can lead to an incomplete perfusion, artificial dilation and rupturing of vascular trees.

The 3D reconstruction of the vascular system was based on CT scans and was achieved using preclinical software such as HepaVision. The quality of the reconstructed vascular tree was directly related to the quality of silicone perfusion. Subsequently computed vascular parameters indicative of vascular growth, such as total vascular volume, were calculated based on the vascular reconstructions. Contrasting the vascular tree with silicone allowed for subsequent histological work-up of the specimen after µCT scanning. The specimen can be subjected to serial sectioning, histological analysis and whole slide scanning, and thereafter to 3D reconstruction of the vascular trees based on histological images. This is the prerequisite for the detection of molecular events and their distribution with respect to the vascular tree. This modified silicone injection procedure can also be used to visualize and reconstruct the vascular systems of other organs. This technique has the potential to be extensively applied to studies concerning vascular anatomy and growth in various animal and disease models.

INTRODUCTION:

Liver regeneration is often determined by measuring the increase of liver weight and volume and by assessing the hepatocyte proliferation rate[16]. However, liver regeneration is not only inducing parenchymal regeneration but also vascular regeneration[6]. Therefore, vascular growth should be further investigated with respect to its role in the progression of liver regeneration. Visualization of the hepatic vascular system is critical to advancing our understanding of vascular regeneration. Numerous indirect methods have been developed to study the underlying molecular mechanisms of hepatic vascular regeneration. Traditionally, detection of cytokines (vascular endothelial growth factor, VEGF)[14], chemokines and their receptors (CXCR4/CXCR7/CXCL12)[4] have been the mainstay for studying vascular regeneration. However, a 3D model together with quantitative analysis of the vasculature would add critical anatomic information to gain a better understanding of the important relationship between hepatic parenchymal and vascular regeneration.

To visualize the hepatic vascular system, which requires contrasting the vascular trees, mice were injected with a radiopaque silicone rubber contrast agent directly into the portal or hepatic venous vascular tree. After polymerization of the silicone and explantation of the organ, the liver samples were subjected to µCT scanning using a CT scanner. The scans resulted in voxel image representations of the silicone-injection specimens[9].

For quality control, the vascular system was first visualized in 3D using preclinical software. Segmentation was performed by setting a threshold between the soft tissue intensity and the vessel intensity. The resulting vessel mask was visualized using surface rendering. The software also allowed for manual determination of two parameters of vascular growth: maximal vessel length and radius.

A preclinical software was then used for 3D reconstruction of vascular trees and subsequent calculation of the supplying or draining vascular territories[13]. In addition, this software automatically determined certain parameters of vascular growth, such as the total length of all visible vascular structures also known as the total edge length or total vessel volume.

The silicone perfusion procedure was performed in naive mice and in mice that underwent 70% partial hepatectomy (PH). Livers were collected at different

observation time points after resection for analyzing vascular and parenchymal liver regeneration using the aforementioned visualization and quantification technique.

The main goals of this film are to: (1) demonstrate the delicate injection-technique required to achieve optimal contrasting and (2) show the potential benefit resulting from a detailed analysis of the resulting specimen using µCT and histological serial sections. After watching this film, the reader should have a better understanding of how to inject silicone compound into a specific vascular system and of the usefulness and applicability of the technique.

PROTOCOL:

Procedures involving animal subjects have been approved by Thüringer Landesamt für Verbraucherschutz Abteilung Tiergesundheit und Tierschutz, Germany. Because the portal venous system was visualized separately from the hepatic venous system, separate animals were needed for the different vascular trees.

1. Reagents preparation.

1.1 Heparin-saline solution

1.1.1 Add 0.1 ml heparin into 10 ml saline (5 IU/ml).

1.2 Silicone compound mixture

1.2.1 Add 2 ml MV-120 in one 5 ml tube. Dilute MV-120 by adding 3 ml MV diluent resulting in a 40% solution.

2 Portal venous system silicone injection.

2.1 Laparotomy.

2.1.1 Place the mouse in the anesthesia induction chamber and anaesthetize it with 2% isoflurane and 0.3 ml/min oxygen.

2.1.2 Fix the anaesthetized mouse on the operating table using tape with continuous inhalation of 2% isoflurane and 0.3 ml/min oxygen. Check the toe-pinch withdrawal reflex of the mouse and start operation if the reflex is absent.

2.1.3 Make a transverse incision on the abdomen using scissors for the skin layer and an electric coagulator for the muscle layer. Move out the intestines to the left side using cotton tips and cover the intestines with saline soaked gauze.

2.2 Catheter insertion.

2.2.1 Dissect portal vein under the microscope using micro-forceps. Place one 6-0 silk suture underneath the extrahepatic portal vein, in approximately 1 mm distance to its bifurcation and tie it loosely for later use.

2.2.2 Inject prepared heparin-saline solution via penile vein (male) or inferior vena cava (female) for systemic heparinization for 5min.

2.2.3 Insert the 26-gauge (26G) catheter with needle into portal vein and fix it with a clamp

2.3 Heparin-saline solution and silicone compound perfusion

2.3.1 Load heparin-saline solution in 5 ml syringe and turn on perfusion device. Fill the catheter fully with heparin-saline solution to avoid air bubbles.

2.3.2 Connect extension tube to the catheter and fix them tightly. Start heparin-saline perfusion with a perfusion rate of 0.4 ml/min.

2.3.3 Ligate pre-placed 6-0 silk suture for double fixing the catheter and blocking blood flow from splenic vein and mesenteric vein. Euthanatize the mouse by exsanguination via perfusion under anesthesia.

2.3.4 Rinse the liver using saline during the whole perfusion procedure in order to keep it moist.

2.3.5 Add 0.1 ml curing agent into the MV-120 tube. Change heparin-saline syringe to silicone syringe.

2.3.6 Start silicone perfusion with a perfusion rate of 0.2 ml/min for approximately 1 minute to prefill the catheter system and to fill the portal vein system. . Stop silicone perfusion when the vessels on the surface turn blue.

2.4 Sampling

2.4.1 Keep the liver *in-situ* until the silicone is fully polymerized after approximately 15 to 30 min. Dissect ligaments connecting liver and adjacent organs with care to keep liver intact. Explant the liver and put it into formalin for fixation.

3 Hepatic venous system silicone injection.

3.1 Perform laparotomy as performed in step 2.1 and expose operative field fully.

3.2 Catheter insertion.

3.2.1 Dissect portal vein under the microscope using micro-forceps. Place one 6-0 silk suture underneath the extrahepatic portal vein, in approximately 1 mm distance to its bifurcation and tie it loosely for later use.

3.2.2 Inject prepared heparin-saline solution via penile vein (male) or inferior vena cava (female) for systemic heparinization for 5min.

3.2.3 Insert one 26G catheter (catheter 1) with needle into portal vein and fix it with a clamp. Insert another 26G catheter (catheter 2) with needle into inferior vena cava and fix it with a clamp.

3.2.4 Ligate the branches of inferior vena cava (including left and right renal veins) and its distal end using 6-0 synthetic, monofilament, non-absorbable polypropylene suture.

3.3 Heparin-saline solution and silicone compound perfusion

3.3.1 Load heparin-saline solution in 5 ml syringe and turn on perfusion device. Fill catheter 1 completely with heparin-saline solution to avoid air bubbles. Connect extension tube to catheter 1 and fix it tightly. Start heparin-saline perfusion at a rate of 0.4 ml/min.

3.3.2 Ligate pre-placed 6-0 silk suture for double fixing the catheter and blocking blood flow from splenic vein and mesenteric vein. Euthanatize the mouse by exsanguination via perfusion under anesthesia.

3.3.3 Rinse the liver using saline during the whole perfusion procedure in order to keep it moist. Add 0.1 ml curing agent into the MV-120 tube. Exchange heparin-saline syringe with silicone syringe.

3.3.4 Place a clamp on the suprahepatic inferior vena cava to obstruct the outflow of the liver.

3.3.5 Connect the extension tube to catheter 2 and start silicone perfusion with a perfusion rate of 0.2 ml/min for approximately 2 minutes to reach an objective hepatic vascular volume as reported. Stop silicone perfusion when the vessels on the surface turn blue.

3.4 Sampling:

3.4.1 Dissect hepatic ligaments avoiding any injury to the liver. Explant the liver and put it into formalin for fixation.

4 Micro-CT (μCT) scanning

To scan the explanted liver sample using μCT, the following steps are needed.

4.1 Take the liver sample out of the fixation solution. Place the liver onto the μCT bed. Put the μCT bed with the liver sample into the μCT.

4.2 Acquire topogram before starting the scan. Use one subscan for the small liver sample and two subscans for large samples.

4.3 Select a µCT protocol with a high resolution (e.g., HQD-6565-390-90). This protocol acquires 720 projections with 1032 x 1012 pixels during one full rotation with the scanning time of 90 s per sub-scan. Start the µCT scan.

5 Histological serial sections

5.1 Embed the liver specimen in paraffin as a whole after µCT scanning. Cut whole paraffin sample into 4 µm sections, resulting in a series of 2000 to 2500 sections.

5.2 Stain sections with appropriate staining technique to visualize molecular events of interest such as Ki-67 as proliferation marker and HMGB1 as a marker of ischemic damage. Determine sequence of staining in respect to scientific question.

5.3 Use a whole slide scanner to digitalize the stained sections.

5.4 Perform 3D-reconstruction of vascular tree(s) (already feasible) and visualize 3D-distribution of molecular events in respect to vascular tree (research in progress).

REPRESENTATIVE RESULTS:

Quality criteria:

The quality of silicone injection can be judged with the naked eye during the procedure. The small vessels on liver surface fill gradually with the blue compound. If the normal vascular structure was observed on the liver surface, the silicone rubber injection quality was good. If the perfusion volume was insufficient, the small vessels on the liver surface were not fully filled. In contrast, over filling caused vascular rupture as indicated by irregular blue spots on the surface of the organ. Both are causing difficulties upon 3D-reconstruction ultimately rendering a procedure a failure.

For better evaluation of the injection quality, µCT scanning followed by 3D vascular reconstruction using preclinical software was performed. Injection was determined to be successful when segmentation resulted in the visualization of an intact complete vascular tree without ruptured structures indicated by visible extravasation. If the vascular tree appeared incomplete (Fig. 1A), perfusion volume was insufficient. If more than one vascular tree appeared or extravasation was seen (Fig. 1B), perfusion volume or pressure was inadequate. This was the most likely reason for a failure. Perfusion pressure can theoretically vary slightly depending on the viscosity of the

solution. Viscosity is dependent on the polymerization time elapsed between mixing the compound and injection into the vascular system. Since some manipulation is required for mixing and injection, time interval can slightly vary between 3 min to 5 min.

If the solution is of low viscosity, perfusion pressure is low. In this case the compound can transfer into the non-injected vascular tree via the sinusoidal system leading to a slightly higher perfusion volume. If the solution is further polymerized leading to a higher viscosity, the perfusion pressure will rise, causing disruption of the vessels and extravasation.

Determination of objective perfusion volume

Since inadequate perfusion or hyperperfusion would cause failure of injection, standardizing the perfusion volume was considered. As reported[2], 6% of the hepatic volume is occupied by blood and 44% of the blood in the liver resides in the large vessels (e.g., hepatic artery, portal vein). Liver volume in mice is about 1.3 ml[11]. Therefore, total vascular volume in portal venous system in normal mice was estimated to range between 0.03 ml and 0.04 ml. Flow rate was set to 0.2 ml/min and total perfusion time was set to approximately 1 minute resulting in a total injected volume of around 0.2 ml.

This seemingly high volume is needed, since the catheter system must be prefilled, which takes about 0.1-0.15 ml. An extra volume of 0.05 ml is needed to fill the proximal portal vein between liver hilum and the ligation of the catheter. Flow rate for hepatic vein injection was also set to 0.2 ml/min but total perfusion time was prolonged to 2 min, resulting in a higher total volume of about 0.4 ml. Total intrahepatic vascular volume was assumed to be similar to the total portal vein vascular volume. However, the volume needed to fill the intrahepatic vena cava between the infrahepatic ligation and the suprahepatic clamp was estimated with 0.2 ml.

Success rate:

A total of 49 animals were subjected to silicone injection: 22 animals into the PV system and 27 animals into the HV system. Our success rate of injection was 55% (12/22) in the PV group and 89% (24/27) in the HV group. Taking into account that the PV group was used to establish the silicone injection technique in the beginning (n=4), the success rate of injection for the PV system should effectively be higher than 55%. However, µCT images obtained from these injections were suitable for 3D

reconstruction and quantitative analysis. Additionally, the vascular trees from either PV or HV of 36 mice could be reconstructed with the Imalytics Preclinical software.

Parenchymal and vascular regeneration:

A time resolved µCT series of murine liver samples after hepatectomy was subjected to a qualitative analysis. Parenchymal regeneration consisted of 3D growth of the remnant liver. Vascular regeneration was defined as tissue that displayed an increase in the length and diameter of the vascular stem, with its main branches and outgrowth of additional terminal branches, in both the portal venous and hepatic venous tree.

Currently, several quantitative parameters suitable for describing vascular growth and the relationship between hepatic parenchymal regeneration and vascular regeneration are under investigation. These include parameters indicative of vascular growth, including maximal vascular length (Fig. 2), vascular radius and vascular density in terms of total vascular length/liver volume or vascular volume/liver volume.

Total liver volume and volume of selected liver lobes were calculated. In normal livers, total liver volume ranged from 1.2 ml to 1.6 ml (n=6, including both the PV group and HV group). It decreased to 0.6 to 0.7 ml after performing an extended liver resection by removing the left lateral and median lobe. The liver volume increased continuously during the liver growth. By post-operative day 7 (POD 7), the liver volume increased to approximately 88% of its original volume, i.e., by 2.6-fold. The increase of liver volume correlated with liver weight recovery.

Total vascular volumes of the PV system and HV system were computed. Total vascular volume of the HV system was higher than in PV system, because part of the intrahepatic inferior vena cava was included. Total vascular volume of PV system ranged from 0.05 to 0.08 ml in normal mice. It decreased to 0.03 to 0.04 ml after 70% partial hepatectomy. By POD 7, total vascular volume of the remnant liver increased to 100% of original volume. Total vascular volume of HV ranged from 0.14 to 0.16 ml. Vascular volume decreased to 0.08 to 0.09 ml after resection. Within the first postoperative week, the total vascular volume of the remnant liver increased by 94% of original value.

As the relation between results, increase in vascular volume and parenchymal volume, a vascular density was calculated, more precisely the vascular volume fraction (vascular volume divided by liver volume). This revealed that vascular volume fraction remained relatively stable throughout the regeneration process.

3D visualization of molecular events:

After CT-scanning the selected specimens were subjected to serial sectioning, yielding to up to 2000 slides, which were fully digitalized and used to reconstruct the portal as well as the hepatic venous tree[12]. This is the prerequisite for the future 3D visualization of molecular events during regeneration in respect to the growing vascular tree.

FIGURE LEGEND:

Figure 1. Monitoring the quality of silicone injection

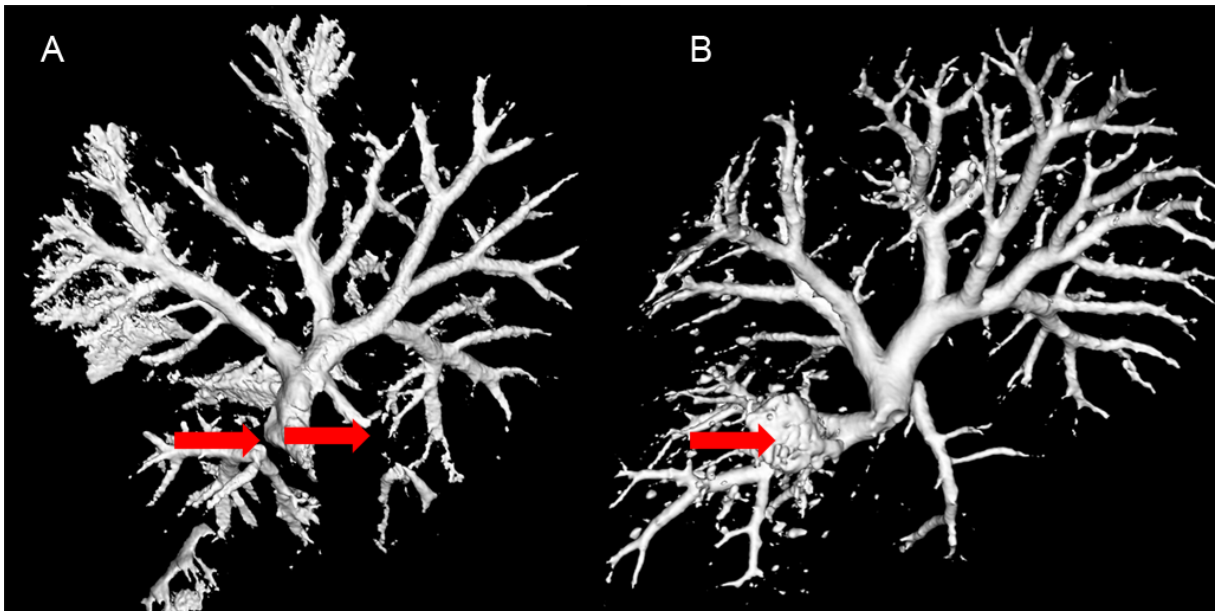

A. Incomplete filling of right inferior portal vein (arrow in the left) and caudate portal vein (arrow in the right) were visualized in Imalytics Preclinical software as discontinuities of the vascular tree. This indicated an inadequate perfusion pressure or perfusion volume or the existence of air bubbles. B. Extravasation of right inferior portal vein was visualized which indicated disruption of a vessel due to inadequate pressure or hyperperfusion.

Figure 2. Measurement of maximal vessel length of right inferior portal vein

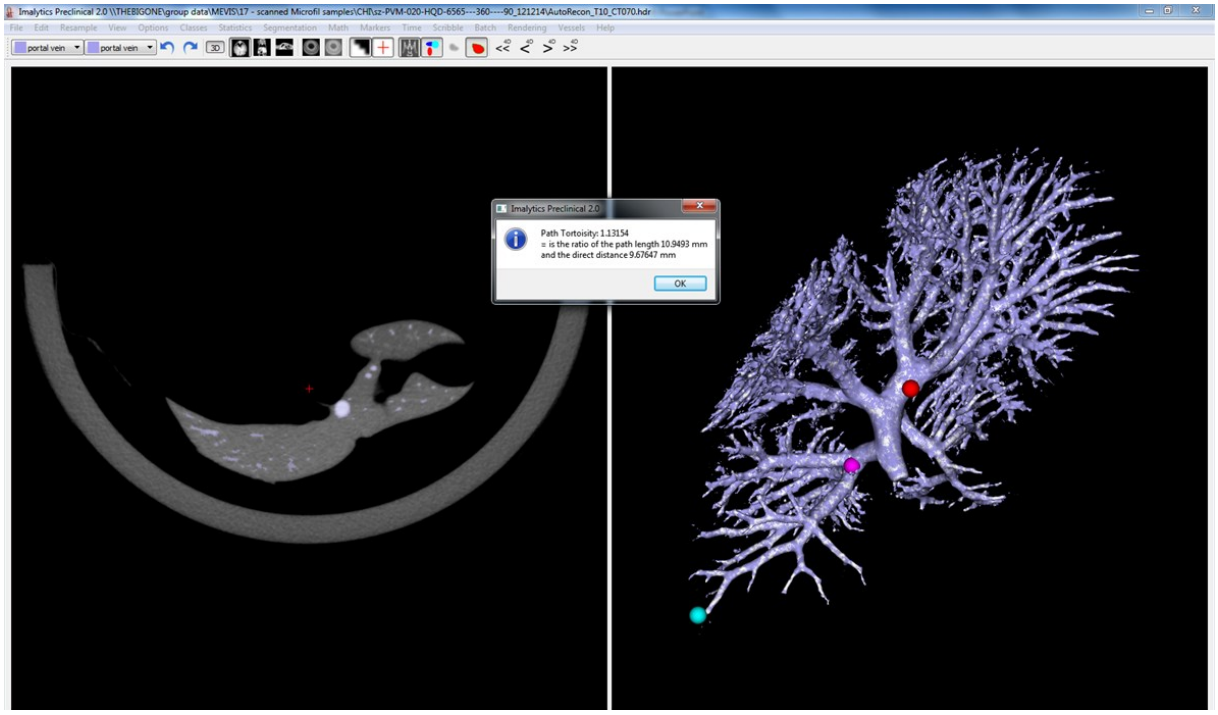

To determine the maximal vessel length, one start point and one end point were placed at the root and distal end of the right inferior portal vein (RIPV) of the vascular mask (blue and magenta ball markers) in preclinical software. The vascular path length of the RIPV (10.95 mm) was obtained as part of evaluating the "Path Tortuosity".

DISCUSSION:

Contrasting the vascular tree by silicone injection and μCT scanning has been introduced in tumor models and neurological disease models frequently to study the angiogenic progression[5,7,8,10]. Improvements in methodology of silicone injection were made in the present study for visualizing and quantifying vascular growth after partial hepatectomy in mice.

There are a number of critical steps needing attention to achieve good perfusion quality. First of all, systemic heparinization is highly recommended before flushing the liver with heparin or saline to avoid blood clotting inside the liver. Elimination of air bubbles from the tubing is also important to achieve good quality of silicone perfusion. The determination of perfusion rate and pressure should first be based on physiological hemodynamic parameters[17]. Perfusion time reflects the total injected

volume and is estimated taking the expected intravascular volume and the prefilling volume of the catheter system into account.

Silicone is a highly viscous compound which differs from blood or saline. Therefore, several trials are needed for adjusting perfusion rate and pressure. Maintaining constant injection flow rate and pressure is necessary to prevent severe dilation or even rupture of small vessels. Perfusion time is set according to the estimated needed injection volume. However, perfusion should be stopped immediately when the blue compound becomes visible in vessels on the surface of the liver. Otherwise, the silicone can drain into sinusoids and into another vascular system which will interfere with later reconstruction and analysis.

Typically, silicone is perfused systematically via the left ventricle in most published reports [1,3,15]. The left ventricle is easy to expose to enable free access to the injection site. However, the disadvantage is that this route is rather indirect because the contrast agent has to undergo circulation before reaching the site of interest. Therefore, the surgical procedure of silicone injection technique has been modified in this study. In contrast to the frequently selected indirect route of application performed by others, silicone compound was directly injected into the vascular system of interest, instead of contrasting the whole body. In this way, the velocity and volume of perfusion can be better controlled. The portal venous system and hepatic venous systems can be perfused and reconstructed separately for later individual analysis, as shown in the video.

The limitation of this modified procedure is the technical difficulty. It is challenging to successfully perform an intraportal injection using highly viscous compound in mice, because the vascular structure is so delicate. It is rather easy to destroy the vessels during the procedure. Thus, portal vein dissection and catheter insertion should be performed gently.

Contrasting of the vascular trees and subsequent µCT imaging of the explanted livers is a useful tool for visualizing and quantifying vascular regeneration after partial hepatectomy. Quantitative vascular parameters can be utilized for better understanding of the kinetic of vascular growth in the progression of liver regeneration. Furthermore, 3D reconstruction of both hepatic vascular systems based on serial sections is technically feasible, albeit representing an enormous work load.

This technique can be applied in multiple models where visualization and quantification of vascular growth is important. Moreover, 3D visualization of molecular events in respect to the underlying vascular tree is at reach. Examples of molecular events of interest could be the detection of proliferation marker such as Ki-67 or markers of ischemic damage such as HMGB1. Assessing the spatially resolved molecular events in the vicinity of the regenerating vascular tree within the regenerating hepatic parenchyma is the prerequisite for advanced multi-scale systems biology modeling. This silicone injection technique is one experimental step towards reaching this goal.

ACKNOWLEDGMENTS:

The authors acknowledge funding by the German Ministry of Education and Research (BMBF) via the systems biology network “Virtual Liver”, grant numbers 0315743 (ExMI), 0315765 (UK Jena), 0315769 (MEVIS).The authors also thank Frank Schubert for technical support.

DISCLOSURE:

The authors declare that they have no competing financial interests.

REFERENCES

1. Bearden, S.E. & Segal, S.S. Neurovascular alignment in adult mouse skeletal muscles. Microcirculation. 12 (2), 161-167, doi:10.1080/10739680590904964 (2005).
2. Brown, R.P., Delp, M.D., Lindstedt, S.L., Rhomberg, L.R., & Beliles, R.P. Physiological parameter values for physiologically based pharmacokinetic models. Toxicol.Ind.Health. 13 (4), 407-484, doi:10.1177/074823379701300401 (1997).
3. Dai, D. et al. Elastase-Induced Intracranial Dolichoectasia Model in Mice. Neurosurgery. doi:10.1227/NEU.0000000000000615 (2015).
4. Ding, B.S. et al. Inductive angiocrine signals from sinusoidal endothelium are required for liver regeneration. Nature. 468 (7321), 310-315, doi:10.1038/nature09493 (2010).
5. Downey, C.M. et al. Quantitative ex-vivo micro-computed tomographic imaging of blood vessels and necrotic regions within tumors. PLoS.One. 7 (7), e41685, doi:10.1371/journal.pone.0041685 (2012).
6. Ehling, J. et al. CCL2-dependent infiltrating macrophages promote angiogenesis in progressive liver fibrosis. Gut. doi:10.1136/gutjnl-2013-306294 (2014).

7. Ehling, J. et al. Micro-CT imaging of tumor angiogenesis: quantitative measures describing micromorphology and vascularization. Am.J.Pathol. 184 (2), 431-441, doi:10.1016/j.ajpath.2013.10.014 (2014).
8. Ghanavati, S., Yu, L.X., Lerch, J.P., & Sled, J.G. A perfusion procedure for imaging of the mouse cerebral vasculature by X-ray micro-CT. J.Neurosci.Methods. 221 70-77, doi:10.1016/j.jneumeth.2013.09.002 (2014).
9. Gremse, F. et al. Hybrid microCT-FMT imaging and image analysis. J.Vis.Exp. (100), doi:10.3791/52770 (2015).
10. Jing, X.L. et al. Radiomorphometric quantitative analysis of vasculature utilizing micro-computed tomography and vessel perfusion in the murine mandible. Craniomaxillofac.Trauma Reconstr. 5 (4), 223-230, doi:10.1055/s-0032-1329540 (2012).
11. Melloul, E. et al. Small animal magnetic resonance imaging: an efficient tool to assess liver volume and intrahepatic vascular anatomy. J.Surg.Res. 187 (2), 458-465, doi:10.1016/j.jss.2013.11.1079 (2014).
12. Schwier, M., Bohler, T., Hahn, H.K., Dahmen, U., & Dirsch, O. Registration of histological whole slide images guided by vessel structures. J.Pathol.Inform. 4 (Suppl), S10, doi:10.4103/2153-3539.109868 (2013).
13. Selle, D., Preim, B., Schenk, A., & Peitgen, H.O. Analysis of vasculature for liver surgical planning. IEEE Trans.Med.Imaging. 21 (11), 1344-1357, doi:10.1109/tmi.2002.801166 (2002).
14. Shergill, U. et al. Inhibition of of VEGF- and NO-dependent angiogenesis does not impair liver regeneration. Am.J.Physiol Regul.Integr.Comp Physiol. 298 (5), R1279-R1287, 10.1152/ajpregu.00836.2009 (2010).
15. Sueyoshi, R., Ralls, M.W., & Teitelbaum, D.H. Glucagon-like peptide 2 increases efficacy of distraction enterogenesis. J.Surg.Res. 184 (1), 365-373, doi:10.1016/j.jss.2013.03.089 (2013).
16. Wei, W. et al. Rodent models and imaging techniques to study liver regeneration. Eur.Surg.Res. 54 (3-4), 97-113, doi:10.1159/000368573 (2015).
17. Xie, C., Wei, W., Zhang, T., Dirsch, O., & Dahmen, U. Monitoring of systemic and hepatic hemodynamic parameters in mice. J.Vis.Exp. (92), e51955, doi:10.3791/51955 (2014).

3.3 Manuscript III

Quantification of hepatic vascular and parenchymal regeneration in mice

Chichi Xie, Lars Ole Schwen, Weiwei Wei, Andrea Schenk, Sara Zafarnia, Felix Gremse, Uta Dahmen

PLOS ONE - Submitted

Authorship

First author

Authors' contribution

Chichi Xie: Performing the surgical procedures, creating the contrasted specimen, identifying the vascular parameters of interest, measuring the circumscribed vascular parameters, alculating all parenchymal and vascular parameters, analyzing the results, generating the graphs and tables, writing the manuscript
Lars Ole Schwen: Identifying and calculating the cumulative vascular parameters, analyzing the results, writing the manuscript
Weiwei Wei: Assisting in performing the surgical procedure
Andrea Schenk: Converting micro-CT data and 3D vascular and territories reconstruction
Sara Zafarnia: Acquiring micro-CT data from contrasted explanted specimen
Felix Gremse: Assisting in acquiring vascular data from the micro-CT images
Uta Dahmen: Initiating the study, identifying the vascular parameters of interest, supervising the project and revising the manuscript

Summary

In this study, we quantitatively described the increase of parenchymal and vascular growth during regeneration, quantified the relationship between regenerating parenchyma and vasculature and compare the observed growth to hypothetical isotropic expansion. Geometric parameters were selected and evaluated in the vascular data sets of normal and liver-resected mice. Determination of parameters different time points provided a quantitative description of vascular regeneration which was, in turn, compared to parenchymal volume recovery to explore the growth pattern. Prospectively, this quantification approach can be used for investigating hepatic vascular regeneration under different conditions.

Quantification of hepatic vascular and parenchymal regeneration in mice

Chichi Xie[1], *Lars Ole Schwen*[2], *Weiwei Wei*[1], *Andrea Schenk*[2], *Sara Zafarnia*[3], *Felix Gremse*[3], *Uta Dahmen*[1]

1. Department of General, Visceral and Vascular Surgery, Jena University Hospital, Jena, Germany
2. Fraunhofer Institute for Medical Image Computing MEVIS, Bremen, Germany
3. Institute for Experimental Molecular Imaging, RWTH Aachen University, Aachen, Germany

Corresponding author
Prof. Dr. med. Uta Dahmen
Uta.Dahmen@med.uni-jena.de (UD)

Key words: Liver parenchymal regeneration; liver vascular regeneration; visualization of liver regeneration; vascular geometry; quantification of liver regeneration; Micro-CT imaging; contrast agent, partial hepatectomy; Mice; growth pattern; isotropic expansion

Abstract

Background Liver regeneration consists of cellular proliferation leading to parenchymal and vascular growth. Quantification of regeneration usually includes determination of cell proliferation rates and liver weight recovery, but not the assessment of vascular growth. This study aims at (1) quantitatively describing parenchymal and vascular regeneration, and (2) determining their relationship. Both together are needed to (3) characterize the underlying growth pattern.

Method Specimens were created by injecting a polymerizing contrast agent in either portal or hepatic vein in normal or regenerating livers after 70% partial hepatectomy (PH). 3D image data were obtained through µCT scanning.

Parenchymal growth was assessed by determining weight and volume of the regenerating liver. Vascular growth was described by manually determined circumscribed parameters (maximal vessel length and radius of right inferior portal/hepatic vein), automatically determined cumulative parameters (total edge length and total vascular volume), and parameters describing vascular density (total edge length/volume, vascular volume fraction).

The growth pattern was explored by comparing the relative increase of these parameters to the increase expected in case of isotropic expansion.

Results Liver volume recovery paralleled weight recovery and reached 90% of the original liver volume within 7 days (POD 7).

Comparing radius-related vascular parameters immediately after surgical resection and after virtual resection in-silico revealed a slight increase, possibly reflecting the effect of resection-induced portal hyperperfusion. Comparing length-related parameters between POD 7 and after virtual resection showed similar vascular growth in PVs and HVs. In contrast, radius-related parameters increased slightly more in the PV-group.

Despite the seemingly homogeneous 3D-growth, the observed vascular parameters were not compatible with the hypothesis of isotropic expansion of liver parenchyma and vascular structures.

Conclusion We present an approach for the quantitative analysis of the vascular systems of regenerating mouse livers. Prospectively, this approach can be used to investigate hepatic vascular regeneration under different conditions.

Introduction

Livers have the remarkable capability to fully regenerate after major loss of parenchyma. Regeneration requires reconstitution of liver parenchyma and vascular structures. Two major cell types involved in the regeneration at a microscopic scale are hepatocytes and liver sinusoidal endothelial cells (LSECs). Proliferation of these cells leads to the increase of liver mass and growth of blood vessels, respectively [1]. The present study focuses on these changes on a meso- and macroscopic scale.

In the past, more efforts were spent on studying parenchymal liver regeneration rather than on vascular regeneration. Parenchymal growth is typically quantified on the cellular level by determining the hepatocyte proliferation index and on the lobule respectively organ level by measuring hepatic weight or volume, see [2] for a review.

In particular, changes in geometry and shape of the hepatic lobes are typically not addressed. Inhomogeneous growth of the liver or of a given liver lobe may point to a disturbance in liver regeneration. Thus, we here investigated the growth pattern in liver regeneration. Based on macroscopic observations, one could assume that liver regeneration resembles isotropic expansion. Therefore we wanted to compare the changes in vascular and parenchymal parameters observed after seven days of regeneration to the ones expected in case of isotropic expansion.

Growth and remodeling of liver vessels seems to be crucial in the process of hepatic regeneration. Vascular regeneration mainly consists of the prolongation of the main vessel branches and outgrowth of small terminal branches. Studying vascular regeneration can facilitate the understanding of the pivotal role of vascular growth for the process of regeneration. Traditionally, vascular growth is assessed on a cellular level indirectly by quantifying proliferation of LSECs with specific markers [3]. However, it is still hard to quantify vascular growth routinely and directly on the macroscopic level.

As the development of imaging techniques, there are several approaches available for visualizing vascular growth [4] on the lobule or organ scale in different organ systems. Silicone injection in combination with micro-CT (μCT) imaging techniques are established and commonly used for assessing vascular growth. This contrasting technique has been used to successfully evaluate vasculature in organs (e.g., brain [5], liver [6] and bone [7;8]) and tumors [9;10]. This technique allows a more thorough structural characterization of vasculature than 2D images. Imaging also provides

quantitative data of vascular growth, which allows a mathematical description of the biological phenomenon of regeneration. Despite these promising advances for visualization and quantification of vascular regeneration, this technique was not well established for livers in small experimental animals. We previously adapted this technique to rodent livers [11]. It proved to be very helpful to identify anatomical variants. This study shows that the technique is also useful for quantifying regeneration.

Quantifying vascular growth requires numerically evaluating the changes in parameters appropriate for describing the geometry of vascular systems. Such parameters include vessel diameter/ thickness [6-8], vessel length [12;13], vessel volume [9;14;15], angles at branchings [16], vessel number [10;17], and vessel cross-section area [18]. Parameters are determined for individual vessel segments or as cumulative quantities in the literature mentioned before. Additionally, the dependency on the hierarchy in vascular trees was considered [18-20]. However, there is no widely accepted standard yet to describe vascular geometries.

The goals of the present study were to (1) quantitatively describe the increase of parenchymal and vascular growth during regeneration, and (2) to quantify the relationship between regenerating parenchyma and vasculature in order to (3) compare the observed growth to hypothetical isotropic expansion.

For this purpose, 70% partial hepatectomy (PH) was performed in mice, specimens of the hepatic vasculature at different time points were created by injection of a radiopaque polymerizing agent, µCT imaging was performed, and geometric representations of the vasculature were obtained from the image data. Geometric parameters evaluated in the vascular data sets of normal and liver-resected mice. Determining parameters at different time points provided a quantitative description of vascular regeneration which was, in turn, compared to parenchymal volume recovery to explore the growth pattern. Furthermore, these changes in geometric parameters were compared to changes expected in case of isotropic expansion. This finally led to the conclusion that the observed regeneration did not resemble isotropic expansion.

Material and Methods

Experimental Design - Workflow Overview

The workflow of creating and scanning specimens of the livers (n=3 animals/ time point in the PV group or the HV group) as well as subsequent image analysis is illustrated in [Figure 1].

Experiments and Image Acquisition

Animals

Animal experiments were performed in male inbred C57BL/6N mice (25 g to 30 g, 8-10 weeks, Charles River, Sulzfeld, Germany). Mice were fed a laboratory diet (Ssniff Spezialdiäten GmbH, Soest, Germany) with water and mouse chow ad libitum until surgery and were kept under constant environmental conditions with a 12-h light–dark cycle. All procedures and housing of the animals were carried out according to the German Animal Welfare Legislation. Procedures involving animals were approved by Thüringer Landesamt für Verbraucherschutz, Abteilung Tiergesundheit und Tierschutz, Thüringen, Germany (Permit number: 02-122/12).

Partial Hepatectomy

All surgical interventions were performed under inhalation of 2 % isoflurane mixed with 0.3 L/min oxygen (Isoflurane vaporizer, Sigma Delta, UK). A precise vessel-oriented, parenchyma-preserving piercing suture ligation method was used for 70% partial hepatectomy [22] in mice. In brief, after fully exposing the liver, a ligation (6-0 silk, Ethicon, US) was performed 3 mm from the main branch of the left lateral hepatic vein for removing the left lateral lobe (LLL). Next, the gallbladder was removed after ligating the cystic duct and artery (7-0 prolene, Ethicon, US). One clamp was placed roughly perpendicular to the surface of the left median lobe (LML) and the LML was removed. After removing the lobe, one piercing suture was placed to ligate the left hepatic vessels. Thereafter, the right median lobe (RML) was clamped and removed in a similar way. After resection, two piercing sutures were placed to ligate the right and median hepatic vein as well as the arterial and portal supply. Finally, the abdomen was irrigated with warm saline solution and closed with a 2-layer running suture (6-0 prolene, Ethicon, US).

After operation, animals received a subcutaneous injection of 0.05 mg/kg (body weight) buprenorphine (Temgesic, Essex Pharma GmbH, Munich, Germany) to achieve analgesia. The animals were placed on a heating pad for postoperative recovery.

In order to allow the comparison of vascular parameters of non-resected lobes before and after surgical resection and to eliminate the immediate effects of the surgery (details discussed below), a virtual resection was performed as explained below in the section “Obtaining Vascular Tree Representations”.

Specimen Preparation

Injection of a polymerizing silicone contrast compound (Microfil, Flow Tech Inc., Carver, US) (Fig.1-A) was performed on anesthetized normal mice and mice subjected to liver resection immediately after surgery, on postoperative day (POD) 2, and on POD 7 under anesthesia (n=3 for each time point and each group, PV and HV) [23]. Systemic heparinization was achieved by injecting heparinized saline (300 U/kg) via the penile vein and waiting for 5 min for fully systemic heparinization. After laparotomy, portal vein was cannulated with a 26-gauge heparinized catheter and flushed with heparinized saline (0.4 ml/min) using a volume-controlled perfusion device (Perfusor VI, B. Braun, Melsungen, Germany) to remove the blood from liver and to prevent blood clotting. The mice were sacrificed by exsanguination after perfusion. Two specimen preparation methods were utilized. In the portal venous system, the silicone compound was injected into the liver via the catheter in portal vein. In the hepatic venous system, the infrahepatic inferior vena cava (IVC) was cannulated with another 26G catheter. After ligating the branches of the infrahepatic IVC and after clamping the suprahepatic IVC, the silicone compound was injected via the IVC into the hepatic venous system.

The quality of silicone injection was monitored by the naked eye under the microscope throughout the procedure.

After polymerization, the specimen was explanted (Fig.1-B) and weighed. Subsequently, the specimen was immersed in formalin for fixation.

Micro-CT Scanning

The formalin-fixed specimens were scanned by µCT (Fig.1-C; Tomoscope Duo CT, CT Imaging GmbH, Erlangen, Germany). The µCT scans were performed using the scan-protocol HQD-6565-390-90 with 720 projections (approx. 1032 x 1012 pixels) during one full rotation with a scanning time of 90 s per subscan [24]. The scans resulted in voxel image representations (Fig.1-D) of the specimens at an isotropic resolution of 70 µm.

Image Processing and Analysis

After an initial quality check, part of the quantitative description of regeneration was obtained using the voxel image representation. Other parameters of the description were computed from an object-based representation obtained as described below. The parameters reported here reflect those parts of the vasculature resolved in the digital representations.

The vascular system was visualized in 3D (Fig.1-F) based on the µCT images. For this purpose, image segmentation was performed by setting a threshold between the soft tissue intensity and the vessel intensity using the Imalytics Preclinical [25]. The resulting 3D vascular mask was visualized using surface rendering and inspected visually to assess the injection quality. Injection and subsequent imaging was classified as successful if segmentation resulted in the visualization of an intact vascular tree without ruptured structures.

Circumscribed Parameters

Circumscribed parameters (maximal vessel length, in/outflow vascular radii of the right inferior portal vein (RIPV) and right inferior hepatic vein (RIPV) were determined in the right inferior lobe (RIL).

Measurement of maximal vessel length: The maximal vessel length of the right inferior portal/hepatic vein (RIPV/RIHV), i.e., the intravascular distance from root to most distant tip, was measured interactively based on the voxel images by Imalytics Preclinical software. A start point marker and an end point marker were placed at the root and distal end of RIPV/RIHV in 3D-vascular mask. The path line distance inside the vessel was determined as part of computing the “Path tortuosity”.

Measurement of in/outflow vascular radius: Similarly, a start point and an end point were set at both sides of the vascular root to measure in/outflow vascular radius of the RIPV/RIHV. They were placed in the center of a vessel using a slice-based

view. The vessel diameters were computed by performing automatic analysis of “Elastic sphere diameters” [26]. The radius was calculated as half the diameter.

Vascular Tree Representations

Vascular tree representations of the whole/remnant liver were obtained from µCT imaging data as follows:

First, a vascular graph representation of the vascular systems in the microfil specimens as well as a mask representation of the liver (both shown in Fig.1-E) and the different liver territories (Fig.1-G) was obtained applying a semi-automatic procedure for clinical liver surgery planning [27;28]. This procedure consists of (a) liver segmentation, (b) vascular segmentation, (c) conversion of portal vein and hepatic vein to graph structures, (d) labeling subgraphs according to the anatomic lobes, and (e) computation of the PV-supplied or HV-drained territories based on the liver segmentation (from step a) and labeled subgraphs (from step d). Organ volumes were immediately obtained from the liver masks. Similarly, the volumes of the territories were computed based on the territory masks.

Second, the vascular graphs were converted to a tree representation (Fig.1-H) of the vascular systems as described in [21]. This result in strictly bifurcative trees with edges represented as cylinders, i.e., each branching connects one edge to two daughter edges, each edge geometrically has straight centerlines and constant radius, in other words represents a simplification of the actual vascular segment.

Virtual Resection

Virtual resection was performed using HepaVision software (Fraunhofer Institute for Medical Image Computing MEVIS, Bremen, Germany). After loading the vascular graph of whole normal liver in the software, vessels which supplied/drained the remnant liver lobes in the surgical resection (RIL, RSL, CIL, and CSL) together with portal stump or partial vena cava were selected and saved as a new graph. The vessels supplying/draining the LLL, LML and RML lobe were thereby omitted from the new vascular graph. The virtual remnant liver was considered as “liver after virtual resection” and was used to eliminate any additional influence of the surgical procedure. Similarly, the subgraph for the RIL was saved separately. Virtually resected liver and RIL subgraphs were separately converted to *tree representations*, in the same way as the full trees, for further separate analysis.

Cumulative Parameters

The tree representation of the vascular systems permits an automatic computation of different quantitative parameters describing the geometry of the vascular system, based on the methods developed for [21;29].

Total edge length and total vascular volume for a given vascular tree were computed as the sum of all lengths and volumes, respectively, of the cylinders representing vascular edges.

To characterize vascular density, vascular volume fraction was computed as the ratio of total vascular volume and parenchymal volume. Similarly, the ratio of total edge length and parenchymal volume was computed.

Similarity of Branching Angles

The similarity of the hepatic vascular systems before resection and at POD 7 was compared in terms of angular features. For this purpose, a scalar numerical measure of similarity as introduced in [21] was used.

Each bifurcation can be fully characterized by three angles ϕa, ϕb, and ϕc [Fig. 1 in [21]]. Based on the classical Strahler orders [30], Strahler* orders were computed for each edge in the vascular tree, as explained in [21]. Histograms of each of the angles ϕ were computed for each order and each vascular tree. Two vascular trees were classified as ‘similar’ in terms of one of the angles ϕ and for a fixed order if a statistical two-sample Kolmogorov–Smirnov (KS) test [31] failed to detect a significant ($p < 0.05$, [32]) difference between the respective histograms. The overall angle similarity at a given observation time point, e.g., PV Normal, was then computed by comparing, for each angle ϕ and each order, each distinct pair of PV trees, and computing the fraction of ‘similar’ comparisons. Finally, the mean (over all angles ϕ) of the weighted averages (over the orders; weighted according to the number of edges with the given order) of these fractions was evaluated. This resulted in a number between 0 (no similarity) and 1 (high similarity).

For a single group, this indicates intra-individual similarity. The similarity of two groups of vascular trees, e.g., PV Normal vs. POD 7, was computed in analogy to the procedure described above by comparing each normal PV to each PV at POD 7. Finally, an average over the three angles was computed. Detailed formulas for this quantification of similarity are given in [21].

Characterizing the Growth Pattern

Growth refers to a positive change in size over a period of time, in our case, includes vascular dilatation and vascular proliferation. The growth pattern was assessed with respect to isotropic expansion, defined as the increase of length by the same factor in all spatial directions.

For this comparison, the observed changes of selected descriptive parameters (choice described below) were compared to those changes expected in case of hypothetical isotropic expansion.

The descriptive parameters introduced above were based on the visible (i.e., digitally represented) vasculature. During regeneration, the liver increased its size. However, visibility is determined by the µCT resolution which is essentially independent of the specimen size and, in particular, independent of the time point relative to surgery. For hypothetical two specimens of the same liver before resection and at POD 7, the increase in visible vasculature would be due to two effects: (a) vascular edges exceeding the "visibility threshold" θ until POD 7 that were not yet visible before resection, and (b) growth of vascular edges already visible before resection. The latter vascular edges were denoted as "θ-visible" here to indicate that they are a subset of all visible edges, a precise criterion for θ-visibility ("thresholded visibility") is given below. To quantify only the actual growth, the analysis was restricted to comparing parameters for the entire visible vascular trees before resection to parameters for the θ-visible part of the vascular trees at POD 7.

Thresholding for Quantitative Comparison

To define θ-visibility, a threshold θ for vascular radii was used. Generally, volume scales with the third power of length. Under the assumption of isotropic expansion, a relative change in length thus corresponds to the cubic root of the relative change in volume.

Conversely and specifically for the data at hand: if ΔV denotes the relative volume change of the RIL from before resection to POD 7, the expected relative change Δd in length under the assumption of isotropic expansion is $\Delta d = V^{1/3}$. So a threshold θ was chosen as $\theta = \Delta d$ times the minimal radius present in the vascular tree on POD 7. Under the assumption of isotropic expansion, any edges of radius ≥ θ would already have been visible in a hypothetical specimen of the same liver created before surgery. Thus, only edges of radius ≥ θ were used for further analysis.

Determining Parameters for Quantitative Comparison

To compare the vascular growth pattern to hypothetical isotropic expansion, parameters which can be evaluated restricted to the θ-visible edges on POD 7 were selected from those above. These parameters were (a) in/outflow vascular radius, (b) total vascular length, (c) total vascular volume, (d) total vascular length/volume, and (e) vascular volume fraction.

In/outflow vascular radius of the RIL is always θ-visible since it was measured at the root of the vessel, so no new determination was needed for POD 7. The other parameters are affected by θ-invisibility and were thus re-evaluated restricted to θ-visible edges on POD 7 ("observed values").

Estimating the Effect of Isotropic Expansion

Based on ΔV, defined above as the relative volume change of the RIL from before resection to POD 7, "expected values" were obtained by scaling the parameter from before resection by appropriate scaling factors. These scaling factors are the relative change in length ($\Delta d = V^{1/3}$, see above) to the power of the dimension of the respective parameter, i.e., $V^{1/3}$ for in/outflow vascular radius and total vascular length, $V^{3/3}=V$ for total vascular volume, $V^{-2/3}$ for total vascular length/volume, and $\Delta V^{0/3}=1$ for the vascular volume fraction (i.e., the latter should remain constant).

Finally, observed and expected values were compared to estimate the extent of growth. In addition, further insight into the growth pattern was gained by quantifying changes in angular features.

Comparing Angular Features

Purely isotropic expansion does not change any angles at bifurcations. Given that specimens before resection and at POD 7 were obtained from different animals, no 1:1 comparison was possible. Instead, the similarity of branching angles between the two time points was compared to the intraindividual similarity at the separate time points. If those similarities were in the same range, this was used as an indicator supporting the hypothesis of purely isotropic growth.

Results

Visualization and Quantification of Regeneration

Based on the macroscopic appearance and visualizations (Fig.2), parenchymal regeneration is described qualitatively as three-dimensional growth of the remaining liver lobes. Vascular regeneration in both portal and hepatic venous system appeared to be as elongation and widening of the main vascular structures in combination with an out-branching of smaller vessels. Starting on POD 2, the vascular trees of remnant lobes elongated. By POD 7, additional small branches from the same main portal vein and hepatic vein became visible.

Quantification of Parenchymal Regeneration

Quantitative analysis focused on evaluation of parameters indicative of parenchymal and vascular liver regeneration at different observation time points after 70%PH.

Liver weight recovery was compared to computed liver volume recovery, resulting in the relation: hepatic volume (in ml) = 0.907 × liver weight (in gram) + 0.053. These two hepatic parameters indicative of parenchymal regeneration were highly correlated (r^2=0.97, $p<0.001$), for all individual cases in both portal and hepatic vascular system. The average density (± standard deviation) of the livers was 1.042 ± 0.050 g/ml, which is nearly the same as the liver density of humans (1.051 ± 0.013 g/ml) [33]. The increase of hepatic volume paralleled the increase of liver weight (Fig.3-A), indicating that the increase of hepatic volume can be utilized as basis for the subsequent quantitative analysis of hepatic parenchymal regeneration.

In normal mice, total liver weight ranged from 1.3 to 1.6 g. Similarly, total computed liver volume ranged from 1.2 to 1.6 ml, irrespective of the vascular tree used for the computation (1.35 ± 0.16 ml in PV group and 1.35 ± 0.20 ml in HV group) (Fig.3-B).

Hepatic volume of the remnant liver was slightly lower after virtual resection compared with the volume after surgical resection. Virtual resection in the PV/HV group resulted in a decrease of mean total hepatic volume to 35% respectively 34%, whereas surgical resection resulted in a remnant hepatic volume of 52% to 48%. The observed volume difference between virtual resection and surgical resection may be attributed to the complete removal of the liver lobe after virtual resection. In contrast, surgical removal of a liver lobe results in a stump which contributes to the volume of the remnant liver, leading to a slightly higher remnant liver volume.

Hepatic volume after virtual resection increased from 0.45 ml in PV-group respectively 0.46 ml in the HV group to about 1.22 ml and 1.19 ml at POD 7. This volume represented about 90% of the starting volume and was equivalent to a 2.7/2.6-fold increase. Similar results were reported when studying liver weight recovery in mice [34].

The volume recovery of the RIL was very similar compared to the total liver volume recovery, indicating a similar parenchymal growth of the liver lobes of the liver lobes. Before surgery, the volume of RIL was 0.16 ± 0.02 ml in PV group and 0.17 ± 0.03 ml in HV group. By POD 7, it reached about 0.41 ml and 0.44 ml, representing a 2.6/2.7-fold increase compared to the mean volume after virtual resection in the PV/HV group.

Quantification of Vascular Regeneration

Assessment of vascular regeneration was based on a comparison of different parameters obtained on POD 7 and after virtual resection. This time point was chosen as the initial state to exclude immediate effects of the surgical intervention.

First, vascular radii and maximal vessel lengths of the main right inferior portal/hepatic vein were measured and compared between different time points (circumscribed data for individual vessels). Next, total edge length and total vascular volume for the whole/remnant liver and separately for the RIL were computed (cumulative data for the vascular trees). Finally, parameters describing the vascular density, i.e., total edge length/hepatic volume and the vascular volume fraction were considered.

Individual Vessels

Vascular radii of RIPV and RIHV (Fig.4-A) increased, albeit to a different extent. Starting from mean in/outflow vascular radius of 0.35 ± 0.02 mm (PV group) and 0.47 ± 0.01 mm (HV group), radii increased by 1.3- and 1.1-fold respectively until POD 7 .

When comparing the RIPV-radius after virtual resection with the radius obtained after surgical resection, a substantial difference was observed, suggesting an effect of portal hypertension. A further increase was observed when comparing the radius after surgical resection and the radius at POD 2. This increase could be the result of vascular growth but also of vascular dilatation, which cannot be discriminated based on the imaging data.

In contrast, the radius of the RIHV remained rather similar until POD 2 and increased thereafter, an observation better attributable to vascular growth.

However, average maximal vessel length of both vascular systems (Fig.4-B) increased in parallel during regeneration. Before surgery, the maximal vessel length was 12.43 ± 0.87 mm (PV group) and 10.59 ± 0.62 mm (HV group). Immediately after surgical resection, maximal vessel length remained almost the same. By POD 7, maximal vessel length of RIPV as well as RIHV increased both up to 1.3-fold.

Vascular Trees

In contrast to the maximal vessel length, the total edge length increased after surgical resection compared to virtual resection.

In normal mice, the total edge length of whole liver (Fig.4-C) was 861.93 ± 179.45 mm in the PV group and 875.87 ± 118.87 mm in the HV group. As expected from the resected volumes after virtual resection, it decreased to 38% and 45% in the PV

group and HV group corresponding to 326.62 ± 75.43 mm in the PV group and 394.35 ± 55.03 mm in the HV group.

However, total edge length was substantially higher after surgical than after virtual resection (568.39 ± 45.94 vs. 326.62 ± 75.43 mm in the PV group and 486.04 ± 22.41 vs. 394.35 ± 55.03 mm in the HV group). On the one hand, this might be due to portal hypertension induced vascular dilatation caused by surgical resection (see Fig. S1). Small terminal vessel branches in both vascular systems, which were invisible in normal liver, might have been dilated and thereby became visible, which contributed to the computed total edge length. On the other hand, the vessels of the remnant stump after surgical resection were taken into account when computing the total edge length. However, the influence of the small stumps to the total edge length of the remnant liver was limited and negligible since the visible vascular trees were rather small.

The total edge length in both portal venous and hepatic venous tree recovered fully by POD 7. By POD 7, total edge length increased by 2.8-fold and 2.3-fold in PV/HV group, respectively. Similarly, RIL edge length increased by 2.6-fold and 2.2-fold in PV/HV group.

Total vascular volume differed between PVs and HVs (Fig.4-D). In the PV group of whole livers, volumes (0.071 ± 0.008 ml) were lower than in the HV group (0.152 ± 0.010 ml) where the volume of the inferior vena cava was also included.

Also for this parameter, we observed a difference between surgical and virtual resection. Total vascular volume in the PV group after surgical resection was slightly higher than after virtual resection (0.035 ± 0.006 ml vs. 0.024 ± 0.003 ml). In the HV group, total vascular volume after surgical resection was slightly lower than after virtual resection (0.084 ± 0.008 ml vs. 0.094 ± 0.011 ml). This might be an indirect effect of portal hypertension leading to a dilation of portal vessels and consecutively leading to a compression of the hepatic venous tree [35].

Despite the absolute differences in the total volume of both vascular trees, the relative volume increases during the regenerative process in both groups were almost comparable. By POD 7, there was a 2.6-fold increase in the PV group and 1.5-fold increase in the HV group, leading to an 89% to 94% recovery within one week. Similar observations were obtained for both vascular trees of the RIL.

Branching angles stayed essentially the same during regeneration, indicating, at first glance, that the growth pattern resembled isotropic expansion. Branching angles at the bifurcations (see Fig. 5) exhibited a high similarity among the normal livers, 0.926 in both the PV and the HV group. These similarities are even larger than previous results for entire mouse livers (0.841 vs. 0.710) reported in [Fig. 2 in [29]], and show a slightly higher similarity among PVs than for HVs also in our data. Among the livers at POD 7, lower similarities of 0.916 and 0.879 (among the PV and HV groups, respectively) were observed. In both cases, the tendency of PVs being more similar than HVs in terms of branching angles could be confirmed, (see [29] for results in mice and [21] in humans). The similarity of normal PVs and those at POD 7 was 0.900 and thus not substantially lower than at the separate time points (0.853 for HVs), showing that branching angles do not change considerably during regeneration.

Relating Parenchymal and Vascular Regeneration

Vascular Density

Given the fact that the extrahepatic part of the vascular systems could not be excluded from the vascular trees due to the technical reasons, the calculation of these parameters describing vascular density (vascular volume fraction and total edge length/hepatic volume) were based on a selected liver lobe (RIL).

Similar to previously mentioned parameters, vascular density also seems to be affected by the surgery-induced portal hypertension as expected based on the edge length and vascular volume described above (see also Fig.4-C and -D). We observed an increase of PV edge length/RIL hepatic volume and a decrease of HV edge length/RIL hepatic volume after resection, possibly also an indirect effect of portal hypertension. During the course of regeneration, this density returned to the values before surgery, see Fig.6-A.

In contrast, the PV volume fraction increased substantially when comparing the RIL before and after resection but reached its maximum on POD 2. This could be explained by portal hypertension still being present, while parenchymal volume is not fully recovered on POD2. The HV volume fraction followed the same kinetic pattern as described for the HV length/RIL volume, see Fig.6-B.

Observed Growth Pattern

To characterize the observed growth pattern, relative changes of the parameters above were computed and compared.

In the PV group (Fig.7-A), the relative increase of vascular radius and maximal vessel length of the RIL (1.4-fold and 1.3-fold) was not that obvious compared to the remaining three parameters: Hepatic volume indicative of parenchymal regeneration increased to 2.6-fold. Total edge length and total vascular volume of RIL increased to 2.6-fold and 4.9-fold, revealing that the radius of vascular branches in the periphery increased in parallel to the radius at the inflow.

Similar results were obtained when computing the relative increase of vascular radius and maximal vessel length in the HV group (1.1-fold and 1.3-fold) (Fig.7-B). The relative increase of hepatic volume in the HV group (2.7-fold) was comparable to the PV group. However, there was a slight difference between the increase of RIL edge length and vascular volume in the PV and HV group. In contrast to the PV group, the increase of total edge length of RIL (2.2-fold) was higher than the increase of vascular volume (2.0-fold) in the HV group. This indicates that the radii in the periphery increased less than the radii at the outflow.

In the PV group, RIL edge length/hepatic volume (Fig.7-C) increased to 1.2-fold immediately after surgical resection. One likely reason could be that the total edge length was enlarged due to the increase of edge visibility caused by portal hypertension-induced vascular dilatation whereas portal hypertension has limited influence to hepatic volume. Altogether, the increase of total edge length was much higher than the increase in hepatic volume leading to a big increase in RIL edge length/hepatic volume right after resection. In contrast to the PV group with a slight increase, RIL edge length/hepatic volume in the HV group had a slight decrease after surgical resection; both with a tendency to recover within the 7 observed days.

The relative changes of vascular volume fraction (Fig.7-D) were different from the changes of RIL edge length/hepatic volume. Vascular volume fraction increased considerably by POD 7 in the PV group (1.9-fold). However, in the HV group, it decreased to 52% after surgical resection, recovered to 76% of normal ranges by POD 7.

These findings could be explained by portal hypertension after resection leading to a dilation of the portal vein tree, and a corresponding compression of the hepatic vein tree.

Comparison of the Observed Growth Pattern to Isotropic Expansion

Taking all data together revealed that the relative increase of parenchymal volume outweighed the relative vascular elongation, suggesting that it could be explained by isotropic expansion. This suspicion is further corroborated by the lack of changes in the branching angles, as only non-isotropic growth can distort bifurcations. The increase of parenchymal volume in the RIL was 2.6-fold (PV group; 2.7-fold for the HV group), whereas the increase of the maximal vessel length was 1.3-fold. In case of isotropic expansion, the 2.6-fold volume increase would correspond to a 1.4-fold increase of lengths and radii. In order to better compare the observed growth pattern of liver regeneration to isotropic expansion, a more elaborate analysis was necessary. The observed relative increase in the parameters describing the vascular system before resection and at POD 7 were compared to the expected increase in case of isotropic expansion, see Fig. 8.

In the PV cases, the increase of inflow vascular radius almost perfectly matched the expected increase in case of isotropic expansion. Total edge length and total edge length/hepatic volume were about 20% lower than expected in case of isotropic expansion, whereas the vascular volume and the vascular volume fraction were about 60% larger. This indicates that the vascular radii in the periphery increased a lot more than expected. In the HV cases, the outflow vascular radius was about 20% lower than the expected increase in case of isotropic expansion, the remaining parameters (total edge length, total edge length/hepatic volume, vascular volume, vascular volume fraction) were about 40% lower than the expected increase in case of isotropic expansion. This could indicate that HVs generally grow/regenerate slower than PVs.

In summary, the changes in the vascular systems, combined with differences between HVs and PVs, contradict the hypothesis of isotropic expansion of liver parenchyma and vascular structures.

Discussion

In this study, we quantitatively described parenchymal and vascular regeneration after PH in mice, and compared the observed hepatic regeneration to hypothetical isotropic expansion. For this purpose, we established the presented framework for high-resolution µCT imaging and qualitative and quantitative analysis of the vascular system in normal and resected mice.

Assessment of liver parenchymal regeneration based on computed volumes is a reasonable approach for several reasons: Liver weight and volume were strongly correlated (see Fig. 3), the resulting density was similar to literature results [33], and the observed volume recovery within one week was comparable to previously published findings [37] for both the PV and HV group in this study.

Assessment of the vascular system based on vascular geometry provided information regarding vascular regeneration which cannot be obtained otherwise, e.g., by classical parameters such as determination of the proliferation rate of the endothelial cells.

Regeneration is not Isotropic Expansion

Relating hepatic parenchymal and vascular growth as well as the similarity of branching angles suggested, at first glance, that regeneration resembles isotropic expansion and thus permits an easy descriptive model. For further investigating the growth pattern, a more detailed analysis was performed: changes in descriptive geometric parameters were compared to those changes expected in case of isotropic expansion. To achieve this comparison, the vascular datasets were thresholded to eliminate the influence of increased visibility of vasculature that would not have been visible in a hypothetical scan of the same individual at an earlier time point (θ-invisible edges). Ultimately, the observed changes were not compatible with the hypothesis of isotropic expansion. These observations indicated that hepatic regeneration might be a more complex process influenced by many factors.

One important factor is portal hypertension. Portal hypertension induced by surgical removal of liver lobes (see Figure S1) might affect these vascular parameters to different extent, not only immediately after resection but also even after 7 days.

In order to investigate immediate effects of surgery, we compared vascular parameters obtained after surgical resection to after virtual resection. We observed

that portal hypertension affected the vascular diameter strongly and the vascular length slightly. These effects were more pronounced in the PV system than the HV system. Here we suggest a cautious interpretation of the respective quantitative data in the early phase of liver regeneration, as it is impossible to discriminate vascular dilatation from vascular growth based on geometric data. In consequence, results from the virtual resection group should serve as control when assessing regeneration in terms of total edge length and total vascular volume of the regenerating remnant liver.

We also considered potentially longer-lasting effects of portal hypertension on vascular geometry. Based on two observations, we conclude that portal hypertension/perfusion may have a persisting effect on the vascular system: On the one hand, PVP has returned to normal ranges after one week (Fig. S1). On the other hand, the geometric parameters and in particular the differences between PVs and HVs on POD 7 (Fig. 7) showed patterns that could be a residue of portal hypertension. However, further work is needed to determine the 3D-growth pattern of regenerating livers and to elucidate the underlying biological processes in targeted studies.

Limitations

The presented approach using silicone injection, µCT imaging of explanted liver specimens and image analysis is useful for quantifying vascular geometries based on standard imaging techniques. It permits the assessment of differences between different post-surgical time points. Still, certain technical limitations should be taken into account when interpreting the resulting data.

First, using the explanted livers from different animals for each time point leads to the side effect of introducing inter-individual variation. Promising technologies are under development allowing repeated in-vivo assessment of the same animals [12], allowing monitoring the kinetic of vascular regeneration of an individual liver. This would permit a better comparison of vascular growth at different time points.

Second, in the HV specimens, the intrahepatic vena cava could not be excluded from silicone injection, leading to artificially large vascular volumes. When comparing between different time points for the entire liver, this mainly affected vascular volumes, whereas the influence on the other vascular geometric parameters was negligible. The analysis of the RIL as a single lobe remained unaffected by this artifact and was therefore performed. Furthermore, a slight discrepancy between

physiological vascular geometry and the silicone-injected specimens might be present.

Third, image resolution in the workflow used here was limited to 70 µm, focusing the investigation on changes in the larger vasculature rather than on angiogenesis occurring at smaller length scale [38]. In the subsequent image analysis, radius and centerline position estimation led to differences between measurements in voxel image data and graph representation. This procedure is known to slightly underestimate vascular volumes [39]. The simplification from vascular graph to vascular tree again led to differences in measurements of lengths, radii, and angles. Moreover, calculating the total vascular volume as sum of vessel represented cylinder volume, overlap/gaps were ignored, introducing two more inaccuracies that only partly compensate for each other. Finally, the concept of θ-visibility could be insufficient to eliminate the influence of increased visibility of vasculature that would not have been visible in a hypothetical scan of the same individual at an earlier time point. Determining the relative importance of these uncertainties on the overall quantitative results will require a detailed sensitivity analysis. This, however, is beyond the scope of the present study.

Future applications

The workflow presented in this study is modular in the sense that it can (a) be applied to various organs, (b) use other imaging modalities (e.g., other contrasting media, other and higher imaging resolution, in vivo scans, MRI), (c) employ different approaches to obtain tree representations of the vasculature, and (d) evaluate additional geometric parameters if deemed relevant. In particular, the methods used here can also be applied to (potentially smaller) specimens scanned at higher resolution to assess changes in finer vasculature, including investigating angiogenesis [6].

Quantitative descriptions of vascular regeneration and, in particular, its spatial inhomogeneity, provide useful information. It can help to identify disturbances in liver regeneration, which is a prerequisite for possibly developing treatment strategies.

Quantitative descriptions of vascular systems are of utmost importance for perfusion studies. Perfusion is, in turn, the basis for distribution of substances from the organism to the liver and in particular for pharmacokinetics. Vascular regeneration thus leads to alterations in pharmacokinetics. Quantifying vascular regeneration can be used to extend PK simulations with spatially resolved livers [40;41] towards

regenerating livers. This approach could be further used to extend simulations involving lobular regeneration [42] to the scale of the entire organ. Ultimately, this could help optimizing therapy for patients undergoing liver regeneration.

This study is an important prelude to further studies on vascular regeneration. In the future, the techniques presented here can be applied in a broad range of conditions associated with the changes of vascular features. Findings could be used as input or for validation of regeneration/growth simulations including vascular structures, e.g., combining approaches like [43] and [29] or as input for simulations estimating the recovery of liver function after resection.

Conclusion

We successfully implemented a workflow for quantifying vascular regeneration in resected mouse livers. The observed growth pattern turned out to be more complex than mere isotropic expansion. Prospectively, this quantification approach can be used for investigating hepatic vascular regeneration under different conditions.

Acknowledgments

The authors thank Stephanie Lange and Isabel Jank from Jena for helping shipping liver specimens. The authors thank Marek Weiler, the technician from Aachen, for helping us scanning liver specimens and reconstructing the µCT data. The authors thank Christiane Engel and Andrea Koller, the technicians from MEVIS, for helping us reconstructing the vascular trees and hepatic territories.

References

[1] Michalopoulos GK. Liver regeneration. J Cell Physiol 2007; 213(2):286-300.doi:10.1002/jcp.21172

[2] Wei W, Dirsch O, Mclean AL, Zafarnia S, Schwier M, Dahmen U. Rodent models and imaging techniques to study liver regeneration. Eur Surg Res 2015; 54(3-4):97-113.doi:10.1159/000368573

[3] Sorensen KK, Simon-Santamaria J, McCuskey RS, Smedsrod B. Liver Sinusoidal Endothelial Cells. Compr Physiol 2015; 5(4):1751-1774.doi:10.1002/cphy.c140078

[4] Upputuri PK, Sivasubramanian K, Mark CS, Pramanik M. Recent developments in vascular imaging techniques in tissue engineering and regenerative medicine. Biomed Res Int 2015; 2015:783983.doi:10.1155/2015/783983

[5] Ghanavati S, Yu LX, Lerch JP, Sled JG. A perfusion procedure for imaging of the mouse cerebral vasculature by X-ray micro-CT. J Neurosci Methods 2014; 221:70-77.doi:10.1016/j.jneumeth.2013.09.002

[6] Ehling J, Bartneck M, Wei X, Gremse F, Fech V, Mockel D et al. CCL2-dependent infiltrating macrophages promote angiogenesis in progressive liver fibrosis. Gut 2014.doi:10.1136/gutjnl-2013-306294

[7] Jing XL, Farberg AS, Monson LA, Donneys A, Tchanque-Fossuo CN, Buchman SR. Radiomorphometric quantitative analysis of vasculature utilizing micro-computed tomography and vessel perfusion in the murine mandible. Craniomaxillofac Trauma Reconstr 2012; 5(4):223-230.doi:10.1055/s-0032-1329540

[8] Bolland BJ, Kanczler JM, Dunlop DG, Oreffo RO. Development of in vivo muCT evaluation of neovascularisation in tissue engineered bone constructs. Bone 2008; 43(1):195-202.doi:10.1016/j.bone.2008.02.013

[9] Downey CM, Singla AK, Villemaire ML, Buie HR, Boyd SK, Jirik FR. Quantitative ex-vivo micro-computed tomographic imaging of blood vessels and necrotic regions within tumors. PLoS One 2012; 7(7):e41685.doi:10.1371/journal.pone.0041685

[10] Ehling J, Theek B, Gremse F, Baetke S, Mockel D, Maynard J et al. Micro-CT imaging of tumor angiogenesis: quantitative measures describing micromorphology and vascularization. Am J Pathol 2014; 184(2):431-441.doi:10.1016/j.ajpath.2013.10.014

[11] Sanger C, Schenk A, Schwen LO, Wang L, Gremse F, Zafarnia S et al. Intrahepatic Vascular Anatomy in Rats and Mice-Variations and Surgical Implications. PLoS One 2015; 10(11):e0141798.doi:10.1371/journal.pone.0141798

[12] Mittal N, Zhou Y, Ung S, Linares C, Molloi S, Kassab GS. A computer reconstruction of the entire coronary arterial tree based on detailed morphometric data. Ann Biomed Eng 2005; 33(8):1015-1026.doi:10.1007/s10439-005-5758-z

[13] Wan SY, Ritman EL, Higgins WE. Multi-generational analysis and visualization of the vascular tree in 3D micro-CT images. Comput Biol Med 2002; 32(2):55-71.doi:10.1016/S0010-4825(01)00034-8

[14] Langheinrich AC, Ritman EL. Quantitative imaging of microvascular permeability in a rat model of lipopolysaccharide-induced sepsis: evaluation using cryostatic micro-computed tomography. Invest Radiol 2006; 41(8):645-650.doi:10.1097/01.rli.0000227494.17444.64

[15] Gayetskyy S, Museyko O, Kasser J, Hess A, Schett G, Engelke K. Characterization and quantification of angiogenesis in rheumatoid arthritis in a mouse model using muCT. BMC Musculoskelet Disord 2014; 15:298.doi:10.1186/1471-2474-15-298

[16] Parker JC, Cave CB, Ardell JL, Hamm CR, Williams SG. Vascular tree structure affects lung blood flow heterogeneity simulated in three dimensions. J Appl Physiol (1985) 1997; 83(4):1370-1382.

[17] Duvall CL, Taylor WR, Weiss D, Guldberg RE. Quantitative microcomputed tomography analysis of collateral vessel development after ischemic injury. Am J Physiol Heart Circ Physiol 2004; 287(1):H302-H310.doi:10.1152/ajpheart.00928.2003

[18] Huang W, Yen RT, McLaurine M, Bledsoe G. Morphometry of the human pulmonary vasculature. J Appl Physiol (1985) 1996; 81(5):2123-2133.

[19] VanBavel E, Spaan JA. Branching patterns in the porcine coronary arterial tree. Estimation of flow heterogeneity. Circ Res 1992; 71(5):1200-1212.

[20] Yen RT, Zhuang FY, Fung YC, Ho HH, Tremer H, Sobin SS. Morphometry of cat pulmonary venous tree. J Appl Physiol Respir Environ Exerc Physiol 1983; 55(1 Pt 1):236-242.

[21] Schwen LO, Preusser T. Analysis and algorithmic generation of hepatic vascular systems. Int J Hepatol 2012; 2012:357687.doi:10.1155/2012/357687

[22] Madrahimov N, Dirsch O, Broelsch C, Dahmen U. Marginal hepatectomy in the rat: from anatomy to surgery. Ann Surg 2006; 244(1):89-98.doi:10.1097/01.sla.0000218093.12408.0f

[23] Chichi Xie, Weiwei Wei, Andrea Schenk, Lars Ole Schwen, Sara Zafarnia, Michael Schwier et al. Visualization of Vascular and Parenchymal Regeneration After 70% Partial Hepatectomy in Normal Mice. J Vis Exp 2016; e53935.doi:10.3791/53935

[24] Gremse F, Doleschel D, Zafarnia S, Babler A, Jahnen-Dechent W, Lammers T et al. Hybrid microCT-FMT imaging and image analysis. J Vis Exp 2015;(100).doi:10.3791/52770

[25] Gremse F, Stark M, Ehling J, Menzel JR, Lammers T, Kiessling F. Imalytics Preclinical: Interactive Analysis of Biomedical Volume Data. Theranostics 2016; 6(3):328-341.doi:10.7150/thno.13624

[26] Gremse F, Grouls C, Palmowski M, Lammers T, de Vries A, Grull H et al. Virtual elastic sphere processing enables reproducible quantification of vessel stenosis at CT and MR angiography. Radiology 2011; 260(3):709-717.doi:10.1148/radiol.11110069

[27] Selle D, Preim B, Schenk A, Peitgen HO. Analysis of vasculature for liver surgical planning. IEEE Trans Med Imaging 2002; 21(11):1344-1357.doi:10.1109/TMI.2002.801166

[28] Schenk A, Zidowitz S, Bourquain H, Hindennach M, Hansen C, Hahn HK et al. Clinical relevance of model based computer-assisted diagnosis and therapy. Medical Imaging 2008: Computer-Aided Diagnosis 2008; 6915:691502-691519.doi:10.1117/12.780270

[29] Schwen LO, Wei W, Gremse F, Ehling J, Wang L, Dahmen U et al. Algorithmically generated rodent hepatic vascular trees in arbitrary detail. J Theor Biol 2015; 365:289-300.doi:10.1016/j.jtbi.2014.10.026

[30] Arthur N.Strahler. Quantitative analysis of watershed geomorphology. Transactions, American Geophysical Union 1957; 38(6):913-920.doi:10.1029/TR038i006p00913

[31] Dudewicz EJ, Mishra SN. Modern Mathematical Statistics. Wiley, 1988.

[32] Stephen Stigler. Fisher and the 5% level. CHANCE 2008; 21(4):12.doi:10.1007/s00144-008-0033-3

[33] Overmoyer BA, McLaren CE, Brittenham GM. Uniformity of liver density and nonheme (storage) iron distribution. Arch Pathol Lab Med 1987; 111(6):549-554.

[34] Blindenbacher A, Wang X, Langer I, Savino R, Terracciano L, Heim MH. Interleukin 6 is important for survival after partial hepatectomy in mice. Hepatology 2003; 38(3):674-682.doi:10.1053/jhep.2003.50378

[35] Ch.Rouiller. Dynamics of the circulation in the liver. The liver: Morphology, Biochemistry, Physiology. Elsevier, 1963: 329-378.

[36] Xie C, Wei W, Zhang T, Dirsch O, Dahmen U. Monitoring of systemic and hepatic hemodynamic parameters in mice. J Vis Exp 2014;(92):e51955.doi:10.3791/51955

[37] Melloul E, Raptis DA, Boss A, Pfammater T, Tschuor C, Tian Y et al. Small animal magnetic resonance imaging: an efficient tool to assess liver volume and intrahepatic vascular anatomy. J Surg Res 2014; 187(2):458-465.doi:10.1016/j.jss.2013.11.1079

[38] Carmeliet P. Angiogenesis in life, disease and medicine. Nature 2005; 438(7070):932-936.doi:10.1038/nature04478

[39] J.DREXL VKHKHKSLBFHSHOP. Accuracy analysis of vessel segmentation for a LITT dosimetry planning system, Perspective in Image-Guided Surgery. in Proceedings of the Scientific Workshop on Medical Robotics, Navigation and Visualization 2004;204-213.

[40] Schwen LO, Krauss M, Niederalt C, Gremse F, Kiessling F, Schenk A et al. Spatio-temporal simulation of first pass drug perfusion in the liver. PLoS Comput Biol 2014; 10(3):e1003499.doi:10.1371/journal.pcbi.1003499

[41] Schwen LO, Schenk A, Kreutz C, Timmer J, Bartolome Rodriguez MM, Kuepfer L et al. Representative Sinusoids for Hepatic Four-Scale Pharmacokinetics Simulations. PLoS One 2015; 10(7):e0133653.doi:10.1371/journal.pone.0133653

[42] Werner L, Guzner-Gur H, Dotan I. Involvement of CXCR4/CXCR7/CXCL12 Interactions in Inflammatory bowel disease. Theranostics 2013; 3(1):40-46.doi:10.7150/thno.5135

[43] Hohmann N, Weiwei W, Dahmen U, Dirsch O, Deutsch A, Voss-Bohme A. How does a single cell know when the liver has reached its correct size? PLoS One 2014; 9(4):e93207.doi:10.1371/journal.pone.0093207

Figures

Figure 1

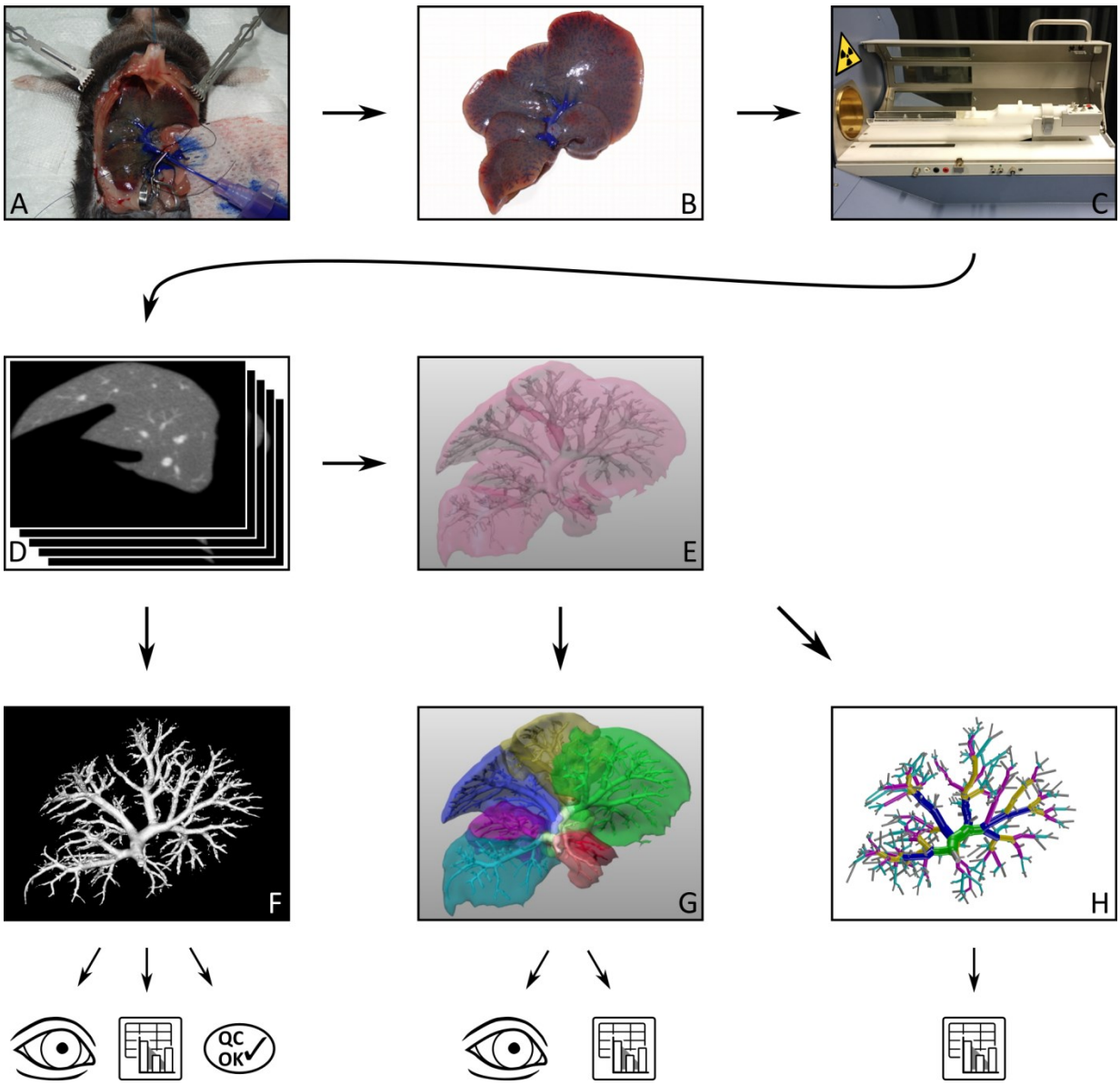

Fig 1. Workflow Sketch. At different time points before and after partial hepatectomy, silicone contrast compound was injected into either portal vein (shown here; naïve liver) or hepatic vein of a mouse liver (A). The liver was explanted (B) and imaged in a micro-CT scanner (C). The resulting voxel image data (D) was thresholded and visualized as a surface rendering (F), where the measurements of maximal vessel length and radius of RIL were performed interactively. From (D), the liver was segmented and the vascular system was segmented and skeletonized, resulting in a graph representation visualized in (E) along with the liver mask. Manually labeling the vascular graph according to anatomical lobes, the respective supplied territories were computed (G; territories shown in different color), permitting both qualitative visual assessment and quantitative volume measurements. The vascular graphs from (E) were converted to strictly bifurcative trees (H, here colored according to Strahler* order [21]). Based on these, automatic measurements of lengths, radii, and angles were performed.

Image credits: The eye and spreadsheet icons at the bottom were adapted from https://openclipart.org/detail/216030/eye-lineart and https://openclipart.org/detail/198552/mono-spreadsheet. Photos in (B) and (C) were edited to remove

Figure 2

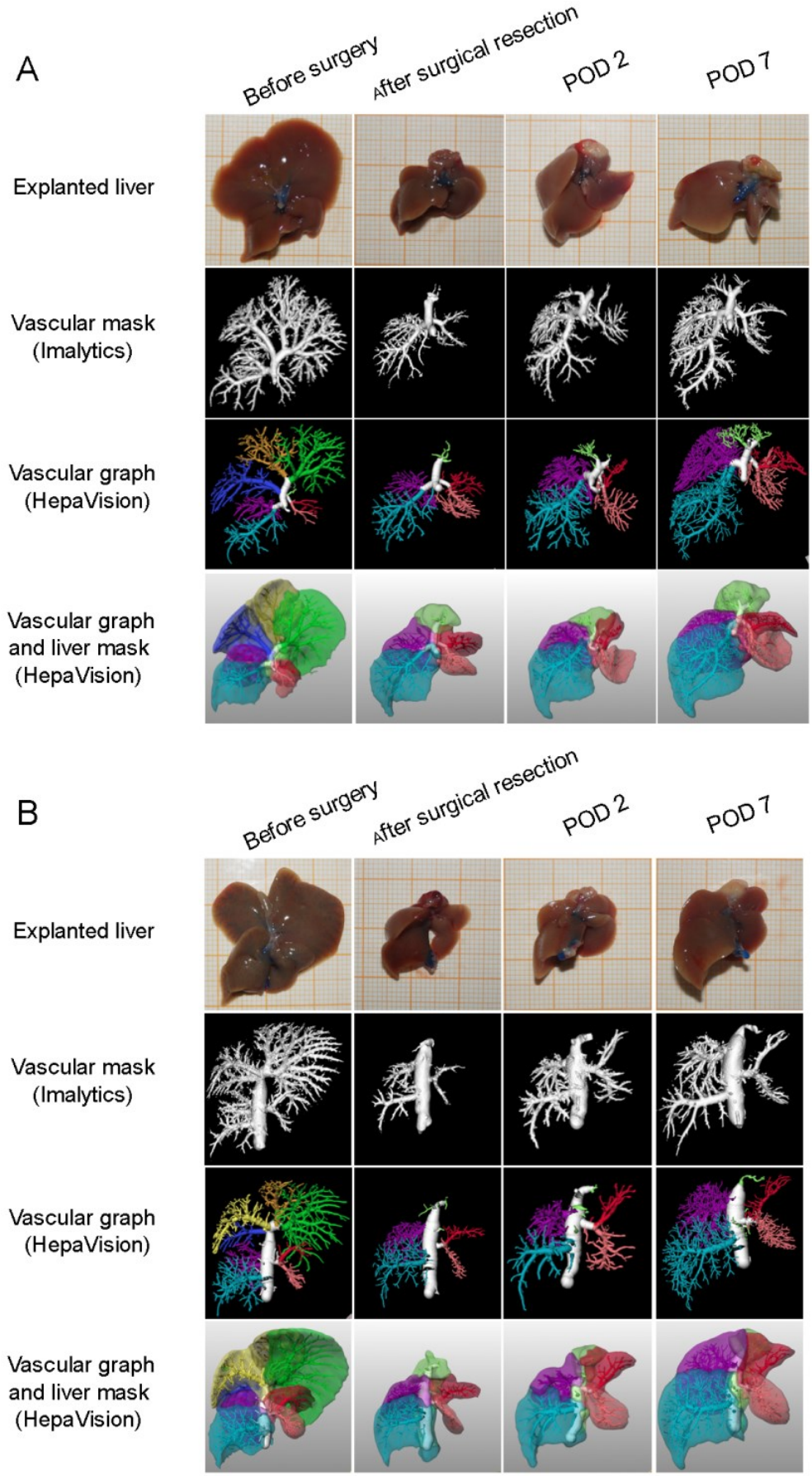
A
Before surgery
After surgical resection
POD 2
POD 7
Explanted liver
Vascular mask (Imalytics)
Vascular graph (HepaVision)
Vascular graph and liver mask (HepaVision)
B
Before surgery
After surgical resection
POD 2
POD 7
Explanted liver
Vascular mask (Imalytics)
Vascular graph (HepaVision)
Vascular graph and liver mask (HepaVision)

Fig 2. Visualization of liver regeneration. Parenchymal and vascular regeneration in the PV group (A) at indicated time points following partial hepatectomy. Left lateral lobe (visualized in green), left median lobe (visualized in yellow), and right median lobe (visualized in dark blue) were removed during PH. These lobes did not regrow during the whole regenerative procedure. Vascular regeneration in both portal and hepatic venous system appeared as elongation of the main vascular structures in combination with an out-branching of smaller vessels. Parenchymal and vascular regeneration in HV group (B) were in parallel to the growth in the PV group.

Figure 3

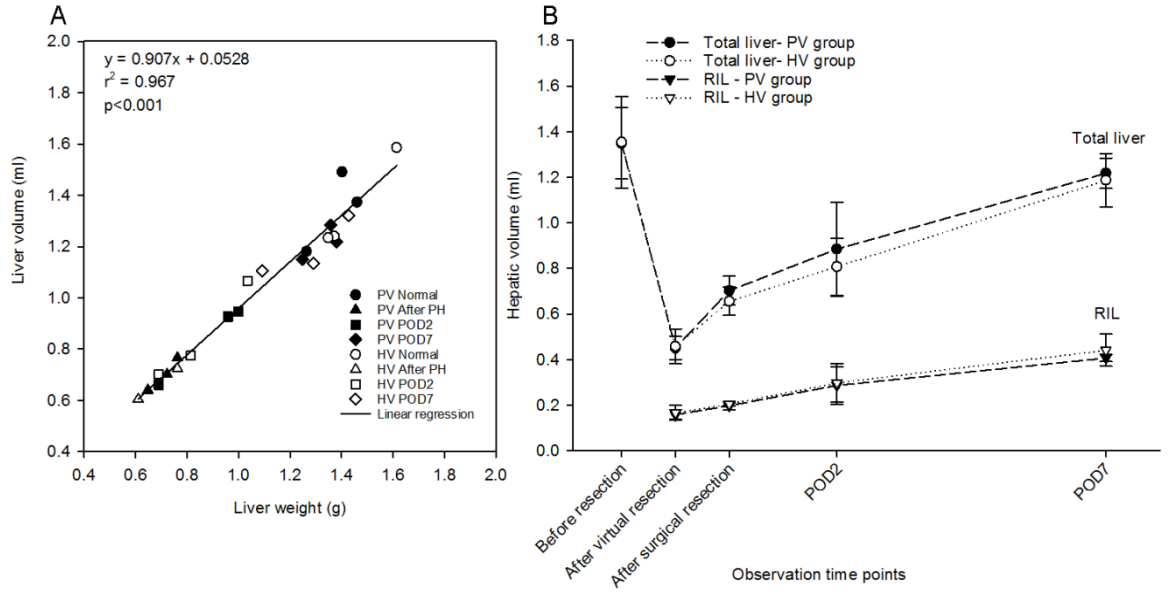

Fig 3. Quantification of Parenchymal Regeneration. (A) Correlation of liver weight and liver volume. Liver weight was compared to computed liver volume, resulting in the relation hepatic volume (in ml) = 0.907 × liver weight (in gram) + 0.053. These two hepatic parameters indicative of parenchymal regeneration were highly correlated (r^2=0.97, p<0.001). (B) Recovery of hepatic volume of total liver and right inferior lobe within the first postoperative week (mean ± SD, n=3/time point). In PV group, virtual resection resulted in a volume reduction from 1.35 ± 0.16 ml to 0.45 ± 0.05 ml, representing a loss of about 70% of the total hepatic volume. In contrast surgical resection caused a reduction to 0.70 ± 0.06 ml, suggesting surgical removal of a liver lobe results in a stump which contributes to the volume of the remnant liver. Liver volume reached 1.22 ± 0.06 ml, representing a 90% recovery. The hepatic volume recovery was almost in parallel in the HV and PV group.

Figure 4

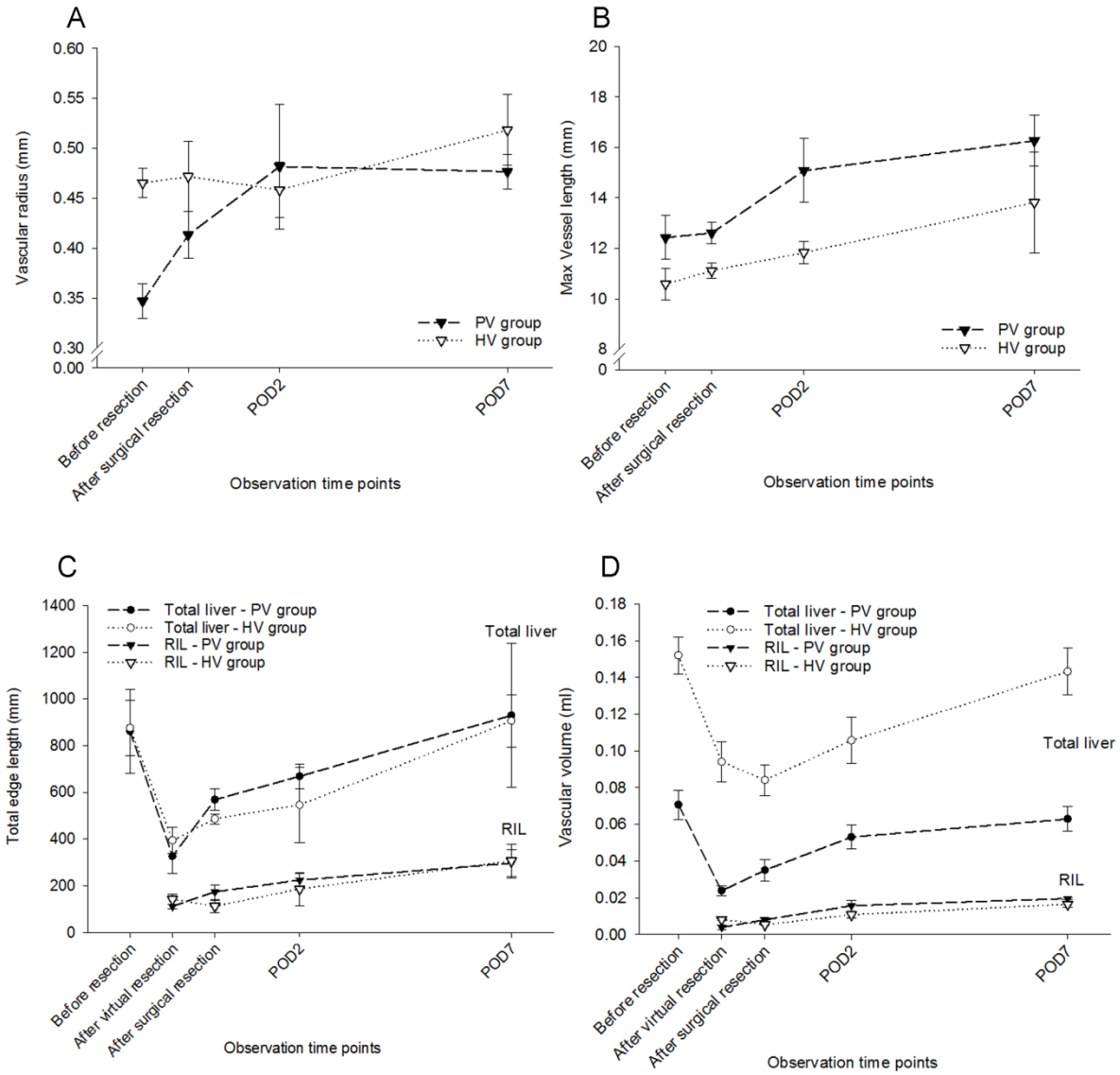

Fig 4. Quantification of Vascular Regeneration. Vascular radius (A) of the right inferior portal vein increased substantially until POD 2 and remained stable thereafter. In contrast, the radius of the right inferior hepatic vein remained rather similar until POD 2 and increased thereafter. However, average maximal vessel length (B) of both vascular systems increased in parallel during regeneration. Total edge length (C) in PV group reduced from 861.93 ± 179.45 ml to 326.62 ± 75.43 ml comparing before and after virtual PH, representing a loss of 62% of the total edge length. In contrast, surgical PH caused a reduction to 568.39 ± 45.94ml, suggesting an effect of portal hypertension. It reached 929.76 ± 308.88 ml, representing a 1.1-fold increase. The increase of total edge length in HV group was almost in parallel in the PV group. However, total vascular volume (D) differed between PVs and HVs. We observed an increase of total vascular volume after surgical resection compared to after virtual resection in PV group but a decrease in HV group. The increases during the regenerative process in both vascular systems were almost comparable.

Figure 5

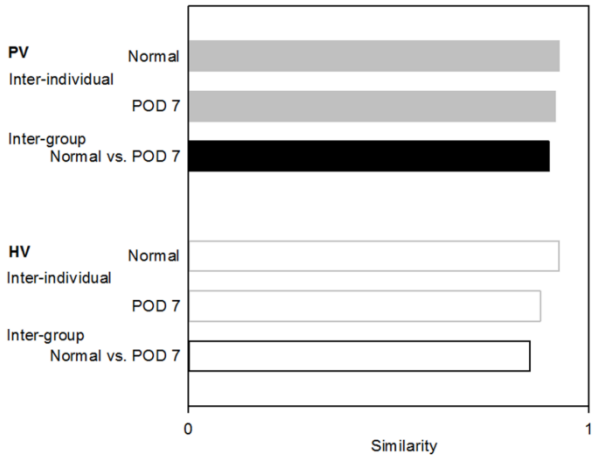

Fig 5. Similarity of Angular Parameters. For time points Normal and POD 7, the plot shows the inter-individual similarity of the angular parameters describing bifurcations for the vascular trees of the RIL, as well as the similarity between the respective vascular trees at the two time points. The similarity measure from [21] is a value between 0 (low) and 1 (high similarity).

Figure 6

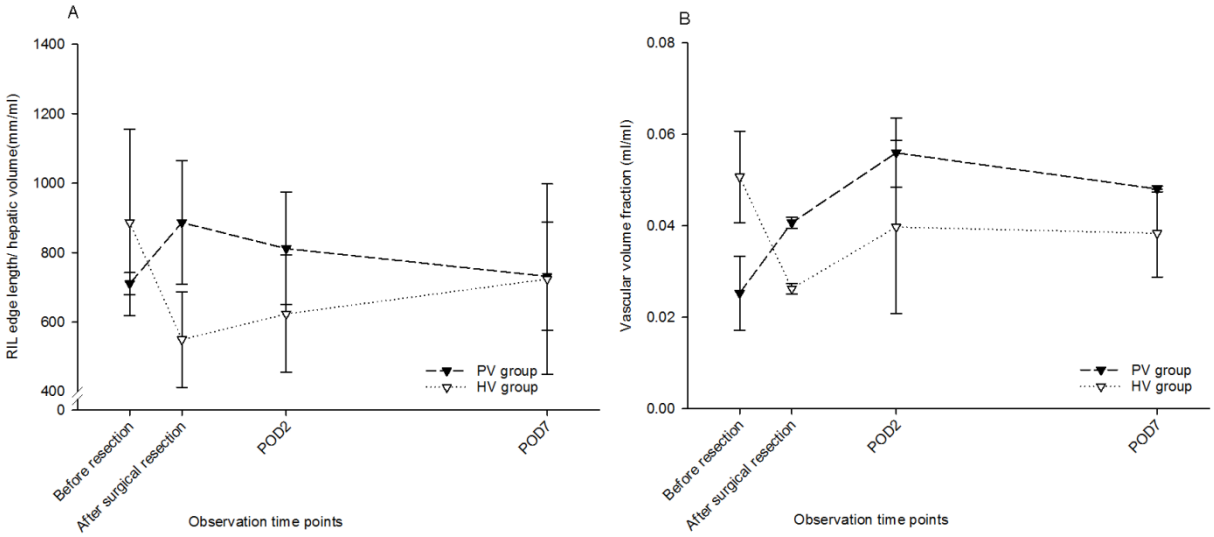

Fig 6. Relating Parenchymal and Vascular Regeneration in RIL. (A) RIL edge length/RIL hepatic volume. We observed an increase of RIL edge length/RIL hepatic volume in the PVs and a decrease of RIL edge length/RIL hepatic volume in the HVs after resection. This density returned to the values before surgery after 7 days' regeneration. (B) Vascular volume fraction of RIL in PVs increased substantially when comparing the fraction before and after resection but reached its maximum on POD 2. However, the vascular volume fraction in HVs followed the same kinetic pattern as described for the HV length/RIL volume.

Figure 7

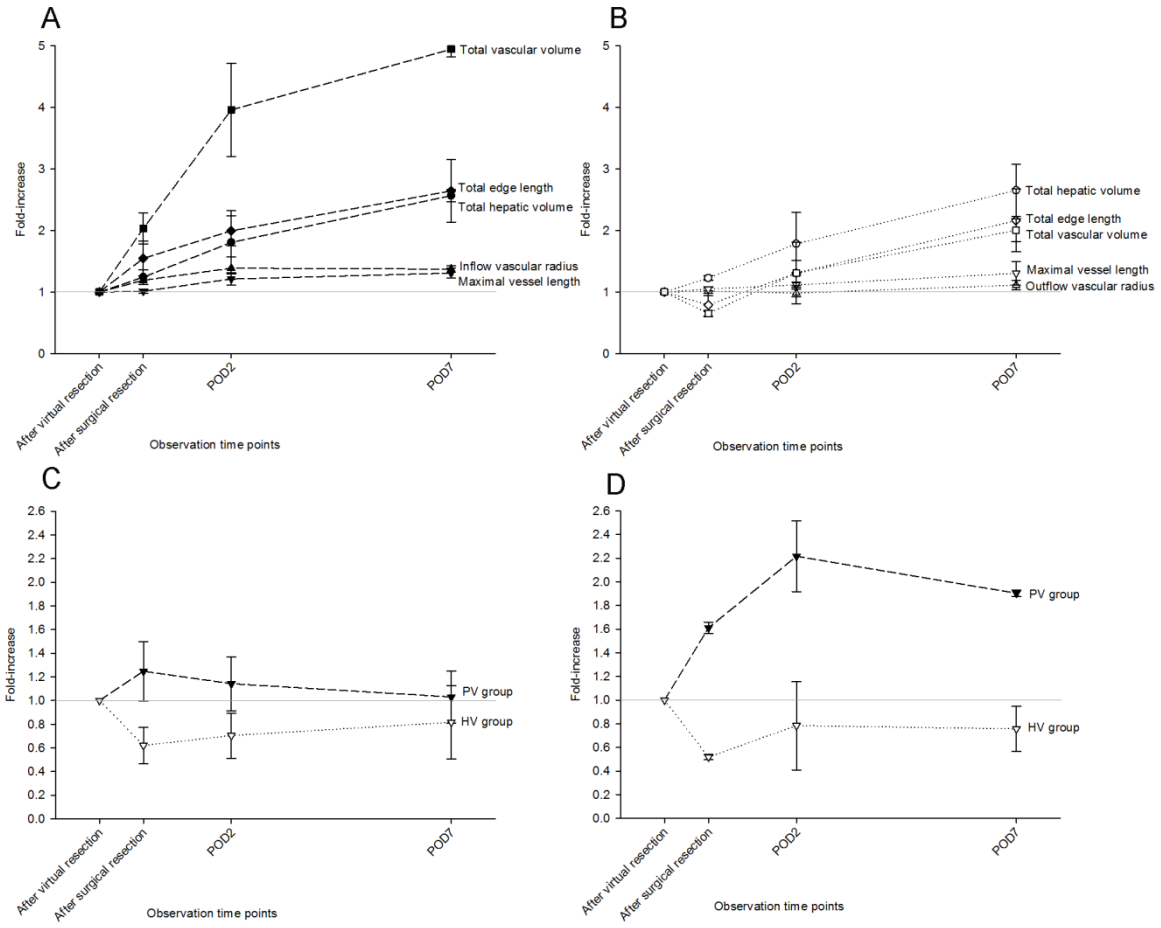

Fig 7. Relative changes of regenerative parameters. The relative changes of five parenchymal and vascular regenerative parameters in PV group (A) and in HV group (B) were related. After 1 week, vascular radius and maximal vessel length in PV group increased to 1.4-fold and 1.3-fold compared with after virtual resection, hepatic volume increased to 2.6-fold, total edge length and total vascular volume increased to 2.6-fold and 4.9-fold, revealing that the radius of vascular branches in the periphery increased in parallel to the radius at the inflow. The relative increases of vascular radius, maximal vessel length and hepatic volume were comparable in HV group and in PV group. However, RIL edge length and vascular volume increased not as pronounced as in PV group, to 2.2-fold and 2.0-fold respectively. This indicates that the radii in the periphery increase less than the radii at the outflow. The relative changes of these two derived parameters referred to vascular density, RIL edge length/hepatic volume (C) and vascular volume fraction of RIL (D) were compared. The increase of total edge length was much higher than the increase in hepatic volume leading to a big increase in RIL edge length/hepatic volume right after resection in the PV group. In contrast, RIL edge length/hepatic volume in the HV group had a slightly decrease after surgical resection.

Figure 8

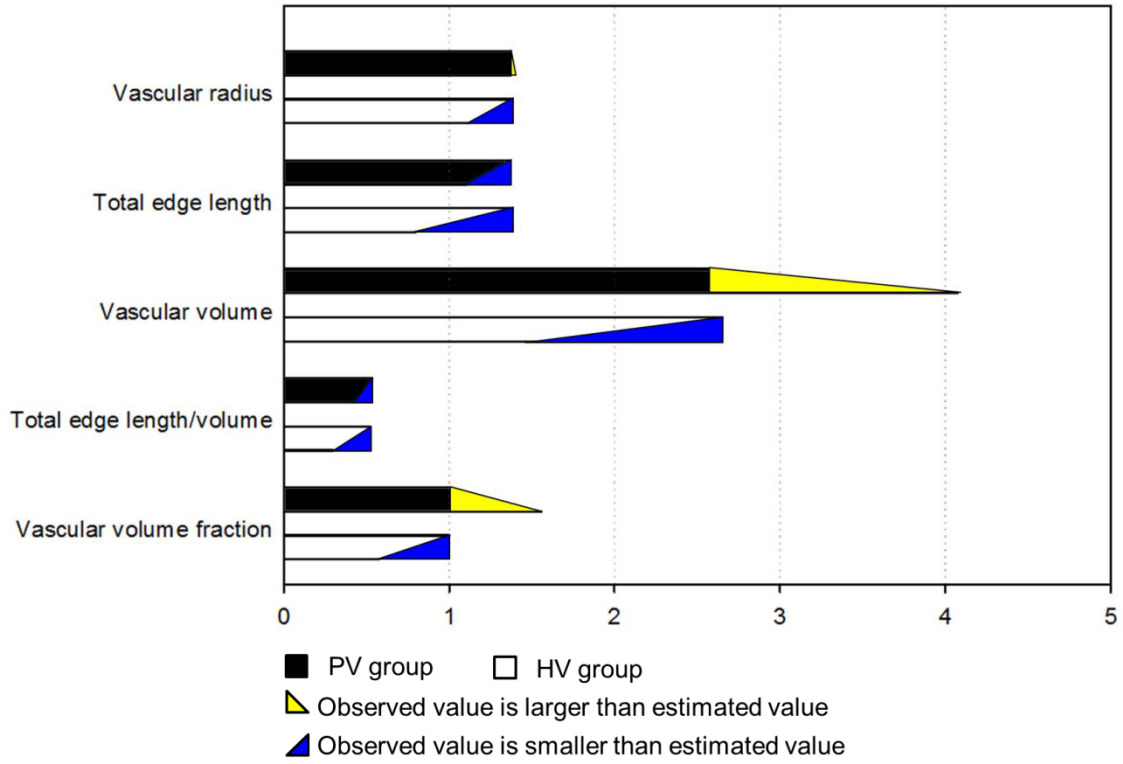

Fig 8. Comparison to Isotropic Expansion. (A) The plot shows the expected increase in case of isotropic expansion and observed relative changes for the RIL from before surgery to θ-visible parameters at POD 7. The expected values (rectangular part of the bar) are computed for the change of mean volume of the RIL from Normal to POD 7, assuming isotropic expansion. Color of the triangle showing direction of difference (blue = observed value is smaller; yellow = observed value is larger)

Supporting Information

S1 Figure

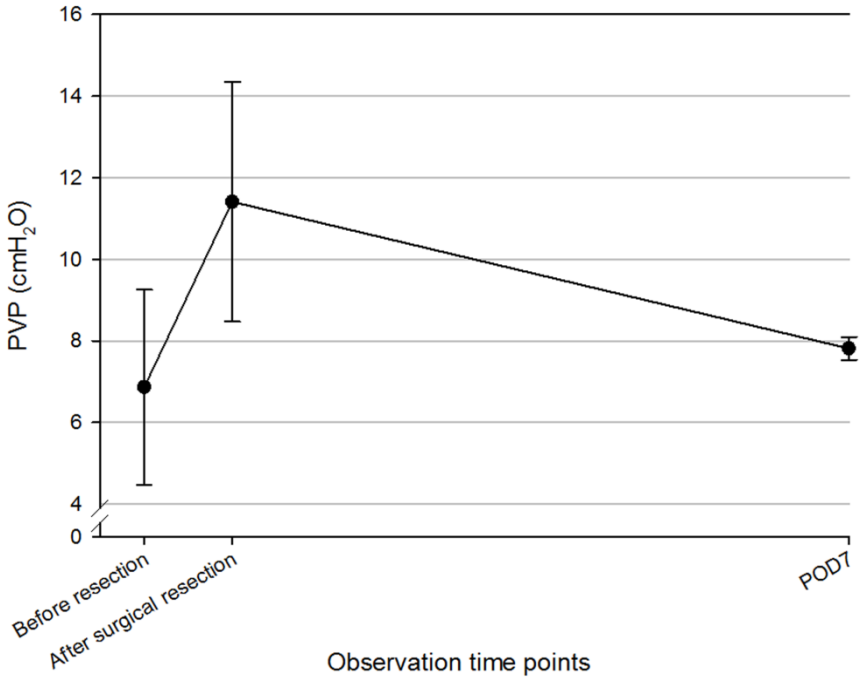

S1 Fig. Portal vein pressure (PVP) after 70% partial hepatectomy. PVP was measured by inserting Millar catheter into the confluence of portal vein at indicated time points. Average PVP before resection was 6.9 ± 2.4 cmH_2O. It increased to 11.4 ± 2.9 cmH2O immediately after surgical resection (Data were reported in [36]). It returned to normal ranges on POD 7 (7.8 ± 0.3 cmH_2O). This revealed that as the new vessel bed developed, the influence of portal hypertension was reduced.

S1 Table. Data evaluation of parenchymal and vascular parameters.

S1 Dataset. Vascular tree datasets used in the geometric analysis. Vascular trees are stored in text format, can thus be read using any text editor or imported in spreadsheets, and viewed interactively in 3D using the viewer tool from [Data S1 in [40]]

3.4 Manuscript IV

Delay of hepatic vascular and parenchymal regeneration after modulating CXCR4-CXCR7-SDF-1α axis in 70% PH mouse model

Chichi Xie, Sara Zafarnia, Felix Gremse, Ralf Stumm, Olaf Dirsch, Uta Dahmen

Manuscript in preparation

Authorship

First author

Authors' contribution

Chichi Xie: Performing 70% partial hepatectomy, injecting silicone compound to create liver specimens, administrating drugs, analyzing results, writing the manuscript
Sara Zafarnia: Acquiring micro-CT data from contrasted explanted specimen
Felix Gremse: Assisting in acquiring vascular data from the micro-CT images
Ralf Stumm: Initiating the project and critical revision of manuscript
Olaf Dirsch: Supervising the project
Uta Dahmen: **I**nitiating and supervising the project, writing the manuscript

Summary

In this study, we visualized and quantified hepatic parenchymal and vascular regeneration after modulating CXCR4-CXCR7-SDF-1α axis by applying either AMD3100 (CXCR4 antagonist) or TC14012 (CXCR4 antagonist and CXC4 agonist) in 70% PH mouse model. We observed that only by blockade of CXCR4 using AMD3100 had limited role in liver regeneration after 70%PH. However, liver regeneration was impaired by administrating TC14012, CXCR4 antagonist and CXCR7 agonist. These results in pilot experiment indicated that, blockade of CXCR4 by AMD3100 after hepatectomy was not capable of inhibiting angiogenesis and vascular growth, because it might be by the compensatory actions through an alternative SDF-1α receptor CXCR7.

Delay of hepatic vascular and parenchymal regeneration after modulating CXCR4-CXCR7-SDF-1α axis in 70% PH mouse model

***Chichi Xie*[1]**, *Sara Zafarnia*[2], *Felix Gremse*[2], *Ralf Stumm*[3], *Olaf Dirsch*[4], *Uta Dahmen*[1]

1. Department of General, Visceral and Vascular Surgery, Jena University Hospital, Jena, Germany
2. Institute for Experimental Molecular Imaging, RWTH Aachen University, Aachen, Germany
3. Institute of Pharmacology and Toxicology, Jena University Hospital, Jena, Germany
4. Klinikum Chemnitz gGmbH, Institute of Pathology, Chemnitz, Germany

Corresponding author
Prof. Dr. med. Uta Dahmen
Uta.Dahmen@med.uni-jena.de

Key words: CXCR4, CXCR7, CXCL12, SDF-1, AMD3100, TC14012, partial hepatectomy, silicone injection, micro-CT imaging, vascular reconstruction

Abstract

Background

Liver regeneration consists of parenchymal regeneration and hepatic vascular growth. SDF-1α and its receptors CXCR4 and CXCR7 are involved in vascular growth during vasculogenesis and angiogenesis. However, the role of this pathway for hepatic parenchymal and vascular regeneration was not yet well explored due to the lack of appropriate methods. We recently established a work flow consisting of contrasting the vascular tree using a silicone compound injection method, micro-CT imaging technique and subsequent image data analysis to quantitatively assess hepatic vascular growth during liver regeneration

The aim of this study was to visualize and quantify hepatic parenchymal and vascular regeneration after modulating CXCR4-CXCR7-SDF-1α axis in 70% PH mouse model. Two drugs were selected for modulating CXCR4-CXCR7-CXCL12 axis: (1) CXCR4 antagonist, AMD3100, for blockade of CXCR4 and (2) CXCR4 antagonist and CXCR7 agonist, TC14012, for blockade of CXCR4 and activation of CXCR7. We hypothesized that after blockade of CXCR4 and activation of CXCR7, liver regeneration would be impaired.

Method

Mice were subjected to 70% partial hepatectomy (PH) (70%PH group, n=6/time point). AMD3100 (10 mg/kg/day, 70%PH+AMD3100 group, n=6/time point) and PBS (70%PH+PBS group, n=6/time point) were administrated by an osmotic pump. TC14012 (5 mg/kg/day, 70%PH+TC14012 group, n=4/time point) was injected subcutaneously every post-operative day before sacrifice. Naïve mice (n=6/time point) and mice subjected to sham operation (n=6/time point) served as control groups.

Postoperative monitoring included daily recording of the body weight for calculating body weight recovery. Liver specimens were explanted and weighed for determining liver weight to body weight ratio. The BrdU.proliferation index was determined in 4 different remnant liver lobes. Three liver specimens in 70%PH+TC14012 group were injected with silicone compound and subjected to µCT scanning. Three dimensional vascular trees and the hepatic territories were reconstructed based on µCT data using Imalytics Preclinical software. Maximal vessel length of right inferior portal vein (RIPV) and the radius of inflow RIPV were measured as well.

Results

Blocking the CXCR4 using the antagonist AMD3100 did not neither affect parenchymal regeneration nor vascular growth. However using TC14012 with a simultaneous effect on both CXCR4 and CXCR7 was associated with a lower parenchymal recovery on POD 2 and 7 as indicated by the LW/BW ratio and the significantly lower liver cell proliferation rate and a reduced vascular growth (maximal vessel length and radius of RIPV on POD 2 and 7 substantially lower compared to the PBS treated group).

Conclusion

Our results elucidated that the blockade of CXCR4 by AMD3100 after hepatectomy is not capable of inhibiting angiogenesis and vascular growth. This finding might be explained by compensatory actions through the alternative CXCL12 receptor CXCR7. This interpretation is further supported by our observation of a reduced and delayed course of liver regeneration, when applying TC14012, a compound not only blocking CXCR4 but also activating CXCR7. Further investigations e.g. focusing on a CXCR7 agonist such as CCX771whichonly plays a role in blocking CXCR7, are needed for better understanding of the molecular mechanism of SDF-1 and its two receptors.

Introduction

CXCR4-CXCR7- SDF-1α pathway is important in vasculogenesis and angiogenesis [1] in normal injured tissue and in tumor.

SDF-1α is a chemokine that acts through its receptors CXCR4 and CXCR7. The tissue and serum expression levels of SDF-1α and CXCR4 are upregulated after liver injury [2;3]. It was observed recently, that upregulation of SDF-1α initiated liver regeneration by activating LSECs through autocrine/paracrine pathways [4] and through the mobilization of hematopoietic cells [5]. However, how this pathway may affect hepatic vascular regeneration still remains elusive.

Thus, we aimed at studying the influence of this pathway on hepatic vascular regeneration using our newly developed workflow for quantifying vascular regeneration (see details in Manuscript III). In brief, this workflow consists of injecting silicone contrast compound followed by explanting the liver and ex-vivo µCT scanning and quantitative analysis of the 3D reconstructed vascular tree.

We decided to modulate CXCR4-CXCR7-SDF-1α pathway by pharmacological interventions and study the effects in liver regeneration after 70%PH. Two reagents,

AMD3100 and TC14012, were chosen for this purpose. AMD3100 is a specific CXCR4 antagonist that inhibits binding and the function of SDF-1α with high affinity and potency [6] and subsequently inhibits CXCR4 calcium signaling [7], which might impair liver regeneration.

In contrast, TC14012 is not only CXCR4 antagonist but also CXCR7 agonist. TC14012 is a much more potent agonist on CXCR7 (EC50 of 350 nM for TC14012 versus 140 μM for AMD3100) and only one log weaker than the natural chemokine agonist SDF-1α (35 nM) [8]. TC14012 can activate the β-arrestin pathway via activation of GRK, leading to internalization of CXCR4 and scavenging of SDF-1α. Thus, we hypothesized that liver regeneration will be impaired by applying TC14012.

Methods

1. **Partial Hepatectomy** – as described in method section of Manuscript III
2. **Drug administration**

2.1 AMD3100/PBS administration

AMD3100 (Sigma Aldrich, Saint Louis, Missouri, US) was applied in a concentration of 10 mg/kg/day [9] using an osmotic pump (1007D, ALZET® Pumps, Charles River Laboratories International, Inc.). Osmotic pump was filled with AMD3100 or PBS and immersed in saline solution at room temperature 8h before implantation. A small incision on the back side of the mouse neck was made after resection for pump implantation.

2.2 TC14012 administration

TC14012 was applied in a concentration of 5 mg/kg/day. TC14012 was injected subcutaneously immediately after surgery and at every post-op day

3 Body weight recovery

Body weight was determined daily. Body weight recovery (%) and used to assess the systemic effect of the surgical procedure and drug administration on body weight development and was calculated based on the formula below:

Body weight recovery% = BW on every post-OP day [g]/ BW on OP day [g] *100%

4 Clinical chemistry

Serum for measuring the levels of liver enzyme was obtained when harvesting and stored at -80C until measurement. The serum levels of aspartate transaminase (AST), alanine transaminase (ALT) were measured using Automated Chemical Analyser (Bayer Advia 1650, Leverkusen, Germany).

5 LW/BW ratio

Liver weight measured on harvesting day was compared with the mouse body weight on operation day for estimating liver weight recovery.

LW/BW ratio= Liver weight on sacrifice day [g]/ body weight on operation day [g]*100%

6 BrdU proliferation index

Mice were injected with 5-bromo-2'-deoxyuridine 1 hour prior to sacrifice. The formalin fixed liver tissue was embedded in paraffin and cut in 4µm thick sections. Thereafter, slides were stained with Bromodeoxyuridine (BrdU). The total positive cells in each slide were counted based on BrdU-stained sections by Histokat software (Fraunhofer MEVIS, Bremen, Germany).

7 Statistical Analysis

Results were expressed as mean ± standard deviation (SD). Differences between groups were analyzed using One-Way ANOVA by Sigmaplot 13.0 (Statcon, Witzenhausen, Germany). Differences were considered significant if p-values of less than 0.05 were obtained (* $P < 0.05$).

Results

1. Body weight recovery was not affected by modulating the CXC4-CXCR7-SDF-1 axis

All animals tolerated the surgical procedure well. As expected, sham operated animals lost maximally 3.4% of their body weight and recovered fully within a week (Figure 1). In contrast liver resected animals experienced a maximal body weight loss of 8.4 % on POD 2 and recovered fully within the first 5 post-operative days and gained more weight thereafter. No significant difference was observed in body weight recovery on POD 7 between treatment groups and non-treatment groups.

Figure 1. Body weight recovery

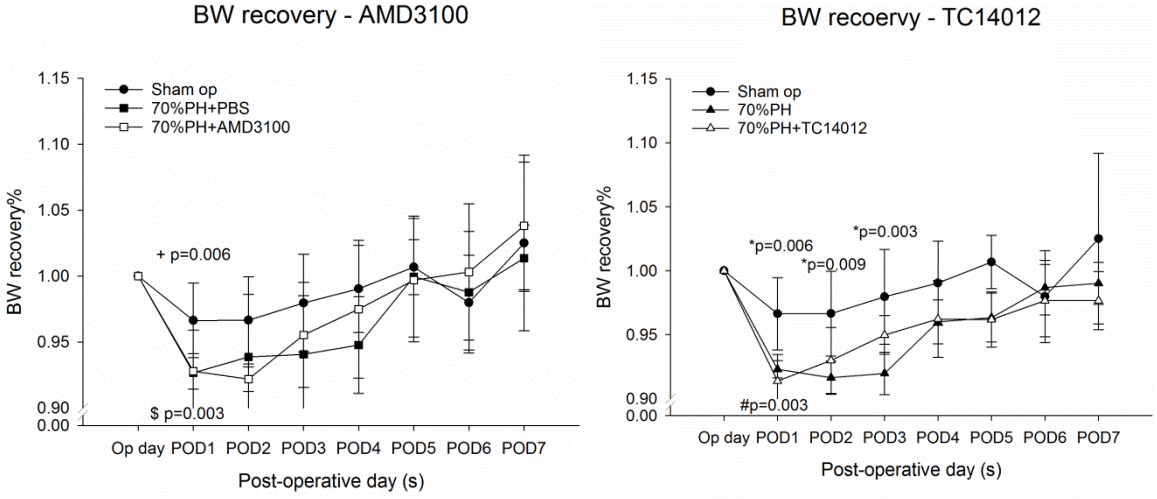

+ Compare 70%PH+PBS group with sham group; $ Compare 70%PH+AMD3100 with sham group;

* Compare 70%PH group with sham group; # Compare 70%PH+TC14012 group with sham group

2. Treatment with CXCR4 antagonist and CXCR7 agonist was associated with higher liver damage

Sham operated animals did not show any signs of liver damage (Figure 2), as expected. Hepatic damage as indicated by serum ALT and AST was highest during the early phase (POD2) after hepatectomy. Liver enzymes reached the normal range within a week after resection indicating full recovery. However, treatment with the CXCR4 antagonist and CXCR7 agonist was associated with significantly higher levels of liver enzymes compared to the control group, suggesting a delayed recovery. In contrast, treatment with the CXCR4 antagonist AMD3100 only did not cause additional damage to the liver.

Figure 2. Liver enzyme – serum ALT and AST

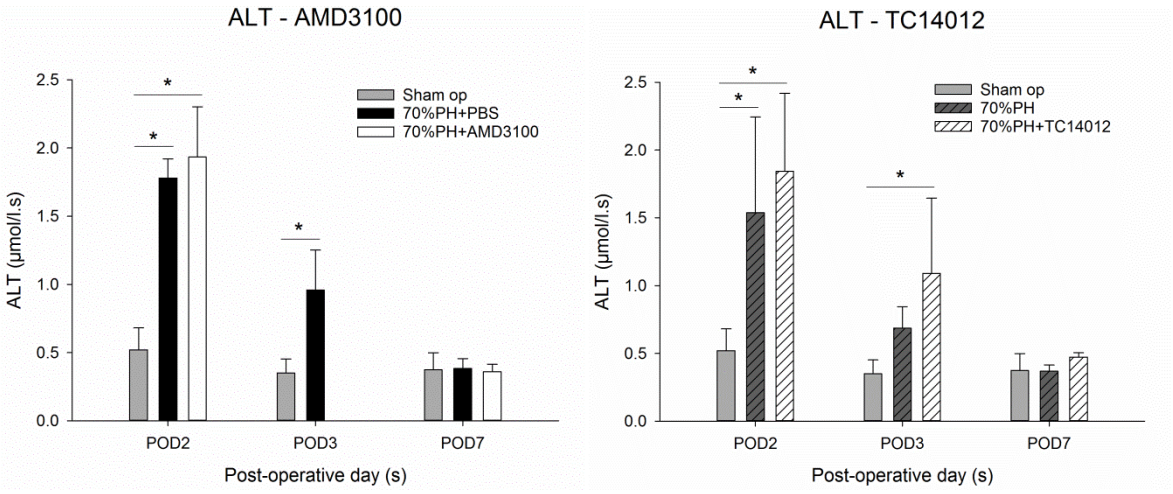

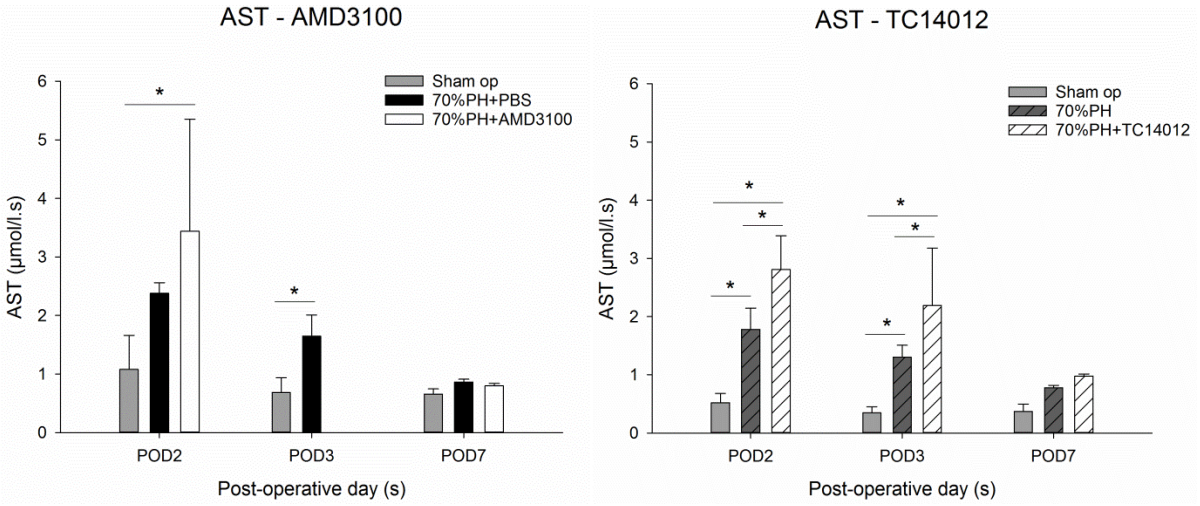

*p<0.05

3. **Treatment with CXCR4 antagonist and CXCR7 agonist was associated with a reduced and delayed liver weight recovery**

   In the sham operated group a transient increase of LW/BW ratio (Figure 3) was observed. However, this was not due to an actual increase in liver weight, but due to the surgery induced decrease of body weight in the first 3 post-operative days. In contrast all liver resected animals experienced a substantial loss of the LW/BW ratio by POD2 as expected, which recovered thereafter. Treatment with the CXCR4 antagonist did not interfere with parenchymal regeneration, where the application of the CXCR4 antagonist and CXCR7 agonist was associated with a more pronounced body weight loss and a reduced and delayed recovery. It indicated that parenchymal liver regeneration was not affected by only blocking CXCR4 using AMD3100, but was impaired by simultaneous activation of CXCR7 when applying TC14012.

Figure 3. Liver weight to body weight ratio

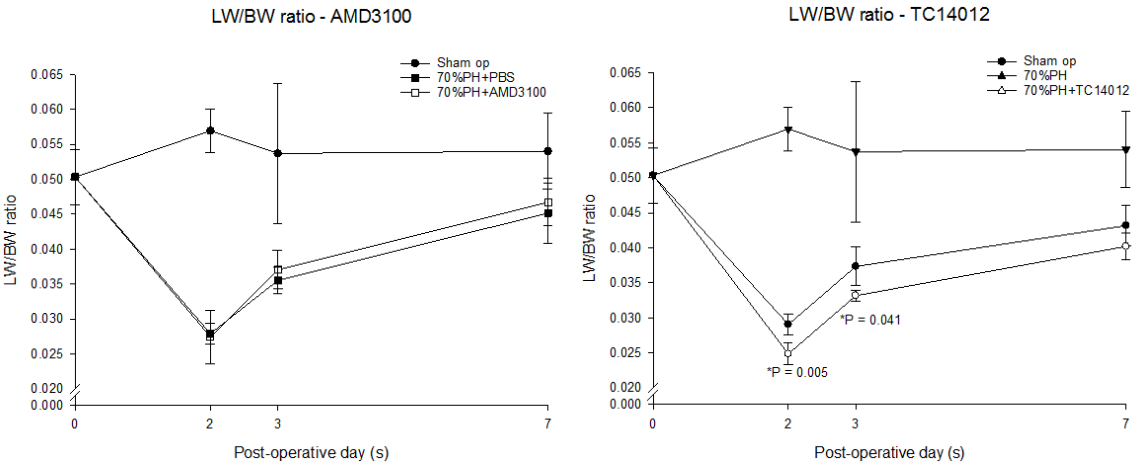

*Compare treatment group with non-treatment 70%PH group.

The peak proliferation index (Figure 4) on POD 2 of total BrdU positive cells was significantly lower in treated group (70%PH+TC14012)compared to untreated 70%PH group control group. It indicated that liver regeneration was impaired. Even on POD3, the proliferation rate remained lower in the treated group, indicating a prolonged impairment of liver regeneration which was also reflected in the lower LW/BW recovery.

Figure 4. Proliferation index of total BrdU positive cells in 70%PH group and 70%PH+TC14012 group at day 2 and day 3

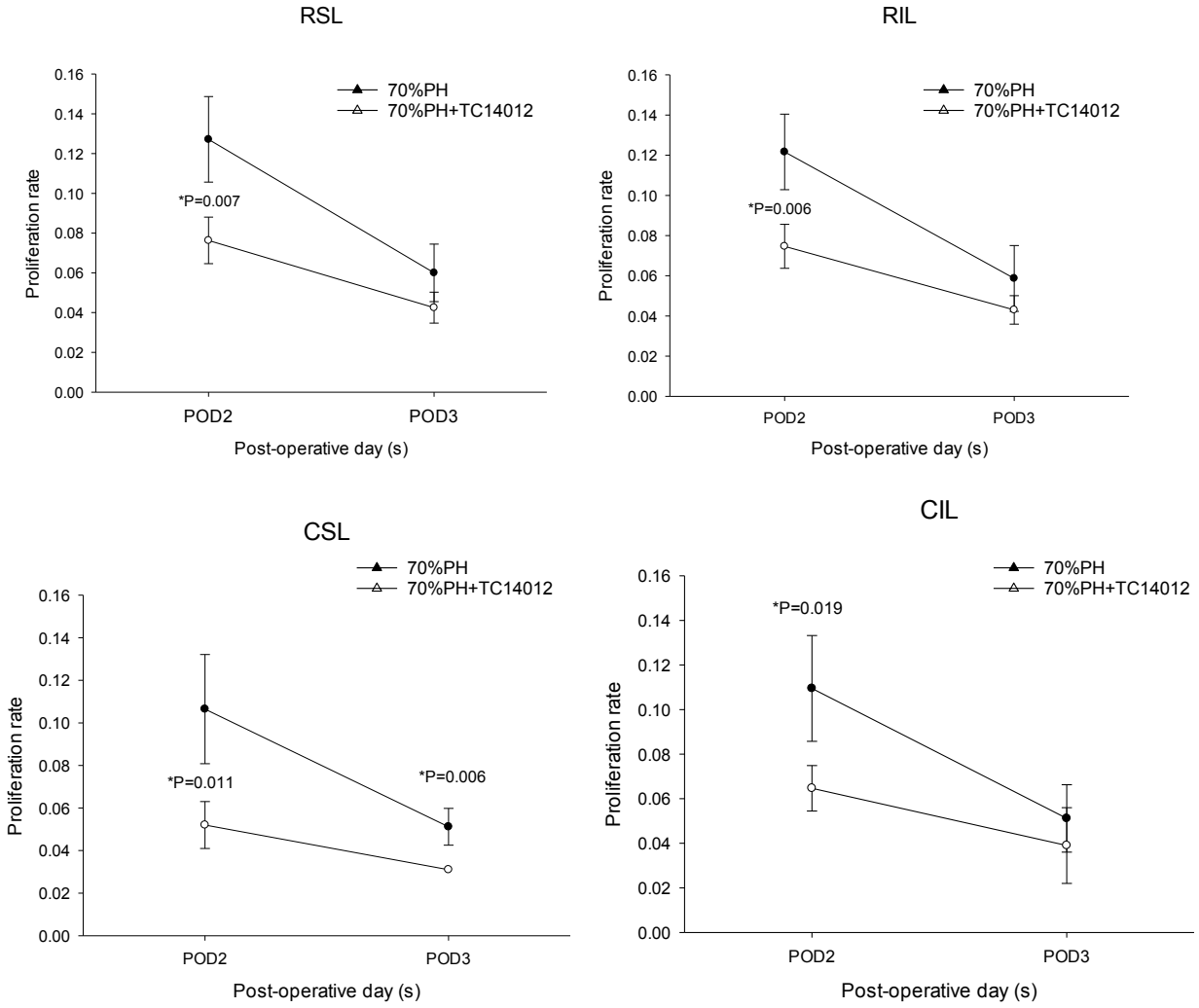

4. Hepatic vascular regeneration was also affect by simultaneously blocking CXCR4 and activating CXCR7

Figure 4. Visualization and quantification of vascular regeneration

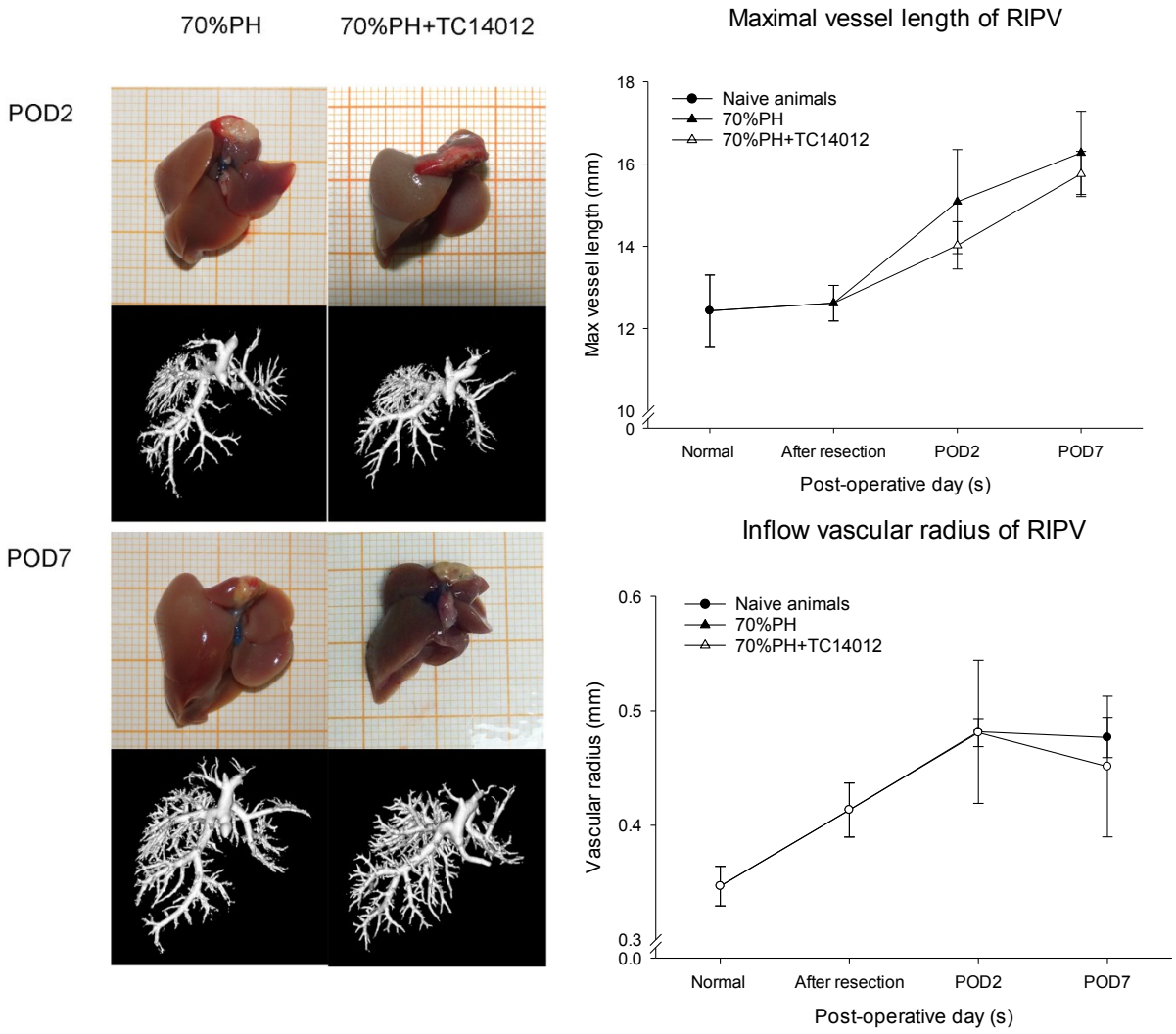

Vascular regeneration was investigated in 70%PH+TC14012 and the untreated 70%PH group. Treatment was associated with a substantially lower maximal vessel length of the RIPV at day 2 and day 7 compared to the non-treated group. It might indicate a delay of hepatic vascular regeneration. However, the average inflow vascular radii in both groups at POD 2 were rather similar. This increase of vascular radius at POD 2 in both groups might be better attributed to portal hypertension than to vascular growth (see our observation in Manuscript III). In other words, vascular radius could hardly reflect the effect of TC14012 to the hepatic vascular systems in the early post-OP time point. Vascular radius in 70%PH+TC14012 group had a substantial decrease at POD 7. This observation was probably due to reduced portal dilatation and delayed vascular expansion

Discussion

In this study, we visualized and quantified hepatic parenchymal and vascular regeneration after modulating the CXCR4-CXCR7-SDF-1 axis. We first applied a CXCR4 antagonist for only blocking CXCR4 in a 70% PH mouse model. Then, we applied CXCR4 antagonist and CXCR7 agonist for not only blocking CXCR4 but also activating CXCR7 using TC14012 in the same resection model in mice.

CXCR4 activation by SDF-1 plays an important role in modulating angiogenesis and haematopoiesis by acting on haematopoietic and vascular endothelial cells. Thus we hypothesized that the blockade of CXCR4 using AMD3100 could dampen the CXCL12-induced angiogenic activity and subsequent impair hepatic vascular regeneration in mouse liver resection model. However, blocking CXCR4 was not associated with any significant differences in terms of the recovery of the body weight, liver enzymes and LW/BW ratio or BrdU proliferation index. It indicated that blocking only CXCR4 using AMD3100 was apparently neither interfering with hepatic regeneration nor with vascular regeneration in normal mouse livers after PH. This might be explained by the multiple roles of the CXCR4 blocking agent AMD3100. AMD3100, also known as Plerixafor, is involved in stem cell mobilization [10]. This role of AMD3100 might be of benefit for liver regeneration. AMD3100 also plays a role in suppressing inflammatory response [11] which might also play a positive role in tissue repair and regeneration.

Expression of CXCR7, another chemokine receptor for SDF-1, is mainly restricted to endothelial cells. It is believed that the primary function of CXCR7 is pivotal in vascular patterning and tumor neo-angiogenesis [12]. TC14012 can activate the β-arrestin pathway via activation of GRK, leading to internalization of CXCR4 and scavenging of SDF-1. Thus, we hypothesized that liver regeneration will be impaired by applying TC14012 via blocking CXCR4 and activating CXCR7.

As expected, when using TC14012 we observed a slower recovery from hepatic injury and a slower recovery of the LW/BW ratio, indicating an impaired course of hepatic regeneration. This prompted to perform the next and key experiment to quantify vascular regeneration. We observed a substantial delay in prolongation of maximal vessel length of RIPV at POD 2 in 70%PH+TC14012 group. We could conclude that vascular liver regeneration might be impaired as indicated by the tested vascular parameter of maximal vessel length. However, this difference did not yet reach statistical significance. . It could be explained by the small group size (n=3), the

observed high inter-group individual variability and vascular parameters obtained restrict to right inferior lobe.

As a next step, we are going to compute the maximal vessel length for the other liver lobes, cumulative vascular parameters for investigating the vascular growth in the whole remnant liver lobes and try to enlarge the group size for reducing the individual variant.

Furthermore, we are also considering todetermine the proliferation rate of hepatocytes and LSEC separately to get a better insight how the drug affects parenchymal versus vascular regeneration.

We also observed that there was no difference in inflow vascular radius in 70%PH+TC14012 compared to 70%PH group. Given the fact that portal hypertension may have residual effect to vascular radius-related parameters, the inflow vascular radius of RIPV was possibly not suitable for detecting the effect of a given drug.

According to our results obtained in TC14012 pilot experiment, it seems that CXCR7 is more related to liver regeneration after partial hepatectomy. It might be explained that CXCR7 could increase the expression of proangiogenic factors, such as interleukin-8 and VEGF, through a G-protein-independent β-arrestin-2-biased receptor resulting in ERK1/2 phosphorylation [12;13].

In summary, using our newly established workflow to assess hepatic vascular regeneration, we confirmed that the CXCR4-CXCR7-SDF-1 pathway is of relevance for liver regeneration. We identified that a substantial decrease in length and radius of RIPV indicated that hepatic vascular regeneration was impaired by administrating TC14012. Our study elucidated that blockade of CXCR4 by AMD3100 after hepatectomy is not capable of inhibiting angiogenesis and vascular growth, possibly due to compensatory actions through the alternative CXCL12 receptor CXCR7.

In the near future, we are going to elucidate this pathway further to detect its molecular mechanism for better understanding the process of liver regeneration. Currently a pilot experiment regarding the changes in mRNA-expression of CXCR4, CXCR7 and SDF-1 after liver resection as detected by in situ hybridization is ongoing. This will serve as a basis when investigating the effects of modulating this axis.

In conclusion, assessment of vascular regeneration by quantifying vascular growth and LSEC proliferation rate in addition to parenchymal regeneration is a useful add-

on for better understanding the relevance of the CXCR4-CXCR7-SDF-1 pathway and liver regeneration in general.

Reference

[1] Liekens S, Schols D, Hatse S. CXCL12-CXCR4 axis in angiogenesis, metastasis and stem cell mobilization. Curr Pharm Des 2010; 16(35):3903-3920.

[2] Wilson GC, Freeman CM, Kuethe JW, Quillin RC, III, Nojima H, Schuster R et al. CXC Chemokine Receptor 4 Signaling Limits Hepatocyte Proliferation After Hepatic Ischemia/Reperfusion in Mice. Am J Physiol Gastrointest Liver Physiol 2015;ajpgi.

[3] Jiang Q, Takahagi S, Uitto J. Administration of bone marrow derived mesenchymal stem cells into the liver: potential to rescue pseudoxanthoma elasticum in a mouse model (Abcc6-/-). J Biomed Biotechnol 2012; 2012:818937.

[4] Mavier P, Martin N, Couchie D, Preaux AM, Laperche Y, Zafrani ES. Expression of stromal cell-derived factor-1 and of its receptor CXCR4 in liver regeneration from oval cells in rat. Am J Pathol 2004; 165(6):1969-1977.

[5] Grunewald M, Avraham I, Dor Y, Bachar-Lustig E, Itin A, Jung S et al. VEGF-induced adult neovascularization: recruitment, retention, and role of accessory cells. Cell 2006; 124(1):175-189.

[6] Rosenkilde MM, Gerlach LO, Jakobsen JS, Skerlj RT, Bridger GJ, Schwartz TW. Molecular mechanism of AMD3100 antagonism in the CXCR4 receptor: transfer of binding site to the CXCR3 receptor. J Biol Chem 2004; 279(4):3033-3041.

[7] Hatse S, Princen K, Bridger G, De Clercq E, Schols D. Chemokine receptor inhibition by AMD3100 is strictly confined to CXCR4. FEBS Lett 2002; 527(1-3):255-262.

[8] Gravel S, Malouf C, Boulais PE, Berchiche YA, Oishi S, Fujii N et al. The peptidomimetic CXCR4 antagonist TC14012 recruits beta-arrestin to CXCR7: roles of receptor domains. J Biol Chem 2010; 285(49):37939-37943.

[9] Chen Y, Huang Y, Reiberger T, Duyverman AM, Huang P, Samuel R et al. Differential effects of sorafenib on liver versus tumor fibrosis mediated by stromal-derived factor 1 alpha/C-X-C receptor type 4 axis and myeloid differentiation antigen-positive myeloid cell infiltration in mice. Hepatology 2014; 59(4):1435-1447.

[10] Mark AL, Sun Z, Warren DS, Lonze BE, Knabel MK, Melville Williams GM et al. Stem cell mobilization is life saving in an animal model of acute liver failure. Ann Surg 2010; 252(4):591-596.

[11] Huang J, Li Y, Tang Y, Tang G, Yang GY, Wang Y. CXCR4 antagonist AMD3100 protects blood-brain barrier integrity and reduces inflammatory response after focal ischemia in mice. Stroke 2013; 44(1):190-197.

[12] Ding BS, Cao Z, Lis R, Nolan DJ, Guo P, Simons M et al. Divergent angiocrine signals from vascular niche balance liver regeneration and fibrosis. Nature 2014; 505(7481):97-102.

[13] Jing XL, Farberg AS, Monson LA, Donneys A, Tchanque-Fossuo CN, Buchman SR. Radiomorphometric quantitative analysis of vasculature utilizing micro-computed tomography and vessel perfusion in the murine mandible. Craniomaxillofac Trauma Reconstr 2012; 5(4):223-230.doi:10.1055/s-0032-1329540

4 DISCUSSION

In experimental research, the 70% partial hepatectomy model in mouse model is of enormous importance for the study of hepatic physiology and pathophysiological disturbances. This liver resection model has been used for years.

However, the mechanism of hepatic vascular regeneration still remains elusive since limited tools are available for studying vascular regeneration. Moreover, due to the small size of the mouse, technical details of determining vascular related parameters were rarely described.

Thus, in the present study, we complemented technical tools for assessing hepatic parenchymal and vascular regeneration. We established an intraoperative monitoring procedure as well as a work flow from silicone injection, µCT-imaging and computational analysis. The results obtained using our adapted experimental approaches were comparable with others (Table1 in Manuscript I and Figure3 in Manuscript III). It indicated that these technical tools are sensitive and suitable for detecting differences in vascular perfusion and vascular growth. Contrasting the vascular tree by silicone injection and µCT scanning provided us the opportunity to study vascular regeneration in a qualitative and quantitative way. Ina previous study, we used the resulting three-dimensional vascular trees for visualizing the variations of hepatic vascular anatomy in normal rats and mice (Sanger et al. 2015).

We acquired quantitative vascular parameters after µCT imaging and performed a quantitative analysis in 70%PH mouse model. Based on these parameters, we explored the growth pattern. Relating hepatic parenchymal and vascular growth as well as determining the similarity of branching angles suggested, at first glance, that regeneration resembled isotropic expansion and thus would represent an easy descriptive model. For further investigating of the growth pattern, a more detailed analysis was performed. Despite the seemingly homogeneous 3D-growth, the observed vascular parameters were ultimately not compatible with the hypothesis of isotropic expansion of liver parenchyma and vascular structures. These observations indicated that hepatic regeneration might be a more complex process influenced by many factors.

One important factor affecting liver regeneration is portal hypertension. Portal hypertension induced by surgical removal of liver lobes might affect these vascular parameters to different extent, not only immediately after resection but also even

after 7 days. Based on the hepatic hemodynamic data obtained 7 days after resection using the established monitoring technique, we were aware of the fact that portal venous pressure returned to normal ranges at POD 7. However, portal hypertension might have residual effects on hepatic vasculature remaining for a longer time. In spite of this limitation, quantitative descriptions of vascular regeneration and, in particular, its spatial inhomogeneity, provided useful information. It can help to identify disturbances in liver regeneration, which is a prerequisite for possibly developing treatment strategies.

Next, we applied silicone injection and micro-CT imaging technique to quantitatively describe hepatic vascular parameters after modulating CXCR4-CXCR7-SDF-1 pathway in 70%PH mouse model. We observed that parenchymal and vascular liver regeneration were not affected by only blocking CXCR4 but were impaired by simultaneous activation of CXCR7 using TC14012.

Our results elucidated that blockade of CXCR4 by AMD3100 after hepatectomy is not capable of inhibiting angiogenesis and vascular growth, because there might be the compensatory actions through the alternative SDF-1 receptor CXCR7. Substantially shorter maximal vessel length RIPV after administration of TC14012 might imply the impairment of hepatic vascular regeneration. This pilot experiment was the first step to study the role of CXCR4-CXCR7-SDF-1 pathway in hepatic vascular regeneration. It was reported that CXCR7-VEGF pathway is related to liver vascular regeneration (DeLeve et al. 2016). Next step, we want to investigate pure CXCR7 antagonist, such as CCX771 (Berahovich et al. 2014), to better understand the role of this pathway for liver regeneration.

Both newly established technical tools can be used in studies evaluating vasoactive drugs in hepatology and hepatobiliary surgery. The monitoring procedure can be utilized to study the effect of drugs affecting hepatic hemodynamic parameters or vascular regenerative parameters. Hemodynamic data can help to characterize the effect of hepatobiliary procedures on the circulatory system. The workflow of silicone injection, μCT imaging, and visualization of the vascular tree and subsequent computation of selective and cumulative vascular parameter technique can be utilized for better understanding the kinetics of vascular growth in the progression of angiogenesis under normal and treatment conditions.

In contrast to corrosion casting, the parenchyma of silicone injected liver specimen remains intact, so that the same specimen can be used for serial sections of the

whole organ for subsequent detection of molecular events during the process of regeneration. Assessing the spatially resolved molecular events in the vicinity of the regenerating vascular tree within the regenerating hepatic parenchyma is the prerequisite for advanced multi-scale systems biology modeling. This silicone injection technique is one experimental step towards reaching this goal. 3D visualization of molecular events in respect to the underlying vascular tree is at reach. Moreover, these procedures also can be applied in different vascular systems of other organs.

However, the major stumbling block to the wider application of these procedures is the technical challenge. First, the perfusion rate for silicone injection, specifically to the hepatic vascular system in mice, was unknown. We successfully adapted the perfusion rate based on the hepatic hemodynamics measurements obtained during the monitoring experiments. Second, in order to master these procedures, substantial microsurgical experience is required. Thus, we reported critical steps in detail in the two published video papers to help the readers for better establishing these useful tools.

In conclusion, in the present study, we successfully established two delicate techniques for acquiring hepatic hemodynamic parameters and parenchymal and vascular regenerative parameters suitable for the use in mice. Furthermore, we established selective and cumulative parameters suitable for quantifying the hepatic vascular tree and applied them for exploring the vascular growth pattern after liver resection. At last, we applied this technique successfully in a pilot study exploring the role of chemokine signaling for liver regeneration.

Altogether our results are an important prelude to further studies on vascular regeneration. In the future, the techniques presented here can be applied in a broad range of conditions where exploration of vascular growth is needed.

5 ABBREVIATIONS

2D	Two dimensional
3D	Three dimensional
CAP	Carotid artery pressure
CHA	Common hepatic artery
CIL	Caudate inferior lobe
CSL	Caudate superior lobe
CVP	Central venous pressure
Fig	Figure
HV	Hepatic vein
IVC	Inferior vena cava
LLL	Left lateral lobe
LML	Left median lobe
LSECs	Liver sinusoid endothelial cells
ML	Median lobe
PH	Partial hepatectomy
POD	Postoperative day(s)
PV	Portal vein
PVP	Portal vein pressure
RIL	Right inferior lobe
RIHV	Right inferior hepatic vein
RIPV	Right inferior portal vein
RL	Right lobe
RML	Right median lobe
RSL	Right superior lobe
SD	Standard deviation
µCT	Micro computed tomography

6 References

Berahovich RD, Zabel BA, Lewen S, Walters MJ, Ebsworth K, Wang Y, Jaen JC, Schall TJ. 2014. Endothelial expression of CXCR7 and the regulation of systemic CXCL12 levels. Immunology, 141 (1):111-122.

Bolland BJ, Kanczler JM, Dunlop DG, Oreffo RO. 2008. Development of in vivo muCT evaluation of neovascularisation in tissue engineered bone constructs. Bone, 43 (1):195-202.

DeLeve LD. 2013. Liver sinusoidal endothelial cells and liver regeneration. JClinInvest, 123 (5):1861-1866.

DeLeve LD, Wang X, Wang L. 2016. VEGF-sdf1 RECRUITMENT OF CXCR7+ BONE MARROW PROGENITORS OF LIVER SINUSOIDAL ENDOTHELIAL CELLS PROMOTES RAT LIVER REGENERATION. AmJPhysiol GastrointestLiver Physiol:ajpgi.

Ding BS, Cao Z, Lis R, Nolan DJ, Guo P, Simons M, Penfold ME, Shido K, Rabbany SY, Rafii S. 2014. Divergent angiocrine signals from vascular niche balance liver regeneration and fibrosis. Nature, 505 (7481):97-102.

Ding BS, Nolan DJ, Butler JM, James D, Babazadeh AO, Rosenwaks Z, Mittal V, Kobayashi H, Shido K, Lyden D, Sato TN, Rabbany SY, Rafii S. 2010. Inductive angiocrine signals from sinusoidal endothelium are required for liver regeneration. Nature, 468 (7321):310-315.

Downey CM, Singla AK, Villemaire ML, Buie HR, Boyd SK, Jirik FR. 2012. Quantitative ex-vivo micro-computed tomographic imaging of blood vessels and necrotic regions within tumors. PLoSOne, 7 (7):e41685.

Duda DG, Kozin SV, Kirkpatrick ND, Xu L, Fukumura D, Jain RK. 2011. CXCL12 (SDF1alpha)-CXCR4/CXCR7 pathway inhibition: an emerging sensitizer for anticancer therapies? ClinCancer Res, 17 (8):2074-2080.

Ehling J, Theek B, Gremse F, Baetke S, Mockel D, Maynard J, Ricketts SA, Grull H, Neeman M, Knuechel R, Lederle W, Kiessling F, Lammers T. 2014a. Micro-CT imaging of tumor angiogenesis: quantitative measures describing micromorphology and vascularization. AmJPathol, 184 (2):431-441.

Ehling J, Bartneck M, Wei X, Gremse F, Fech V, Mockel D, Baeck C, Hittatiya K, Eulberg D, Luedde T, Kiessling F, Trautwein C, Lammers T, Tacke F. 2014b. CCL2-dependent infiltrating macrophages promote angiogenesis in progressive liver fibrosis. Gut.

Faber A, Roderburg C, Wein F, Saffrich R, Seckinger A, Horsch K, Diehlmann A, Wong D, Bridger G, Eckstein V, Ho AD, Wagner W. 2007. The many facets of SDF-1alpha, CXCR4 agonists and antagonists on hematopoietic progenitor cells. JBiomedBiotechnol, 2007 (3):26065.

Gayetskyy S, Museyko O, Kasser J, Hess A, Schett G, Engelke K. 2014. Characterization and quantification of angiogenesis in rheumatoid arthritis in a mouse model using muCT. BMCMusculoskeletDisord, 15:298.

Ghanavati S, Yu LX, Lerch JP, Sled JG. 2014. A perfusion procedure for imaging of the mouse cerebral vasculature by X-ray micro-CT. JNeurosciMethods, 221:70-77.

Hu J, Srivastava K, Wieland M, Runge A, Mogler C, Besemfelder E, Terhardt D, Vogel MJ, Cao L, Korn C, Bartels S, Thomas M, Augustin HG. 2014. Endothelial cell-derived angiopoietin-2 controls liver regeneration as a spatiotemporal rheostat. Science, 343 (6169):416-419.

Huang W, Yen RT, McLaurine M, Bledsoe G. 1996. Morphometry of the human pulmonary vasculature. JApplPhysiol (1985), 81 (5):2123-2133.

Jiang Q, Takahagi S, Uitto J. 2012. Administration of bone marrow derived mesenchymal stem cells into the liver: potential to rescue pseudoxanthoma elasticum in a mouse model (Abcc6-/-). JBiomedBiotechnol, 2012:818937.

Jing XL, Farberg AS, Monson LA, Donneys A, Tchanque-Fossuo CN, Buchman SR. 2012. Radiomorphometric quantitative analysis of vasculature utilizing micro-computed tomography and vessel perfusion in the murine mandible. CraniomaxillofacTrauma Reconstr, 5 (4):223-230.

Kandilis AN, Koskinas J, Tiniakos DG, Nikiteas N, Perrea DN. 2010. Liver regeneration: focus on cell types and topographic differences. EurSurgRes, 44 (1):1-12.

Langheinrich AC, Ritman EL. 2006. Quantitative imaging of microvascular permeability in a rat model of lipopolysaccharide-induced sepsis: evaluation using cryostatic micro-computed tomography. Invest Radiol, 41 (8):645-650.

Liekens S, Schols D, Hatse S. 2010. CXCL12-CXCR4 axis in angiogenesis, metastasis and stem cell mobilization. CurrPharmDes, 16 (35):3903-3920.

Mittal N, Zhou Y, Ung S, Linares C, Molloi S, Kassab GS. 2005. A computer reconstruction of the entire coronary arterial tree based on detailed morphometric data. AnnBiomedEng, 33 (8):1015-1026.

Parker JC, Cave CB, Ardell JL, Hamm CR, Williams SG. 1997. Vascular tree structure affects lung blood flow heterogeneity simulated in three dimensions. JApplPhysiol (1985), 83 (4):1370-1382.

Rosenkilde MM, Gerlach LO, Jakobsen JS, Skerlj RT, Bridger GJ, Schwartz TW. 2004. Molecular mechanism of AMD3100 antagonism in the CXCR4 receptor: transfer of binding site to the CXCR3 receptor. JBiolChem, 279 (4):3033-3041.

Sanger C, Schenk A, Schwen LO, Wang L, Gremse F, Zafarnia S, Kiessling F, Xie C, Wei W, Richter B, Dirsch O, Dahmen U. 2015. Intrahepatic Vascular Anatomy in Rats and Mice-Variations and Surgical Implications. PLoSOne, 10 (11):e0141798.

Sato Y, Koyama S, Tsukada K, Hatakeyama K. 1997. Acute portal hypertension reflecting shear stress as a trigger of liver regeneration following partial hepatectomy. SurgToday, 27 (6):518-526.

Schwen LO, Preusser T. 2012. Analysis and algorithmic generation of hepatic vascular systems. IntJHepatol, 2012:357687.

Schwier M, Bohler T, Hahn HK, Dahmen U, Dirsch O. 2013. Registration of histological whole slide images guided by vessel structures. JPatholInform, 4 (Suppl):S10.

Tsuchiya A, Imai M, Kamimura H, Takamura M, Yamagiwa S, Sugiyama T, Nomoto M, Heike T, Nagasawa T, Nakahata T, Aoyagi Y. 2012. Increased susceptibility to severe chronic liver damage in CXCR4 conditional knock-out mice. DigDisSci, 57 (11):2892-2900.

Upputuri PK, Sivasubramanian K, Mark CS, Pramanik M. 2015. Recent developments in vascular imaging techniques in tissue engineering and regenerative medicine. BiomedResInt, 2015:783983.

Wan SY, Ritman EL, Higgins WE. 2002. Multi-generational analysis and visualization of the vascular tree in 3D micro-CT images. ComputBiolMed, 32 (2):55-71.

Wilson GC, Freeman CM, Kuethe JW, Quillin RC, III, Nojima H, Schuster R, Blanchard J, Edwards MJ, Caldwell CC, Lentsch AB. 2015. CXC Chemokine Receptor 4 Signaling Limits Hepatocyte Proliferation After Hepatic Ischemia/Reperfusion in Mice. AmJPhysiol GastrointestLiver Physiol:ajpgi.

7 Ehrenwörtliche Erklärung

Hiermit erkläre ich, dass mir die Promotionsordnung der Medizinischen Fakultät der Friedrich-Schiller-Universität bekannt ist,

ich die Dissertation selbst angefertigt habe und alle von mir benutzten Hilfsmittel, persönlichen Mitteilungen und Quellen in meiner Arbeit angegeben sind,

mich folgende Personen bei der Auswahl und Auswertung des Materials sowie bei der Herstellung des Manuskripts unterstützt haben: Weiwei Wei, Tao Zhang, Andrea Schenk, Lars Ole Schwen, Sara Zafarnia, Michael Schwier, Felix Gremse, Isabel Jank, Ralf Stumm, Olaf Dirsch, Uta Dahmen

die Hilfe eines Promotionsberaters nicht in Anspruch genommen wurde und dass Dritte weder unmittelbar noch mittelbar geldwerte Leistungen von mir für Arbeiten erhalten haben, die im Zusammenhang mit dem Inhalt der vorgelegten Dissertation stehen,

dass ich die Dissertation noch nicht als Prüfungsarbeit für eine staatliche oder andere wissenschaftliche Prüfung eingereicht habe und

dass ich die gleiche, eine in wesentlichen Teilen ähnliche oder eine andere Abhandlung nicht bei einer anderen Hochschule als Dissertation eingereicht habe.

Ort, Datum Unterschrift des Verfassers

8 Acknowledgement

I am very thankful to Prof. Dr. med. Utz Settmacher, Director of the Department of General, Visceral and Vascular Surgery, Jena University Hospital for giving me the possibility to conduct my research work in his department.

I want to give my sincerely and special thanks to my dear supervisor, Prof. Dr. med. Uta Dahmen, the leader of our experimental surgery group, who gave me the opportunity to come to Germany and study in experimental surgery lab. I am grateful to her for spending a lot of time on designing and supervising my project and providing constructive comments and criticism throughout the whole doctoral period as well as keeping me active in research field.

I owe my gratitude to Dr. Olaf Dirsch for his generous help and guidance regarding histological evaluation of my study.

I want to give my gratitude and sincere compliments to Weiwei Wei as an excellent colleague and a nice friend, who introduced me into experimental microsurgery and giving valuable suggestions regarding surgical work.

I am thankful for Isabel Jank, who had already helped me before my arrival in Germany and her constant and kind helps in research work for language advices and in daily life for helping me solve problems all the time.

Sincerely I thank Dr. rer. nat. Franziska Mußbach supporting me with optimistic and meaningful advice and I feel happy cooperate with her.

Many thanks to Constanze Sänger for her continuously help in imaging 3D vascular and territories reconstruction.

I wish to express my warmest thanks to my sincere friend and teammate Tianjiao Zhang for her nice friendship, constant help and support during my work and leisure time.

I am happy to have Dr. rer. nat. Haoshu Fang and Chunyi Kan as nice teammates and work with them.

I thank my excellent colleges for a fruitful collaboration. I am grateful to Dr. rer. nat. Claudia Schindler, Janine Arlt and Dr. med. Beate Richter for an efficient teamwork.

I feel grateful to have wonderful cooperation partners. I want to give my special thanks to Dr. Andrea Schenk for providing endless help with micro-CT data reconstructions and imaging technique support. I want to give my special thanks to Dr. Lars Ole Schwen, thank his great efforts for mathematic calculation of vascular

parameters and wonderful suggestions for writing manuscript III. I also want to thank Sara Zafarnia and Dr. Felix Gremse from Aachen for helping me with the scanning of explanted liver specimens and micro-CT data reconstructions.

Special thanks to excellent technicians in our group for helping me and assisting my project all time:

I want to thank technicians from our group. Thank Stephanie Lange, Elke Oswald and Kathrin Schulze for helping me with histological work for my samples. Thank Bianca Göhrig, Juliana Neumann, Ulrike Vetterling and Max Bergmann for assisting me.

I also want to thank the technicians from MEVIS, Christiane Engel and Andrea Koller, and technician from Aachen Marek Weiler for helping me generate micro-CT image data and perform 3D reconstructions.

I also would like to thank Prof.Ralf Stumm with his kind help in CXCR4 porject. I also want to give my thanks to the technicians from Prof.Stumm's group, Christine Anders and Heike Stadler, for their kind help in assisting me for CXCR4 project.

At last, I want to thank my families and my husband for their patience and support for me.

9 Academic achievements

Publications

Anding Liu, Haoshu Fang, Weiwei Wei, Chunyi Kan, **Chichi Xie**, Uta Dahmen, Olaf Dirsch " G-CSF pretreatment aggravates LPS-associated microcirculatory dysfunction and acute liver injury after partial hepatectomy in rats. " *Histochem Cell Biol.* 2014 Dec;142(6):667-76.

Chichi Xie, Weiwei Wei, Tao Zhang, Olaf Dirsch, Uta Dahmen " Monitoring of systemic and hepatic hemodynamic parameters in mice"*J Vis Exp.* 2014 Oct 4;(92):e51955.

Chichi Xie, Weiwei Wei, Andrea Schenk, Lars Ole Schwen, Sara Zafarnia, Michael Schwier, Felix Gremse, Isabel Jank, Olaf Dirsch, Uta Dahmen "Application of Microfil injection technique for the visualization of vascular liver regeneration in mice" *J Vis Exp. – Accepted*

Chichi Xie, Lars Ole Schwen, Weiwei Wei, Andrea Schenk, Sara Zafarnia, Felix Gremse, Uta Dahmen "Quantification of hepatic vascular and parenchymal regeneration in mice" *PLOS One - Submitted*

Constanze Sänger , Andrea Schenk, Lars Ole Schwen, Lei Wang, Felix Gremse, Sara Zafarnia, Fabian Kiessling, **Chichi Xie,** Weiwei Wei, Beate Richter, Olaf Dirsch, Uta Dahmen "Intrahepatic Vascular Anatomy in Rats and Mice—Variations and Surgical Implications" *PLOS One*. 2015 Nov 30;10(11):e0141798.

Weiwei Wei, Tianjiao Zhang, Sara Zafarnia, Andrea Schenk, **Chichi Xie**, Chunyi Kan, Olaf Dirsch, Utz Settmacher, Uta Dahmen "Establishment of a rat model: Associating liver partition with portal vein ligation for staged hepatectomy" *Surgery*. 2016 Feb 12. pii: S0039-6060(15)01033-8.

Franziska Mußbach, Uta Dahmen, Olaf Dirsch, **Chichi Xie,** Utz Settmacher „Bioengineered livers" – a new tool for drug testing and a promising solution to meet the growing demand for donor organs" *European surgical research – In revision*

Presentations

Chichi Xie, Weiwei Wei, Tao Zhang, Olaf Dirsch, Uta Dahmen "Monitoring of hepatic perfusion in the mouse" *24th Biotest Wilsede-Workshop,* Wilsede, Germany, Jul 2013

Chichi Xie, Weiwei Wei, Olaf Dirsch, Uta Dahmen "Monitoring of mice hepatic hemodynamics in experimental surgery" *25th Biotest Wilsede-Workshop*, Wilsede, Germany, Jul 2014

Chichi Xie, Weiwei Wei, Andrea Schenk, Lars Ole Schwen, Sara Zafarnia, Uta Dahmen " Visualization of liver regeneration after 70% partial hepatectomy in mice" *the 132th DGCH (Deutsche Gesellschaft für Chirurgie)*, Munich, Germany, May 2015

Chichi Xie, Lars Ole Schwen, Weiwei Wei, Andrea Schenk, Sara Zafarnia, Uta Dahmen " Visualization of liver parenchymal and vascular regeneration after 70% partial hepatectomy in mice" *the 19th Chirurgische Forschungstage*, Würzburg, Germany, Oct 2015

Chichi Xie, Lars Ole Schwen, Weiwei Wei, Andrea Schenk, Sara Zafarnia, Uta Dahmen " Visualization of liver parenchymal and vascular regeneration after 70% partial hepatectomy in mice" *the 24th Deutschen Transplantationsgesellschaft*, Dresden, Germany, Oct 2015

Posters

Chichi Xie, Weiwei Wei, Sara Zafarnia, Felix Gremse, Michael Schwier, Olaf Dirsch, Uta Dahmen " Visualization of liver regeneration after 70% partial hepatectomy in mice" *the 50th EASL (European Association for the Study of the Liver)*, Vienna, Austria, Apr 2015

10 Curriculum vitae

Personal Information

Name	XIE, Chichi
Gender	Female
Date of Birth	25. 08. 1987
Place of Birth	Zhejiang, China
Nationality	P. R. China
Marital State	Married
E-mail	popxcc@gmail.com
Handy Number	0049-015777133219
Address	Stauffenberg Str.9
	07747, Jena

Education

Primary School

Sep 1994 ~ Jun 2000	Wenyi Rd Primary School, Hangzhou, China

Middle school

Sep 2000 ~ Jun 2003	Hangzhou No.13 Middle School, Hangzhou, China

High school

Sep 2003 ~ Jun 2006	Hangzhou Xuejun High School, Hangzhou, China

Bachelor Degree

Sep 2006 ~ Jun 2010	ZheJiang University City College, Medical College, Hangzhou, China
Sep 2010 ~ Jun 2011	One year clinical rotation as an intern in The Second Affiliated Hospital of Zhejiang University, School of Medicine, Hangzhou, China

Master Degree

Sep 2011~Jun2014	Major: Reproductive Medicine
	Institute of Reproductive Medicine, The First Affiliated Hospital of Wenzhou Medical University, Wenzhou Medical University, Wenzhou, China
	Academic Advisor: Prof. Ying Zhou

Doctoral degree

Mar 2013 ~ Now	Doctoral candidate in Experimental Transplantation Surgery, the department of General, Visceral and Vascular Surgery, Jena University Hospital, Germany
	Supervisor: Prof.med. Uta Dahmen

Experimental experience

Period of pursuing Master Degree in China

Mouse and rat anatomical identification	N=5
Rat vascular anastomosis (Carotid, Femoral artery)	N=30
End to end microvascular anastomosis in mouse cadaver	N=10
End to side microvascular anastomosis in mouse cadaver	N=20
Mouse heart donor operation	N=45
Mouse heterotopic heart transplantation(Neck)	N=40
Mouse heterotopic heart transplantation(Abdomen)	N=5
Rabbit heterotopic ovary transplantation(Neck)	N=15
Rabbit orthotropic ovary transplantation(contralateral ovarian vessel)	N=5

Period of pursuing doctoral degree in Germany

Systemic and hepatic hemodynamics monitoring in normal and partial hepatectomized mice	N=10 (Full monitoring) N=20 (Hepatic monitoring)
Partial hepatectomy (PH)	N=167 (70%PH) N=16 (90%PH)
Bile duct ligation	N=10
Microfil injection technique for visualization and quantification of hepatic vascular system in normal and partial hepatectomized mice	N=26 (PV system) N=28 (HV system)
Establishment of liver decellularization	N=20 (Normal liver) N=11 (90%PH liver) N=14 (fatty liver) N=10 (fibrotic liver) N=4 (Liver from died mice)